ไฮโดรเทอร์โมไลซิสของคาร์โบไฮเดรตด้วยโลหะรองรับบนอะลูมิโนซิลิเกต

นางสาวสิรินาถ เสือเจริญ

วิทยานิพนธ์นี้เป็นส่วนหนึ่งของการศึกษาตามหลักสูตรปริญญาวิทยาศาสตรมหาบัณฑิต

สาขาวิชาปิโตรเคมีและวิทยาศาสตร์พอลิเมอร์

คณะวิทยาศาสตร์ จุฬาลงกรณ์มหาวิทยาลัย

ปีการศึกษา 2554

HYDROTHERMOLYSIS OF CARBOHYDRATES USING METAL SUPPORTED ON ALUMINOSILICATE

Miss Sirinart Suacharoen

A Thesis Submitted in Partial Fulfillment of the Requirements
for the Degree of Master of Science Program in Petrochemistry and Polymer Science
Faculty of Science
Chulalongkorn University
Academic Year 2011

Thesis Title	HYDROTHERMOLYSIS OF CARBOHYDRATES USING METAL SUPPORTED ON ALUMINOSILICATE
By	Miss Sirinart Suacharoen
Field of Study	Petrochemistry and Polymer Science
Thesis Advisor	Duangamol Tungasmita, Ph.D.

Accepted by the Faculty of Science, Chulalongkorn University in Partial Fulfillment of the Requirements for the Master's Degree

……..Dean of the Faculty of Science

(Professor Supot Hannongbua, Dr. rer. nat.)

THESIS COMMITTEE

……..Chairman

(Associate Professor Supawan Tantayanon, Ph.D.)

……..Thesis Advisor

(Duangamol Tungasmita, Ph.D.)

……..Examiner

(Associate Professor Wimonrat Trakarnpruk, Ph.D.)

……..External Examiner

(Gamolwan Tumcharern, Ph.D.)

สิรินาถ เสือเจริญ : ไฮโดรเทอร์โมไลซิสของคาร์โบไฮเดรตด้วยโลหะรองรับบนอะลูมิโนซิลิเกต. (HYDROTHERMOLYSIS OF CARBOHYDRATES USING METAL SUPPORTED ON ALUMINOSILICATE) อ.ที่ปรึกษาวิทยานิพนธ์หลัก: อ. ดร. ดวงกมล ตุงคะสมิต, 110 หน้า

ได้สังเคราะห์ตัวเร่งปฏิกิริยาเอสบีเอ-15 เป็นซิลิกาที่มีรูพรุนขนาดกลางด้วยวิธีทางความร้อน ใช้ไทรบล็อกโคพอลิเมอร์ชนิด P123 (พอลิเอทิลีนออกไซด์$_{20}$-พอลิโพรพิลีนออกไซด์$_{70}$-พอลิเอทิลีนออกไซด์$_{20}$) เป็นสารชี้นำโครงสร้าง มีองค์ประกอบของเจลเป็น 1.0 TEOS: 0.0165 P123: 6.95 HCl: 140 H_2O ทำการตกผลึกที่อุณหภูมิ 100 องศาเซลเซียส เป็นเวลา 48 ชั่วโมง อะลูมิเนียม-เอสบีเอ-15 เตรียมโดยการเติมอะลูมิเนียมไปในโครงสร้างเอสบีเอ-15 นอกจากนี้ได้เตรียมโลหะนิกเกิลและรูทีเนียม บนตัวรองรับเอสบีเอ-15 และอะลูมิเนียม-เอสบีเอ-15 โดยวิธีทำให้เอิบชุ่ม จากนั้นตรวจสอบลักษณะเฉพาะของวัสดุที่สังเคราะห์ได้ด้วยเทคนิคการเลี้ยวเบนของรังสีเอกซ์ เทคนิคการดูดซับแก๊สไนโตรเจน อะลูมิเนียมนิวเคลียร์แมกเนติกเรโซแนนซ์สำหรับสถานะของแข็ง กล้องจุลทรรศน์แบบส่องกราดติดตั้งร่วมกับเครื่องกระจายพลังงานของรังสีเอ็กซ์ และกล้องจุลทรรศน์แบบส่องผ่าน นำตัวเร่งปฏิกิริยาที่สังเคราะห์ได้ไปประยุกต์กับปฏิกิริยาไฮโดรเทอร์โมไลซิสของสารประเภทคาร์โบไฮเดรต โดยใช้กลูโคส ซูโครส และแป้งเป็นสารตั้งต้น ได้ศึกษาผลของปัจจัยต่างๆในการเกิดปฏิกิริยา ได้แก่ ชนิดของสารตั้งต้น ชนิดของตัวเร่งปฏิกิริยา ปริมาณของตัวเร่งปฏิกิริยา และอุณหภูมิ จากผลการทดลองภาวะที่เหมาะสมของกลูโคสคือตัวเร่งปฏิกิริยา 20%Ru-ZSM-5 ปริมาณ 15 เปอร์เซ็นต์โดยน้ำหนักสารตั้งต้น ที่อุณหภูมิ 200 องศาเซลเซียส เป็นเวลา 1 ชั่วโมง ให้ปริมาณกรดลีวูลินิกสูงสุดที่ 44.0 เปอร์เซ็นต์ ภาวะที่เหมาะสมของซูโครสคือตัวเร่งปฏิกิริยา 20%Ru-Al-SBA-15 ปริมาณ 15 เปอร์เซ็นต์โดยน้ำหนักสารตั้งต้น ที่อุณหภูมิ 200 องศาเซลเซียส เป็นเวลา 1 ชั่วโมง ให้ปริมาณกรดลีวูลินิกสูงสุดที่ 40.8 เปอร์เซ็นต์และภาวะที่เหมาะสมของแป้งคือตัวเร่งปฏิกิริยา 20%Ru-Al-SBA-15 ปริมาณ 10 เปอร์เซ็นต์โดยน้ำหนักสารตั้งต้น ที่อุณหภูมิ 300 องศาเซลเซียส เป็นเวลา 1 ชั่วโมง ให้ปริมาณกรดลีวูลินิกสูงสุดที่ 38.6 เปอร์เซ็นต์

สาขาวิชา ปิโตรเคมีและวิทยาศาสตร์พอลิเมอร์ ลายมือชื่อนิสิต.....

ปีการศึกษา 2554 ลายมือชื่อ อ.ที่ปรึกษาวิทยานิพนธ์หลัก.....

5272723523: MAJOR PETROCHEMISTRY AND POLYMER SCIENCE
KEYWORDS: HYDROTHERMOLYSIS / CARBOHYDRATE / ALUMINOSILICATE

SIRINART SUACHAROEN: HYDROTHERMOLYSIS OF CARBOHYDRATES USING METAL SUPPORTED ON ALUMINOSILICATE. ADVISOR: DUANGAMOL TUNGASMITA, Ph.D., 110 pp.

Mesoporous silica SBA-15 was synthesized by hydrothermal method using triblock P123 (poly(ethylene oxide)$_{20}$-poly(propylene oxide)$_{70}$-poly(ethylene oxide)$_{20}$) copolymer as a structure directing agent. The gel molar composition of SBA-15 was 1.0 TEOS: 0.0165 P123: 6.95 HCl: 140 H_2O. The gel was crystallized at 100°C for 48 h. The Al-SBA-15 was synthesized by incorporating SBA-15 with aluminium via post synthesis. In addition, the Ni and Ru metal supported on SBA-15 and Al-SBA-15 were prepared by aqueous wet impregnation method. The synthesized materials were characterized by X-ray powder diffraction, nitrogen sorption analysis, solid state ^{27}Al-nuclear magnetic resonance, scanning electron microscopy equipped with energy dispersive spectrometer, and transmission electron microscopy. Synthesized catalysts were applied in hydrothermolysis of carbohydrates using glucose, sucrose, and starch as starting materials. The various reaction parameters such as starting material type, catalytic type, catalytic amount, and temperature were studied. From the results, the optimum condition for glucose over 20%Ru-ZSM-5 in amount of 15 wt.% of starting material at 200°C for 1 h which gave the maximum levulinic acid selectivity as 44.0%. The optimum condition for sucrose over 20%Ru-Al-SBA-15 in amount of 15 wt.% of starting material at 200°C for 1 h which gave the maximum levulinic acid selectivity as 40.8%. The optimum condition for starch over 20%Ru-Al-SBA-15 in amount of 10 wt.% of starting material at 300°C for 1 h which gave the maximum levulinic acid selectivity as 38.6%.

Field of Study:Petrochemistry and Polymer Science Student's Signature .....

Academic Year: 2011 Advisor's Signature .....

ACKNOWLEDGEMENTS

The accomplishment of this thesis can be attributed to the extensive support and assistance from Dr. Duangamol Tungasmita, my thesis advisor. I would like to sincere gratitude to her for valuable advice and guidance in this research as well as extraordinary experiences throughout the work.

I would like to thank sincerely to Associate Professor Dr. Supawan Tantayanon, Associate Professor Dr. Wimonrat Trakarnpruk, and Dr. Gamolwan Tumcharern as the chairman and examiner of this thesis committee, respectively, for all of their kindness and useful advice in the research.

I would like to gratefully thank the contribution of Center of Innovative Nanotechnology, Petrochemicals and Advanced Materials, Chulalongkorn University and the Department of Chemistry and Program of Petrochemistry and Polymer Science, Faculty of Science, Chulalongkorn University for the valuable knowledge and experience.

Many thanks go in particular to the members of Materials Chemistry and Catalysis Research Unit for their sincere help and kindness. Finally, I would like to express my deepest gratitude to my family and my friend for their entirely care and understanding during my graduate study.

CONTENTS

CHAPTER **Page**

CHAPTER **Page**

CHAPTER **Page**

CHAPTER **Page**

LIST OF TABLES

LIST OF FIGURES

Figure **Page**

Figure **Page**

Figure **Page**

LIST OF SCHEMES

LIST OF ABBREVIATIONS

Å	Angstrom
a.u.	Arbitrary unit
BET	Brunauer-Emmett-Teller
BJH	Barret, Joyner, and Halenda
^{o}C	Degree Celsius
CMC	critical micelle concentration
EDX	Energy dispersive spectrometer
GC	Gas chromatography
g	Gram (s)
h	Hour
µm	Micrometer (s)
ml	Milliliter (s)
min	Minute (s)
M	Molarity
nm	Nanometer (s)
%	Percentage
SEM	Scanning electron microscopy
TEM	Transmission electron microscope
XRD	X-ray diffraction

CHAPTER I

INTRODUCTION

1.1 Background

In recent years, economic growth requires safe, sustainable and environment friendly resources for industrial production and it should be available for long term. The formation of fossil resources from biomass is a very slow process, and at present these resources are being depleted faster than they are being formed. Using abundant renewable biomass to replace petroleum as raw materials for the chemical industry has important strategic significant. Carbohydrate feedstocks are invaluable as an ton-scale accessible and relatively cheap resource to provide the initial feedstock in the development of large biobased chemical products such as reducing sugars, furfural, various carboxylic acids including levulinic acid, succinic acids and lactic acid, etc. [1-3].

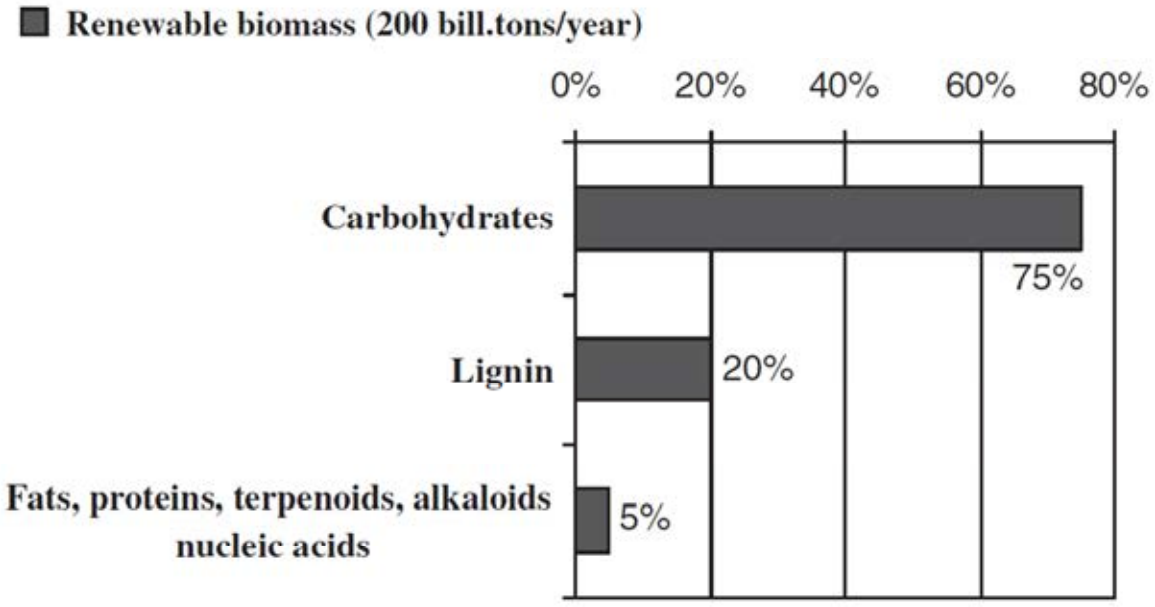

Figure 1.1 Composition of renewable biomass [1].

Generally, the conversion of biomass to chemicals represent a major challenge because of the complex nature of the substrates. Therefore, the catalysts play an important role in increasing the reaction rates and optimizing the yields of targeted products [4]. For this reason, the conversion of carbohydrates to bio-chemicals by heterogeneous catalysis has received much attention in recent years. Aluminosilicate catalysts have the potential to promote the production of oxygenated hydrocarbon from carbohydrate. Zeolites and mesoporous compounds have high concentration of acid sites, high hydrothermal stability, less toxic, non-corrosive and enhanced shape selectivity. In this research, focus on ZSM-5 and SBA-15 due to ZSM-5 is a zeolite with an tetrahedral micropore structure which can improve the reaction rate and product selectivity for the acid-catalyzed dehydration of glucose to hydrocarbon [5] while SBA-15 possesses a hexagonal mesopore structure, is a high hydrothermal stability material and composes of parallel cylindrical pores with axes arrange in a hexagonal unit cell. Acidity of SBA-15 increased by aluminosilicate postsynthesis and the catalyst was designated as a Al-SBA-15 which have aluminosilicate structure.

In this work, the appropriate reaction condition in hydrothermolysis of carbohydrates was investigated. The reaction temperature was varied in the range 200 to 300^{o}C and catalytic amount was varied from 5 to 15 wt.% based on starting material. The starting materials namely glucose, sucrose, and starch were representative of carbohydrate for molecular size comparison. In addition, incorporated with Ni and Ru on Al-SBA-15 for improve property of catalyst and compared to ZSM-5 in hydrothermolysis for pore size comparison under the optimum conditions on each starting material for synthesis of levulinic acid (LA).

1.2 Objectives

The objectives of this research were:

1. To synthesize Al-SBA-15 and metal (Ni and Ru) supported on SBA-15, Al-SBA-15, and ZSM-5.
2. To study reaction parameters based on levulinic acid yield and product selectivity in hydrothermolysis of carbohydrates with aluminosilicate catalysts.

1.3 Scopes of work

1. To synthesize SBA-15 by hydrothermal methods.
2. To synthesize Al-SBA-15 by post synthesis methods.
3. To synthesize metal (Ni and Ru) supported SBA-15, Al-SBA-15, and ZSM-5 materials by wet impregnation method.
4. Characterization of all prepared catalysts.
5. Determination of the optimum condition of carbohydrate hydrothermolysis by studying the effect of type of metal supported on SAB-15 and ZSM-5, catalytic amount, reaction temperature and type of starting material.

1.4 Literature reviews

1.4.1 Hydrothermolysis of carbohydrate

In 2002, Cha *et al.* [6] have performed hydrolysis of corn starch with dilute sulfuric acid by extrusion processing, and then converted to levulinic acid using a pressure reactor. The result indicated maximum yield of levulinic acid was 47.5% when extruded corn starch was reacted at 200^{o}C after being extruded mixture of corn starch(70%), sulfuric acid(5%) and water(25%) at 180^{o}C and 20 rpm screw speed.

In 1987, Jinder *et al.* [7] studied a catalytically dehydrating molten D-fructose to levulinic acid over LZY zeolite within batch reactor at 140^{o}C and nitrogen was purged. After 15 h, the maximum yield of levulinic acid was 43% of original D-fructose, but net yield of hydroxymethylfurfural (HMF) was only 4% of original D-fructose.

In 1997, Khavinet *et al.* [8] studied the partial dehydration of glucose solution to organic acids in both microporous (HY-zeolite and montmorillonite) and mesoporous (MCM-20 and MCM-41) aluminosilicate catalysts. Microporous molecular-sieving catalysts also promoted the decomposition of reaction products to coke, which in turn lowered the product yield and selectivity. Coke formation was less significant with the mesoporous MCM catalysts.

In 1999, Cheriti *et al.* [9] studied hydrothermolysis of carbohydrate fraction of the biomass (glucose and cellobiose) as aqueous solution 0.1M in a continuous tube reactor at 350^{o}C under alkaline condition (NaOH 0.01M) compared with neutral condition. In alkaline condition, the results showed formation of products HMF, 2-furaldehyde and hydroxyhydroquinone were inhibit. Contrary to the formation of CO_2 and CO was increased.

1.4.2 Al-SBA-15 catalysts

In 1998, Zhao *et al.*[10] successfully synthesized mesoporous molecular sieves (SBA-15) which was used copolymer as template under acidic condition. SBA-15 exhibited pore sized in the range of 50 to 300 Å, pore volume fractions up to 0.85 and wall thickness about 31 to 64Å that refered to hydrothermal stability.

Mesoporous silica SBA-15 can be incorporated with aluminum via two different synthesis procedures that are direct synthesis and post synthesis procedure. The direct synthesis procedure often required a specialized synthesis condition depending on the respective structures of the materials, and the incorporation of aluminum into the silica matrix usually caused a decrease in the structure ordering. In 1999, Yue *et al.*[11] synthesized Al-SBA-15 by changing the synthesis condition from a strongly acidic condition (pH<0) to a pH value of 1.5. The resulting materials retain the hexagonal order and physical properties of purely siliceous SBA-15. The Al-SBA-15 catalysts exhibited higher catalytic activity in the cumene cracking reaction than Al-MCM-41.

In 2005, Kao *et al.* [12] developed the post-synthesis aluminum method for SBA-15 using an aqueous $(NH_4)_3AlF_6$ solution as the aluminum source. The Al-SBA-15 materials thus obtained a high framework aluminum content (up to a bulk Si/Al molar ratio near 5), good structural integrity, and well-developed Brønsted acidity.

In 2007, Ooi *et al.* [13] have prepared aluminum-containing SBA-15 material using two different methods in order to compare their cracking activity in gasoline production from waste used palm oil. The catalyst prepared *via* direct synthesis possessed disorder pore size distribution whereas the catalyst prepared *via* post-synthesis had narrow pore size distribution. The regenerated Al-SBA-15 prepared via post-synthesis gave better activity and yield of gasoline fraction than Al-SBA-15 prepared *via* direct synthesis.

1.4.3 Metal incorporation in catalyst

In 2005, Xiu-Ki *et al*. [14] investigated the effects of using fumed SiO_2, MCM-41, and SBA-15 as supports for Ru and Ni catalysts on ammonia decomposition. The loading of metal component and potassium promoter onto the supports was done by the incipient wetness impregnation method. The highly active Ru and Ni catalysts have been fabricated for the generation of CO_x-free H_2 from ammonia. The Ru catalysts were more active than the corresponding Ni catalysts.

In 2007, Yasuharu *et al*. [15] studied the catalytic activities of various noble metal (Pt, Pd, Rh and Ru) supported on siliceous SBA-15 and Al-containing SBA-15 for hydrodesulfurization (HDS) of thiophene at 350^{o}C. The catalysts were characterized by XRD analysis, N_2 adsorption, 2-propanol dehydration, cumene cracking and FT-IR. The order of activities of these catalysts was Pt/SBA-15 > Pd/SBA-15 > Rh/SBA-15 > Ru/SBA-15. In the same year, Vizcaino*et al*. [16] prepared Ni-Cu supported catalysts (MCM-41, SBA-15, and ZSM-5 nanocrystalline) by incipient wetness impregnation and tested in ethanol steam reforming reaction. The best metal dispersion due to smaller metallic crystallite size is achieved over SBA-15, which offers higher metal contents, leading to the highest hydrogen selectivity. Nickel monometallic catalyst showed good catalytic performance but copper monometallic catalyst presented poor catalytic activity.

In 2011, Yang *et al*. [17] have performed Fenton-like degradation reaction of cellulose over Mn/ZSM-5 under 53% phosphoric acid medium at 100^{o}C for 5 h. The Mn/ZSM-5 was prepared by incipient impregnation method. Cellulose can be degraded to small molecular chemicals such as levulinic acid (LA), 5-hydroxymethylfurfural (HMF) which higher than the other products.

CHAPTER II

THEORY

2.1 Catalysts

A catalyst is a substance that increased the rate of a chemical reaction by reducing the activation energy (E_a) as shown in Figure 2.1. The highest peak position performing the highest energy refers to the transition state. In typically reaction, the energy required to enter the transition state is high, whereas the energy to transition state decreases in catalytic reaction. In addition, the catalyst may participate in multiple chemical transformations and is not consumed by the reaction.

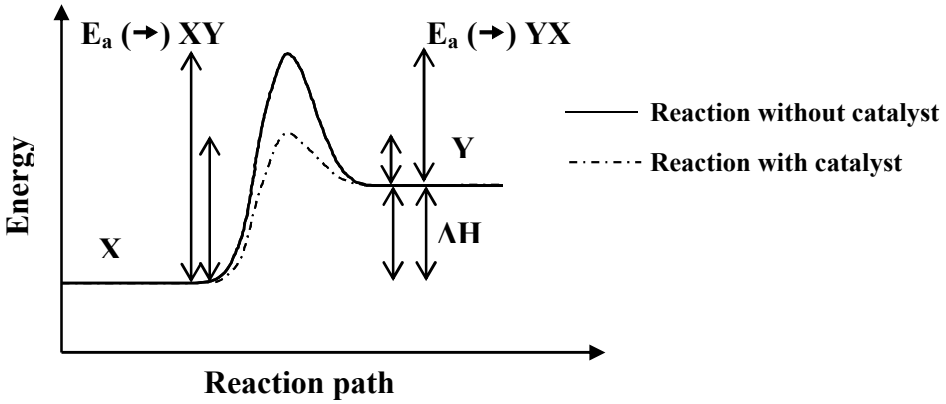

Figure 2.1 The relationship between activation energy (E_a) and enthalpy (ΔH) of the reaction with and without a catalyst [18].

2.2 Properties of industrial catalysts

In general, the suitable catalysts for industrial processes are considered mainly on the three properties [19]:

1) Activity is a measure of how fast one or more reaction proceed which can be defined in term of kinetics. A high activity catalyst will be given high productivity when the less amount of the catalyst is utilized or the reaction is performed in mild operating condition, particularly temperature, which enhances selectivity and stability if the thermodynamic is more favorable. It is appropriate to measure reaction rates in the temperature that will be occurred in the reactor.

2) Selectivity of a reaction is the fraction of the starting material that is converted to the expected product. High selectivity catalyst produces high yield of a desired product, whereas undesirable competitive and consecutive reactions are suppressed. This means that the texture of the catalyst (in particular pore size and pore volume) should be improved toward reducing limitation by internal diffusion, which in case of consecutive reactions rapidly reduces selectivity.

3) Stability of a catalyst determines its lifetime in industrial processes. Catalyst stability is influenced by various factors such as decomposition, coking and poisoning. Catalyst deactivation can be followed by measuring activity or selectivity as a function of time. Deactivated catalysts can often be regenerated before they ultimately have to be replaced. The catalyst lifetime is a crucial importance for the economics of process.

Nowadays, the efficient use of raw materials and energy is of major importance, and it is preferable to optimize existing processes than to develop new ones. For various reasons, the target quantities should be given the following order of priority:

Selectivity > Stability > Activity

2.3 Type of the catalysts

Catalysts can be classified into two main types by the boundary of the catalyst and the reactant. Heterogeneous reaction, the catalyst is in a different phase from the reactants, whereas the catalyst in the same phase of reactant is called homogeneous reaction. Thus, the solid catalysts are identified as heterogeneous catalysts, and the liquid catalysts are specified as homogeneous catalysts when assume reactant is liquid. Homogeneous catalysts have a higher degree of dispersion than heterogeneous catalysts only the surface atoms are active [19]. Summary of the advantage and disadvantage of two-type catalyst is presented in Table 2.1.

Table 2.1 Comparison of homogeneous and heterogeneous catalysts

Consideration	Homogeneous catalyst	Heterogeneous catalyst
1. Active centers	All metal atoms	Only surface atoms
2. Concentration	Low	High
3. Selectivity	High	Low
4. Diffusion problems	Practically absent	Present (mass-transfer-controlled reaction)
5. Reaction conditions	Mild (50-200°C)	Severe (often >250°C)
6. Applicability	Limited	Wide
7. Activity loss	Irreversible reaction with product (cluster formation), poisoning	Sintering of the metal crystallites, poisoning
8. Structure/ Stoichiometry	Defined	Undefined
9. Modification possibility	High	Low
10. Thermal stability	Low	High
11. Catalyst separation	Sometimes laborious (chemical decomposition, distillation, extraction)	Fixed-bed: unnecessary Suspension: filtration
12. Catalyst recycling	Possible	Unnecessary (fixed-bed) or easy (suspension)
13. Cost of catalyst losses	High	Low

The major disadvantage of homogeneous catalyst is the difficulty of separating the catalyst from the product. Heterogeneous catalysts are either automatically removed in the process (*e.g.* vapor-phase reaction in fixed bed reactor) or separated by simple methods such as filtration or centrifugation. However, in more complicated processes, distillation, liquid-liquid extraction and ion exchange are necessarily used homogeneous catalysts.

2.4 Porous molecular sieves

Molecular sieves are porous materials that exhibit selective adsorption properties which can be classified on the IUPAC definitions into three main types depending on their pore sizes that are microporous materials, mesoporous materials, and macroporous materials. Properties and examples of these materials are shown in Table 2.2.

Table 2.2 IUPAC classification of porous materials

Type of porous molecular sieve	Pore size (Å)	Examples
Microporous materials	< 20	Zeolites, Activated carbon
Mesoporous materials	20 – 500	M41s, SBA-15, Pillared clays
Macroporous materials	> 500	Glasses

2.4.1 Zeolites

Zeolites are ordered, porous, and regid crystalline aluminosilicates that contain uniform pores and cavities with molecular dimentions. The structures of zeolites consist of an extensive three-dimensional network of SiO_4 and AlO_4 tetrahedral. The tetrahedral are cross-linked by the sharing of oxygen atoms as shown in Figure 2.2

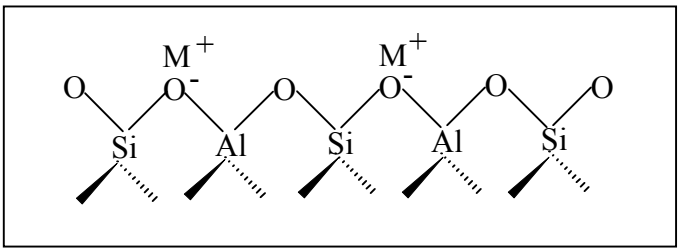

Figure 2.2 The partial structure of zeolites [20].

The AlO_2^- tetrahedral in the structure determines the framework charge. This is balanced by cations that occupy nonframework positions. The general formula for the composition of zeolite is best expressed for the crystallographic unit cell as:

$$M_{x/n}\,[(AlO_2)_x\,(SiO_2)_y].\ w\ H_2O$$

When M is the cation of valence n, generally from the group I or II ions, although other metals, nonmetals, and organic cations (e.g. sodium or ammonium) are also possible, w is the number of water molecules. Water molecules presented are located in the channels and cavities, by surrounding the cations that neutralize the negative charge created by the presence of the AlO_2^- tetrahedral unit in the structure.

2.4.1.1 Zeolite structures

The structure of zeolite consisted of a three-dimension framework of the tetrahedral primary building units when tetrahedral atoms are silicon or aluminum as shown in Figure 2.3.

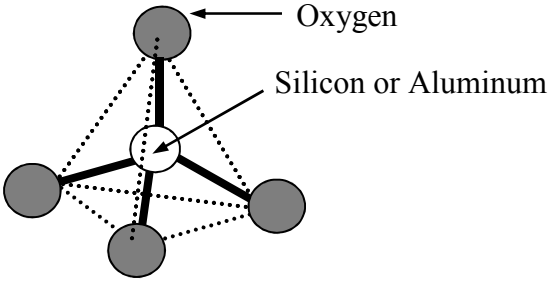

Figure 2.3 A primary building unit of zeolites [20].

Zeolites have a common subunit of structure so called primary building units of $(Al,Si)O_4$ tetrahedral, therein the Si or Al distribution is neglected. A secondary building unit (SBU) consists of selected geometric groupings of those tetrahedral. There are sixteen such building units, which can be used to describe all of the known zeolite structures. The secondary building unit (SBU's) consist of 4, 5, 6 and 8-membered single rings, 4-4, 6-6, and 8-8-member double rings, and 4-1,5-1 and 4-4-1 branched rings. The secondary building units (SBU) are shown in Figure 2.4.

Most zeolite framework can be generated from different SBUs. For example, the sodalite framework can be build from either the single 6-member ring or the single 4-member ring. Some of them are shown in Figure 2.5

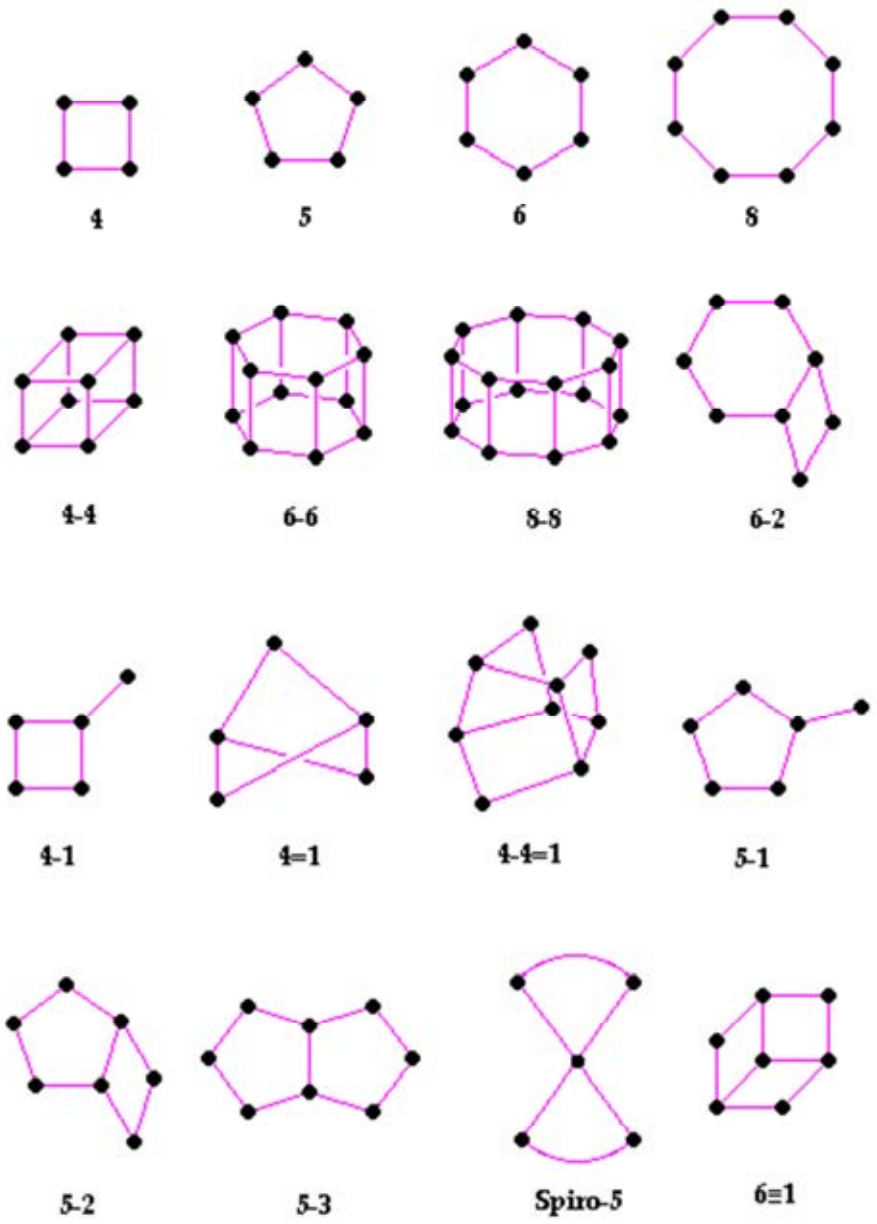

Figure 2.4 Secondary building units (SBUs) in zeolites [21].

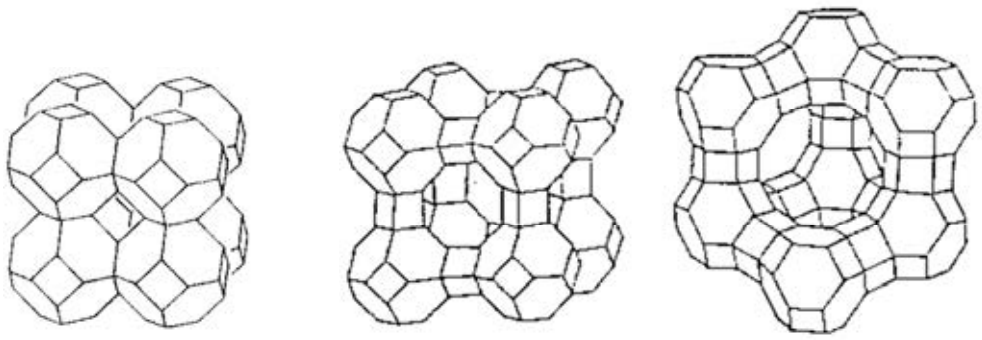

Figure 2.5 The structure of sodalite, zeolite A and faujasite-type zeolites.

The different ring sizes found in zeolites, based on the different number of tetrahedral atoms defining the opening, are shown in Figure 2.6. The ring sizes are often mentioned as the number of oxygen atoms which are equal to the number of tetrahedral atoms.

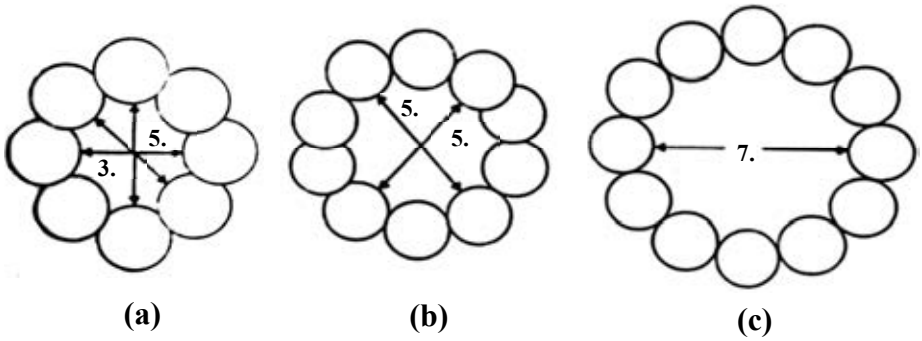

Figure 2.6 Examples of the three types of pore openings in the porous material molecular sieves (a) an 8 ring pore opening (small pore), (b) a 10 ring pore opening (medium pore) and (c) a 12 ring pore opening (large pore) [20].

2.4.1.2 Shape and size selectivity of porous materials

Shape and size selectivity presents a very important role in catalysis. Highly crystalline and regular channel structures are among the principal features that porous material used as catalysts offer over other materials. Shape selectivity is divided into

3 types: reactant shape selectivity, product shape selectivity and transition-state shape selectivity. These types of selectivity are shown in Figure 2.7.

1) Reactant shape selectivity

Reactant shape selectivity refers to the selectivity occurring because of the different sized of the reactants when a mixture of at least two reactants with different sizes is fed into the zeolite molecular dimensions. The larger reactants cannot enter the zeolite pores and reach most of the active sites in the channel. Those banned bulkier reactants may contact external active sites to finish the conversion or leave the zeolite molecular dimensions without being converted to the products.

2) Product shape selectivity

In product shape selectivity, all reactants are so small that they all can enter into the channels of the zeolite where they may form isomers with different sizes inside the channels because the dimensions at the intersections at the intersections are often larger than the pore openings. But only those species that are smaller than pore openings can escape from the channels of the zeolite and join the reaction mixture. The bulkier species are unable to escape from the channel and are excluded from the reaction mixture. The product-shape selectivity model was always used to explain the product distributions in the reaction if toluene alkylation with methanol over zeolite ZSM-5, the slimmer *p*-xylene, the main product, diffuses out of the channel 100-1000 times faster the other bulkier *o*-, and *m*- isomers.

3) Transition state shape selectivity

Transition state shape selectivity is based on the instrinsic shape of the channels in the zeolite, not on the path length. The transition state selectivity depends on neither the reactant nor the product, but the certain reaction mechanism of transition state that occurs in the zeolite crystal size. For example, three are two (parallel or consecutive) reactions. One reaction is going via a bulky transition state or intermediate which cannot be accommodated inside the zeolite pores, thus this reaction is entirely suppressed.

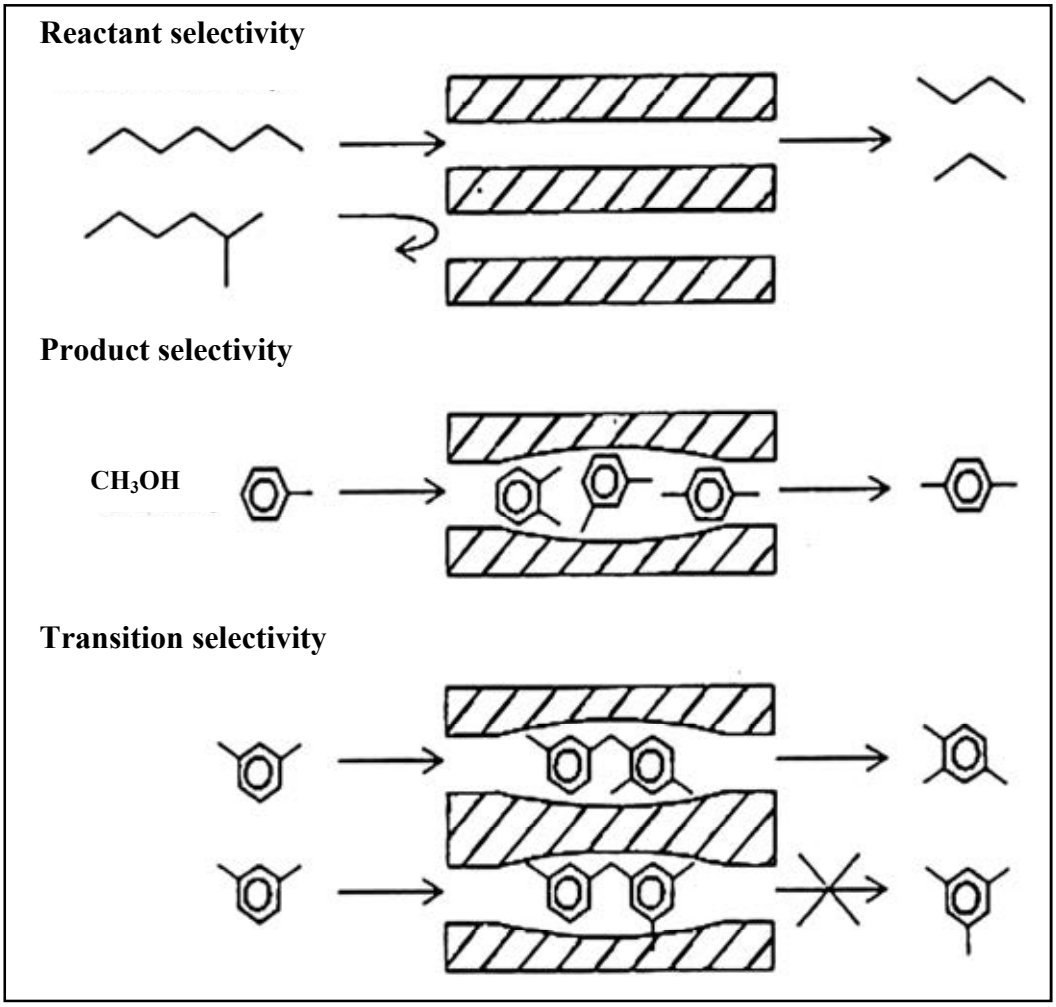

Figure 2.7 Three types of selectivity in porous materials: reactant, product and transition-state shape selectivity [22].

2.4.1.3 Acid sites of zeolites

In addition to the shape and size selective catalysis, the generation of acidic sites in the zeolite pores leads to a high efficiency in solid-acidic catalysis. The isomorphous replacement of silicon atom with aluminum atom in a tetrahedral site gives rise to a charge imbalance because aluminum atom has lower coordination ability than silicon atom and must be neutralized. This is achieved in two ways in natural zeolites:

- The length of Al-O bond becomes slightly longer.
- A coordination site is made profit for cation to counter the excess negative charge.

In natural zeolites, the excess negative charge is balanced by various cations are present in the neighboring environment *e.g.* K^+, Na^+, Mg^{2+} and Ca^{2+} as exhibited in Figure 2.8 and Figure 2.9. The type of counter ion used to balance the charge plays an important part in the use of the zeolite. For uncomplicated understanding, the cation is replaced with a proton by hydrothermal treatment to form a hydroxyl group at the sharing oxygen atom. The acid site formed behaves as a classic Brønsted, proton donating acidic site as shown in Figure 2.10.

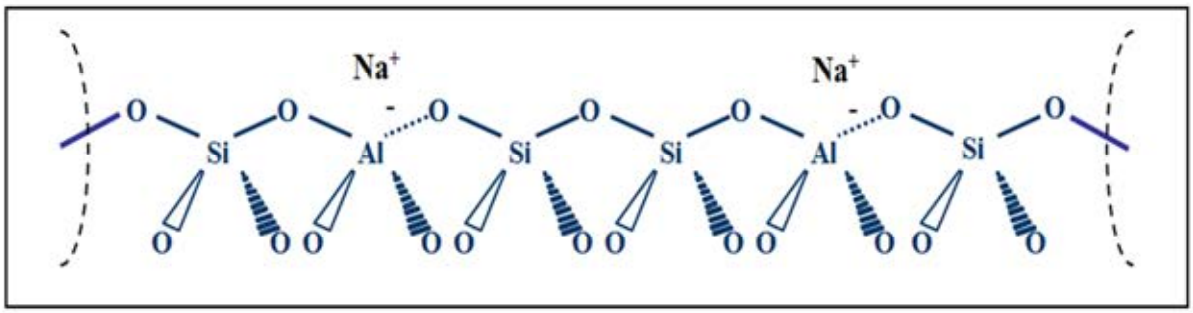

Figure 2.8 Sodium balanced zeolite framework [23].

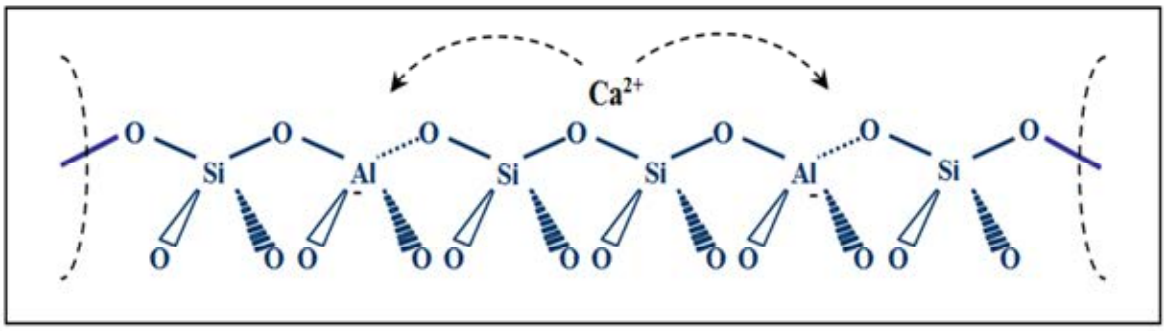

Figure 2.9 Calcium balanced zeolite framework [23].

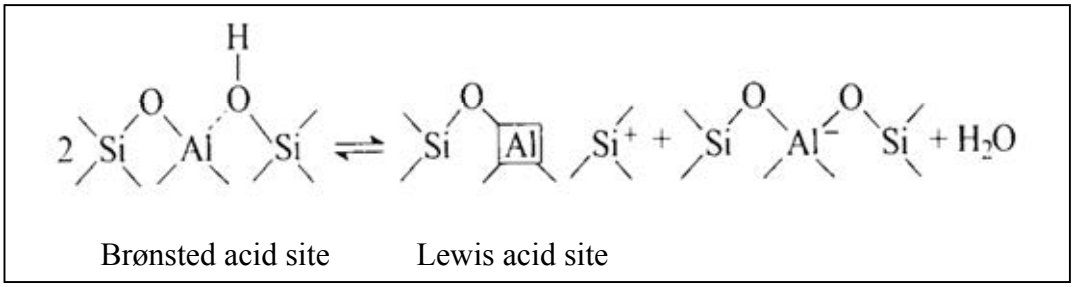

Figure 2.10 Brønsted and Lewis acid sites in zeolites [19].

The highly acidic sites combined with the high selectivity arising from shape selectivity and large internal surface area makes the zeolite as an ideal industrial catalyst. The significance of this acidic proton can be shown easily by comparisons of the experiments in H^+-exchanged zeolites and their equivalent cations from zeolite. For example, the methanol-to-gasoline (MTG) process is highly depended on the presence of the Brønsted proton. If the H-ZSM-5 catalyst is replaced by the purely siliceous analogue of ZSM-5, it has no Brønsted protons; the reaction does not take place at all. Therefore, the modification of zeolite structure could be increased their activity, which are very economically important step for industry.

2.4.2 ZSM-5

The oil company Mobil first synthesized ZSM-5, Zeolite Socony Mobil-Five, in 1972 and its structure code is MFI [22, 24-27]. The tetrahedral units are linked to form the chain-type building block as shown in Figure 2.11. Rings consisted of five oxygen atoms are evident in this structure; the name pentasil is therefore used for describing its structure. ZSM-5 is a medium-pore zeolite having an orthorhombic crystal structure. The pore opening is composed of a 10-member ring. The ZSM-5 framework contains two types of intersection channels: one type is straight, has elliptical (0.51 x 0.58 nm) opening, and run parallel to the b-axis of the orthorhombic unit cell, while the other has near-circular (0.54 x 0.56 nm) opening, is sinusoidal (zigzag) and direction along the a-axis. Figure 2.12 exhibits the structure of ZSM-5 and schematic illustration of three-dimention channels.

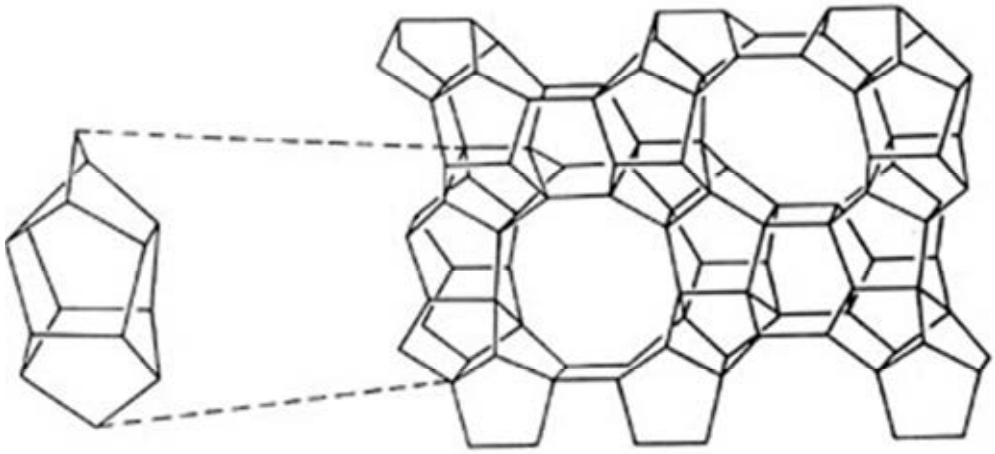

Figure 2.11 The 5-1 secondary building unit (a) to form the chain units (b) found in the ZSM-5 and ZSM-11 structure [22]

Zeolite ZSM-5 is one of the most efficient molecular sieve catalysts in a number of chemical processes. The catalytic activity of ZSM-5 is associated qith different active sites such as Brønsted acid sites, Lewis acid sites, metal ion in cationic positions, transition metal ions in zeolite lattice positions, extra-lattice transition metal compounds in channels and cavities of a zeolite and metal particles in zeolite cavities.

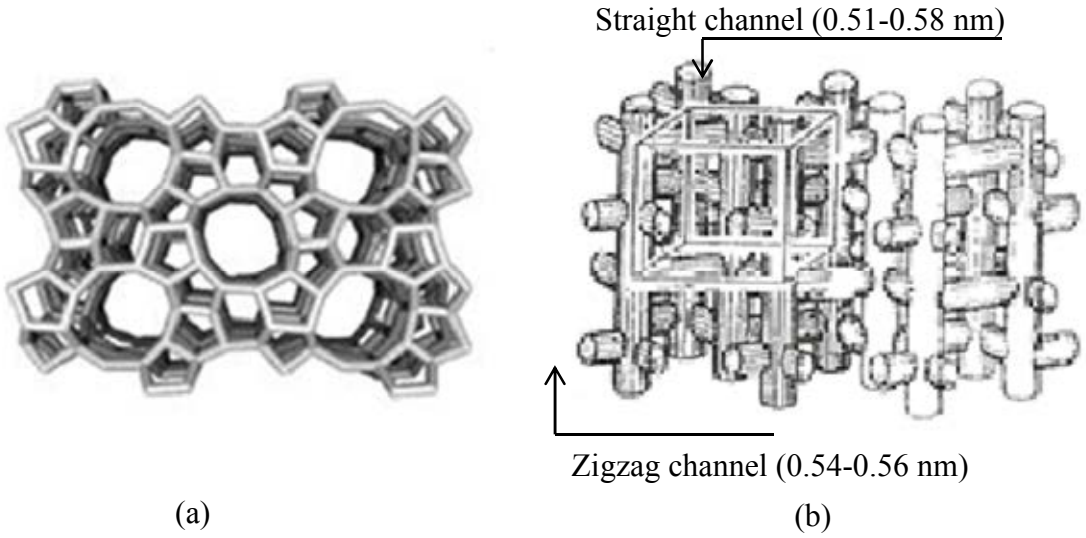

Figure 2.12 (a) Structure of ZSM-5 (MFI). View shows the straight channel. The sinusoidal channels run perpendicular to the straight channels [27]. (b) Schematic illustration of the three-dimensional channels in ZSM-5 [26].

2.4.2.1 Shape selectivity of ZSM-5

The shape selectivity of the zeolite means that both the pore dimension and catalytic sites residing inside the channels are used to control the selectivity of the product. The ZSM-5 is known as molecular sieve, a very important role in zeolite catalyst, since it allows the adsorption molecular of certain dimensions while refuses those of larger dimensions.

The accessibility to the catalytic active sites in ZSM-5 is best viewed by considering its channel system as illustrated in Figure 2.12 (b) [26]. The particular shape-selectivity properties of ZSM-5 result from the conjugation of four different structurally interrelated features:

1) A channel (or pore) opening consisting of a 10-member oxygen ring which is intermediate between that of classical shape-selective zeolites (such as erionite,

ferrierite, gmelinite, and zeolite A) and that of large pore zeolites (such as faujasite, mordenite, and fault-free offretite) as shown in Figure 2.13.

2) The presence of channel intersections (or intersecting elements) which offer a free space of larger dimentions (about 0.9 nm); the latter may play a distinct role in the ordering of simple molecules and could be the site for catalytic activity.

3) The absence of cages along the channel, such cages which ofer a larger available space may be detrimental to catalytic activity, as shown in the case of erionite, being the preferential site for the formation of carbonaceous residues.

4) The occurrence of slightly differentiated channel networks. Aromatic and branched paraffins were indeed fond to preferentially be adsorbed in the linear channels which are elliptical. This may be led to preferential diffusion paths and eventually prevent major counter diffusion effects.

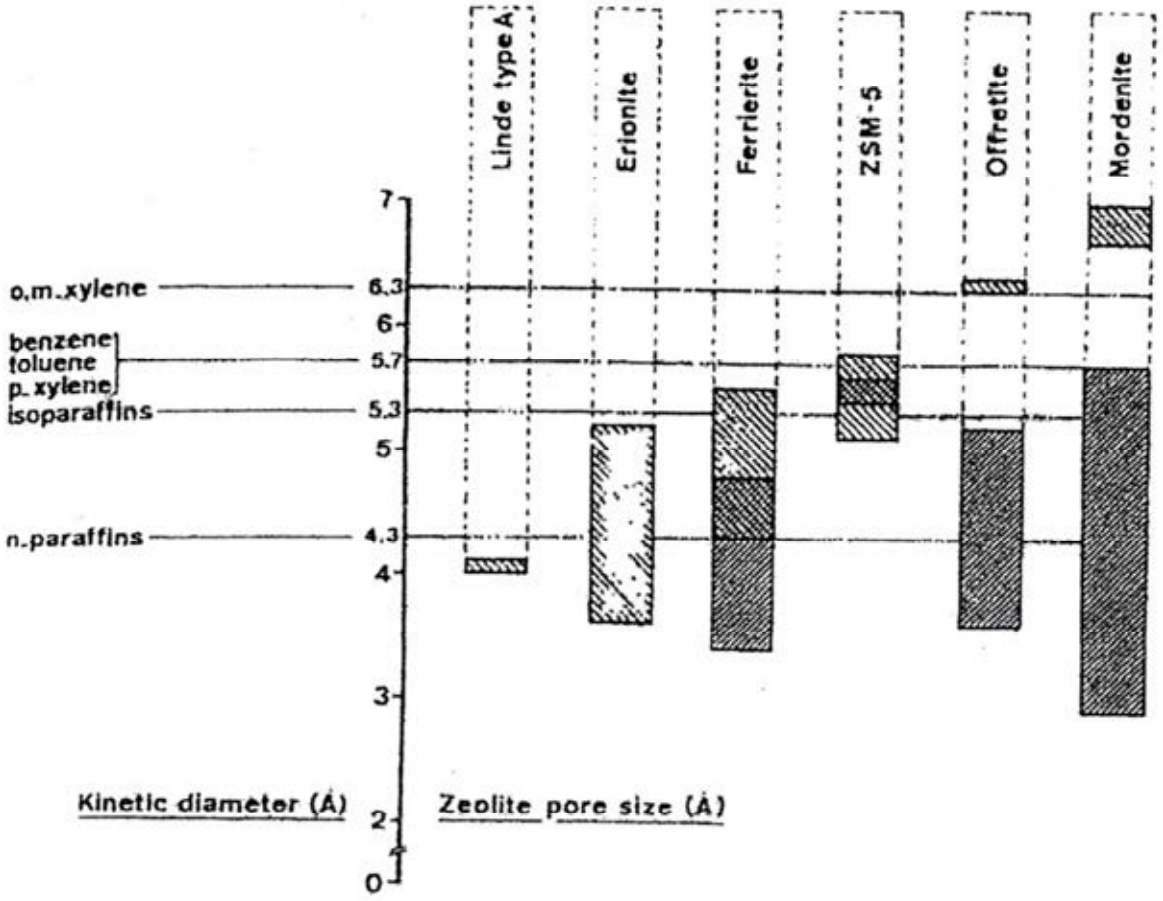

Figure 2.13 Correlation between pore size of various zeolites and kinetic diameter of some molecules [26]

2.4.2.2 Chemical composition of ZSM-5

The chemical formular of a typical unit cell of hydrated Na-ZSM-5 is

$$Na_n[Al_nSi_{96-n}O_{192}.16H_2O],\ n<27.$$

That seem to be a limit on the Al incorporation in the framework. The lowest Si/Al ratio known in the ZSM-5 lattice is 10. ZSM-5 is used in many industrially catalytic processes [27]. The catalytic activity of the material is inextricably linked to its composition and structure.

2.4.3 The templating process

For long time, more than 40 years, the templateing process has been taken as the process responsible for the production of zeolites and molecular sieves. It was not until 1994 that Burkett and Davis [28] showed that the formation of molecular sieves depended heavily on the bonding of amines or quaternary ammonium ions first to water and then to small silicate species, as shown in Figure 2.14.

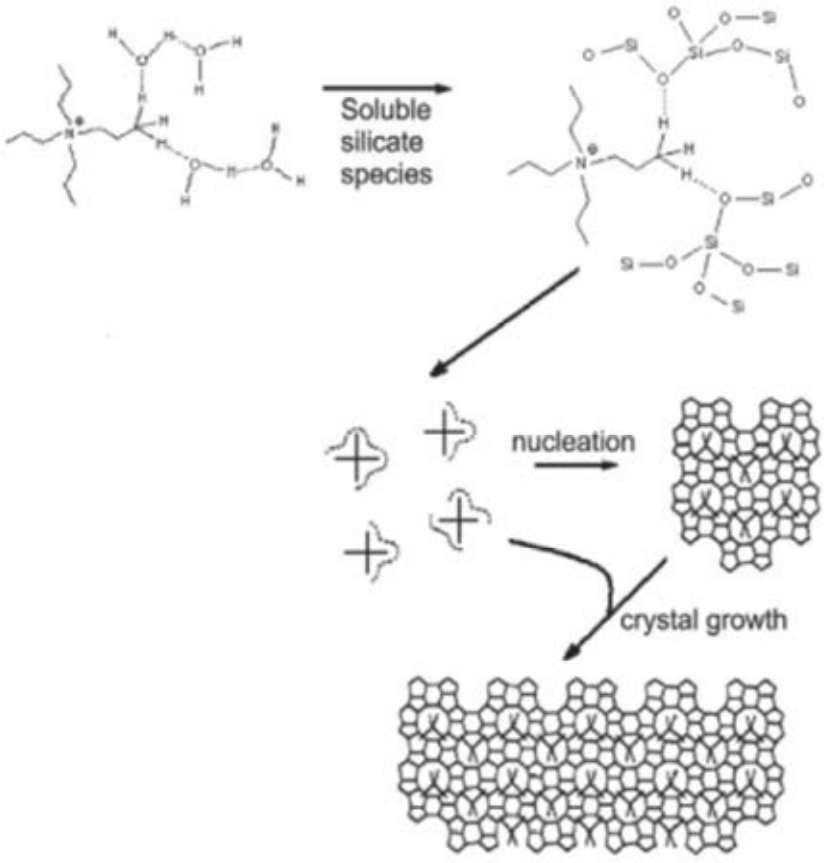

Figure 2.14 The formation of zeolite ZSM-5 according to the idea by which it is the interaction of organics ion and silicate.

In the aqueous solution of quaternary ammonium ions, tetrapropyl ammonium in this case, water molecules are associated with the ions through van de Waals interaction. The addition of silicate species causes the displacement of water and establishes a network of properly organized silicate species, in a high pH solution, that are spatially organized and ready to condense, forming the first nucleus which, and upon further condensation, leads to the formation of the zeolite framework. Therefore, short distance interaction is the major component in the direct synthesis of molecular sieves in general, the structure directing agent has not only the role of filling the voids of the porous structure but also the function of interesting with the framework and stabilizing it, most of the time aided by water and other ions [29].

2.5 Mesoporous materials

Mesoporous materials are a type of molecular sieve, such as silicas or transitional aluminas or modified layered materials such as pillared clays and silicates. Mesoporous silica has uniform pore sizes from 20 to 500 Å and has found great utility as catalysts and sorption media because of the regular arrays of uniform channels. Larger surface area is desired for enhancing of the efficient in the reactions [28].

2.5.1 Classification of mesoporous materials

Mesoporous materials can be classified by different synthetic methods. By varying different types of templates used and pH of gel, synthesizing hexagonal mesoporous materials can be obtained. The interaction of various types of template with inorganic species for assembling these materials are different as summarized in Table 2.3, together with the condition typically employed for a synthesis [28-30].

Table 2.3 Various synthesis conditions of hexagonal mesoporous materials and the types of interaction between templates and inorganic species

Materials	Template	Assembly	Solution
MCM-41	Quaternary ammonium salt	Electrostatic	base or acid
FSM-16	Quaternary ammonium salt	Electrostatic	base
SBA-15	Amphiphilic triblock copolymer	H- bonding	acid (pH<2)
HMS	Primary amine	H- bonding	neutral

MCM-41 and FSM-16 can be synthesized using quaternary ammonium salt as a template. In case of SBA-15, amphiphilic tribock copolymer can be modified as a template and must be synthesized in acidic condition of hydrochloric acid. On the other hand, HMS can be prepared in neutral and environmentally benign condition using primary amine as a template. Although these materials have the same hexagonal structure, some properties are different as shown in Table 2.4.

Table 2.4 Properties of some hexagonal mesopore materials

Material	Pore size (Å)	Wall thickness (nm)	BET specific surface area (m^2/g)	Framework structure
MCM-41	15-100	1	>1000	Honey comb
FSM-16	15-32	-	680-1000	Folded sheet
SBA-15	46-300	3-6	630-1000	Rope-like
HMS	29-41	1-2	640-1000	Wormhole

2.5.2 Synthesis strategies of mesoporous materials

Crystalline molecular sieves are generally obtained by hydrothermal crystallization. The reaction gel, usually, contains cations (*e.g.* Si^{4+} for silicate materials, Al^{3+} for aluminate materials) to form the framework; anionic species (*e.g.* OH^- and F^-); organic template and solvent (generally water). Typically, the nature of template can be considered into two parts that are hydrophobic tail on the alkyl chain side and hydrophilic head on the other side. The examples of templates used are primary, secondary tertiary and quaternary amines, alcohols, crown or linear ethers, and as well as polymers. An understanding of how organic molecules interact with each other and with the inorganic frameworks would increase the ability to design rational routes to molecular sieve materials. The organic templates are frequently occluded in the pores of the synthesized material, contributing to the stability of mineral backbone.

2.5.2.1 The behavior of surfactant molecules in an aqueous solution

In a simple binary system of water-surfactant, surfactant molecules can aggregate to form micelles in various types at a particular concentration. The shapes of micelle depend on the concentrations as shown in Figure 2.11.

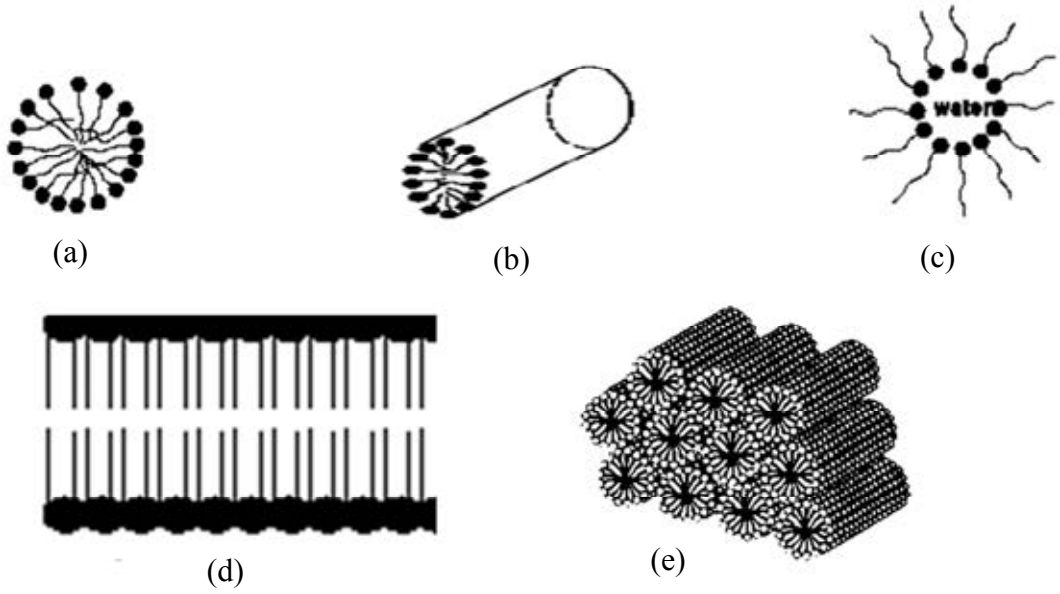

Figure 2.15 Phase sequence of the surfactant-water binary system (a) spherical micelle, (b) rod-shaped micelle, (c) reverse micelle, (d) lamellar phase, and (e) hexagonal phase [31].

At low concentration, they energetically exist as isolated molecules. With increasing concentration, surfactant molecules aggregate together to form isotropic spherical and rod shaped micelles by directing the hydrophobic tails inside and turning the hydrophilic heads outside in order to decrease the system entropy. The initial concentration threshold at which those molecules aggregate to form isotropic micelle is called critical micelle concentration (CMC). The CMC determines thermodynamic stability of the micelles. When the concentration is continuously increased, the micellar shape changes from sphere or rod shapes to hexagonal, lamellar, and inverse micelles. The particular phase present in a surfactant aqueous solution depends not only on the concentrations but also on the natural of surfactant molecules such as its length of the hydrophobic carbon chain, hydrophilic head group, and counter ion. Besides the ionic strength, pH value, and temperature including other additives are the factors determining the shape of micelles.

2.5.2.2 Interaction between inorganic species and surfactant micelles

A number of models have been proposed to explain the formation of mesoporous materials and to provide a rational basis for synthesis routes [18]. On the common level, these models are predicted upon the presence of surfactants in a solution to direct the formation of inorganic mesostructure from stabilized inorganic precursors. The type of interaction between the surfactant and the inorganic species is significantly different

depending on the various synthesis routes as shown in Table 2.5

Table 2.5 Example routes for interactions between the surfactant and the inorganic soluble species

Surfactant type	Inorganic type	Interaction type	Example materials
Cationic (S^+)	I^-	S^+I^-	MCM-41, MCM-48
	I^+X^-	$S^+X^-I^+$	SBA-1, SBA-2, zinc phosphate
	I^0F^-	$S^+F^-I^0$	silica
Anionic (S^-)	I^+	S^-I^+	Al, Mg, Mn, Ga
	I^-M^+	$S^-M^+ I^-$	alumina, zinc oxide
Neutral S^0 or N^0	I^0	S^0I^0 or N^0I^0	HMS, MSU-X, aluminum oxide
	I^+X^-	$S^0X^-I^+$	SBA-15

Where S^x or N^x : surfactant with charge of X

I^x : inorganic species with charge of X

X^- : halogenide anions

F^- : fluoride anion

M^{n+} : with charge of X

Using ionic surfactant (S^+ and S^-), the hydrophilic head mainly binds with inorganic species through electrostatic interactions. There are two possible formation routes. Firstly, direct pathway: surfactant and inorganic species of which charges are opposite interact together directly (S^+I^- and S^-I^+). Another is the indirect pathway, occurring when the charges of surfactant and inorganic species are the same, so the counter ions in solution get involved as charge compensating species for example the $S^+X^-I^+$ path takes place under acidic conditions, in the present of halogenide anions ($X^- = Cl^-$ or Br^-) and the $S^-M^+ I^-$ route is the characteristic of basic media, in the existence of alkaline cation ($M^+ = Na^+$ or K^+). Figure 2.15 shows the possible hybrid inorganic-organic interfaces.

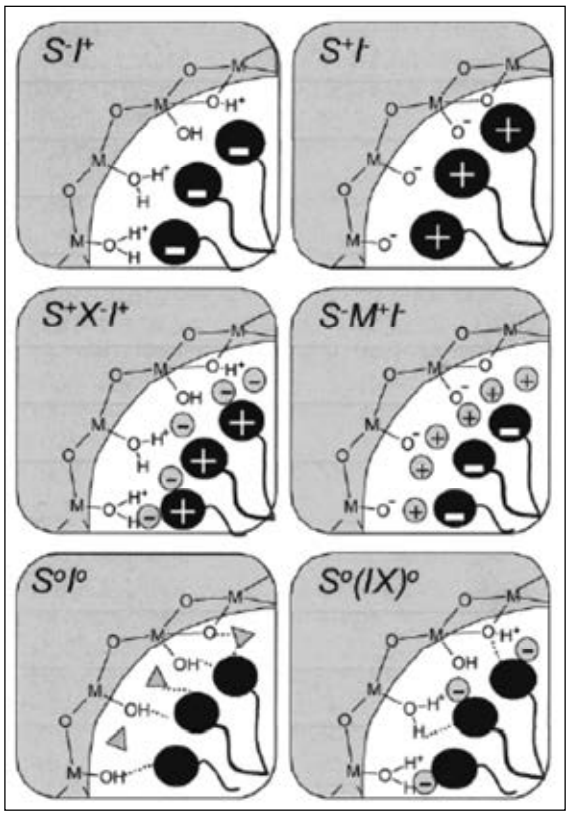

Figure 2.16 Schematic representation of the different types of silica-surfactant interfaces. Dashed line corresponded to H-bonding interactions [32].

In case of non-ionic surfactant (S^0 or N^0), the main interaction between template and inorganic species is hydrogen bonding or dipolar, which is called neutral path i.e. S^0I^0 and $S^0F^-I^+$. Nowadays, non-ionic surfactants give important commercial advantages in comparison to ionic surfactants because they are easily removable, nontoxic, biodegradable and relatively cheap.

2.5.2.3 Formation mechanism of mesoporous materials

Mechanism of mesoporous formation can be classified on the basis of synthetic route into three types exhibited in Figure 2.16:

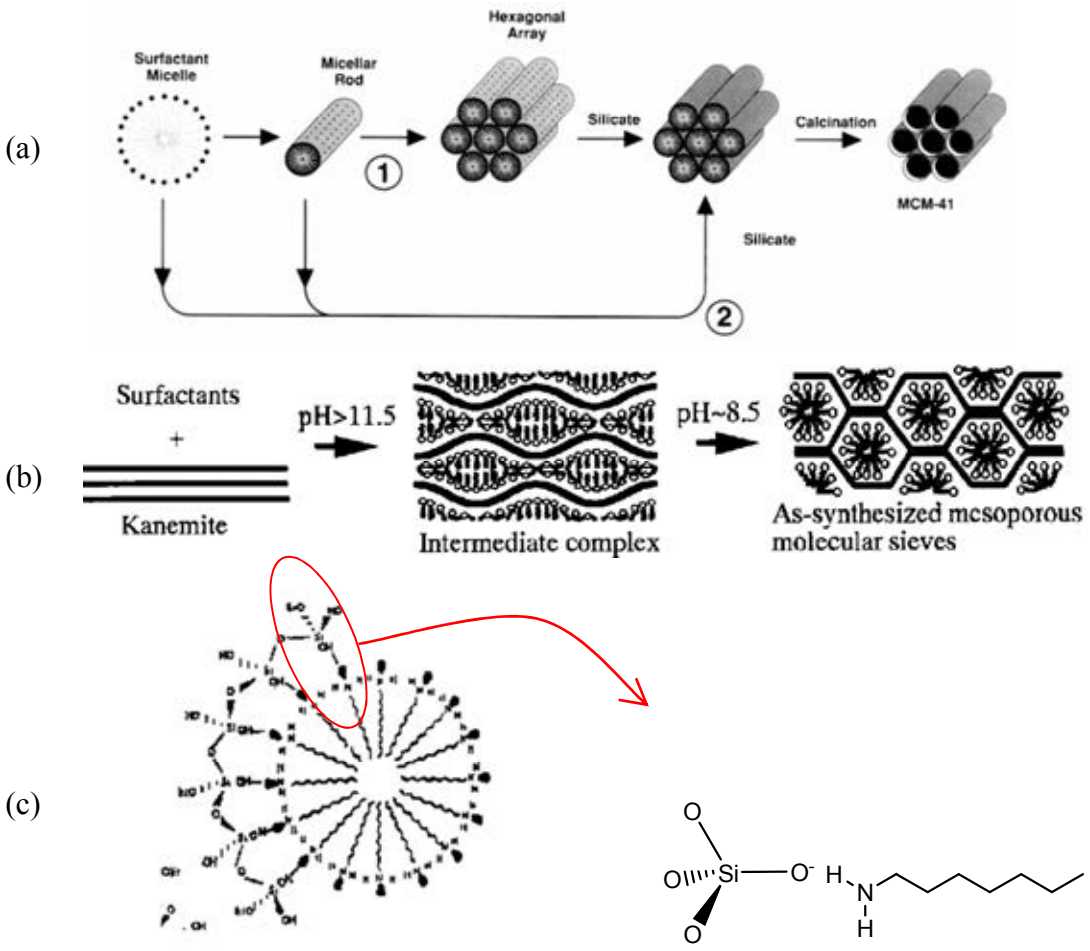

Figure 2.17 Mechanism of mesoporous formation (a) LCT of MCM-41 formation, (b) Folding sheet formation of FSM-16 and (c) H-bonding interaction in HMS formation [31-32]

(a) Liquid crystal Templating mechanism *i.e.* MCM-41. From Figure 2.12(a) there are two main pathways; firstly, liquid crystal phase is intact before silicate species are added or another pathway is the addition of the silicate results in the ordering of the subsequent silicate-encased surfactant micelles.

(b) Folding sheet formation *i.e.* FSM-16. The intercalation of ammonium surfactant into hydrate sodium silicate, which composes of single layered silica sheets called "kanemite" (ideal composition $NaHSi_2O_5.3H_2O$), produces the lamellar-to-hexagonal phase in FSM-16. After the surfactants are ion exchanged into layered structure, the silicate sheets are thought to fold around the surfactants and condense into a hexagonal structure.

(c) Hydrogen-bonding interaction The neutral templating produces mesoporous materials with thicker walls and higher thermal stability as compared to the LCT-derived silicates.

2.5.3 Synthesis strategy of mesoporous material using block-copolymer as structure directing agent

In the synthesis of mesoporous materials such as MCM-41, FSM-16 ionic surfactant *i.e.* the cationic, alkyltrimethyl ammonium (C_nTA^+, $8<n<18$), and anionic surfactant, tertiary amine ($C_nH_{2n+1}N^+(CH_3)_3$) are used as template, respectively. These syntheses are done in extreme (alkaline) pH condition and the obtained materials have pore size in the range of 15 to 100 Å only. However, by this mean, two limitations occur:

(1) The lower stability of the obtained materials: due to the thinner pore wall of materials (8-13 Å).

(2) Difficult to expanding the pore size: the ionic surfactants give a limited pore size. The only way to expand the pore size is in employing swelling agents such as 1,3,5-trimethyl benzene, involving complicate synthesis.

Thus, the block copolymer has been used to solve these problems. Generally, amphiphilic block copolymer has been used in the field of surfactants, detergent manufacturing, emulsifying, coating, etc. The properties of block copolymer can be continuously tuned by adjusting solvent composition, molecular weight, or type of polymers. Figure 2.17 shows typical block copolymer used as templates.

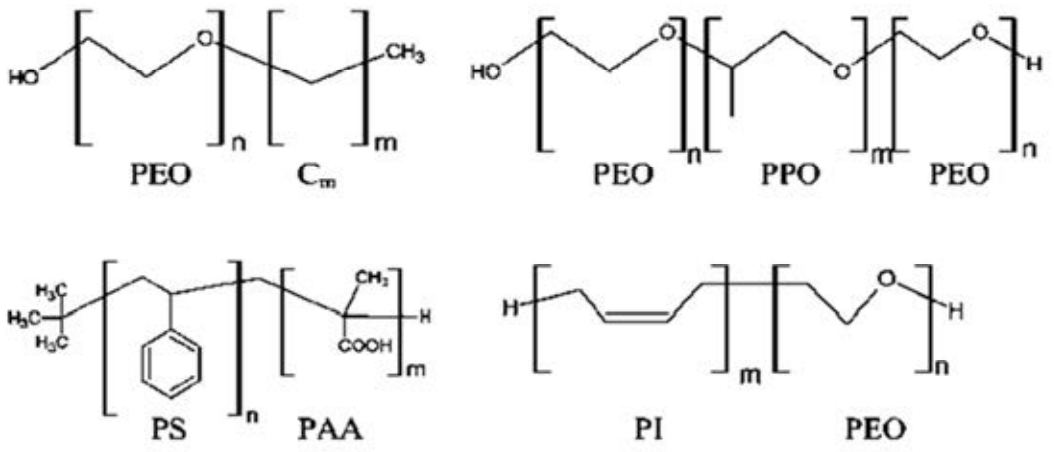

Figure 2.18 Block copolymer used in mesostructured generation [33].

Some advantages of using these block copolymer are:

(1) The thicker wall thickness (about 15-40 Å), enhancing hydrothermal and thermal stability of materials.

(2) Pore diameter can be tuned easier by varying type or concentration of polymer.

(3) Easier to remove from mineral framework by thermal treatment or solvent extraction. Due to the hydrogen bonding interaction between template and inorganic framework, therefore, it should be easier to dissociate as compared to ionic templates (electrostatic interaction).

Interaction between block copolymer template and inorganic species, calls hybrid interphase (HI), is particularly important, especially in PEO-PPO based one. Different possible interactions take place at the HI are schematized in Figure 2.11. Most of the fine HI characterization has been performed on PEO-based (di or triblock) templates. Melosh *et al*. [33] determined that in F127-templated silica monoliths, organization arose for polymer weight fractions higher than 40%. For lower polymericsilica ratios, non-ordered gels were formed. This lack of order was due to a relatively strong interaction (probably of H-bonding type) of the (Si–O–Si) polymers forming the inorganic skeleton with both PEO and PPO blocks.

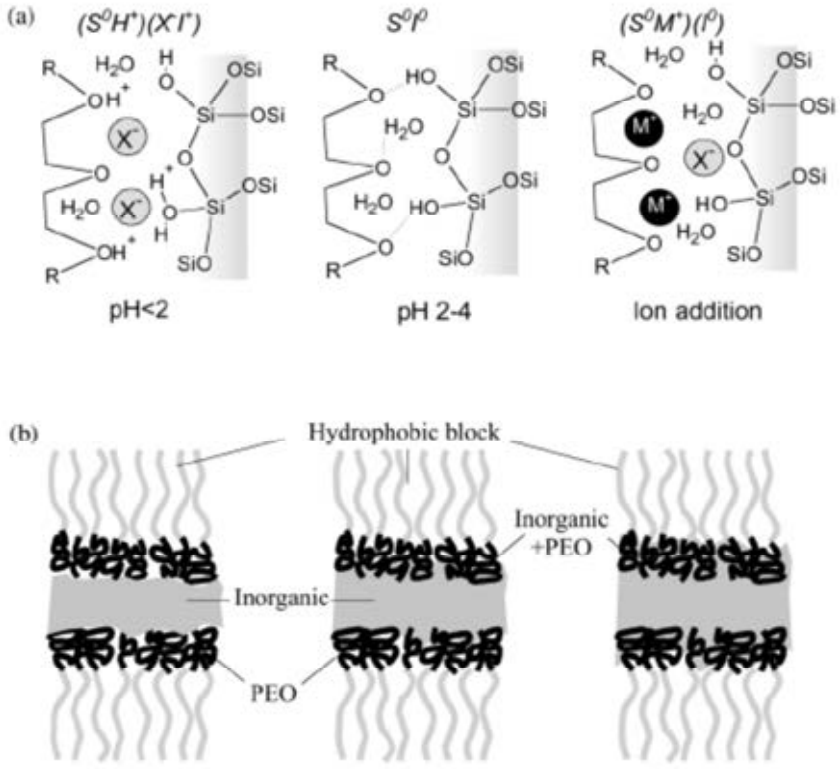

Figure 2.19 (a) Schematic view of the $(S^0H^+)(X^-I^+)$, S^0I^0, and $(S^0M^+)(X^-I^0)$ hybrid interphases (HIs) (b) Three possible structures of a HI composed by a nonionic polymer and an inorganic framework [34].

2.6 SBA-15

2.6.1 Structure and properties of SBA-15

SBA-15 mesoporous material has been synthesized under acidic condition using triblock copolymer as a structure directing agent. This mesoporous material has shown higher hydrothermal stability as compared to MCM-41 due to its thicker pore walls (3.1-6.4 nm). They also posses uniform and hexagonal-structured channel similar to MCM-41 with larger pore size which make them more desirable to deal with bulky molecule. Some properties of MCM-41 and SBA-15 are compared as described in Table 2.6. According to the properties listed in Table 2.6, SBA-15 shows a better performance than MCM-41 in almost of properties.

Table 2.6 Comparison of two well-known mesoporous materials, MCM-41 and SBA-15 in their characteristic properties [31, 35]

Properties	MCM-41	SBA-15
Pore size (Å)	20-100	46-300
Pore volume (mL/g)	>0.7	0.8-1.23
Surface area (m^2/g)	>1000	690-1040
Wall thickness (Å)	10-15	31-64

2.6.2 Synthesis of SBA-15 and formation mechanism

For SBA-15 materials, aging time and temperature are particularly important. Some research found that mesoporous SBA-15 prepared from calcination of an 'as-prepared' hybrid precursor contained a significant fraction of microporosity; further aging of the precursor in the mother liquors leads to an improvement on the pore size distribution (Figure 2.12), in agreement with the first work by Stucky *et al*. [35].

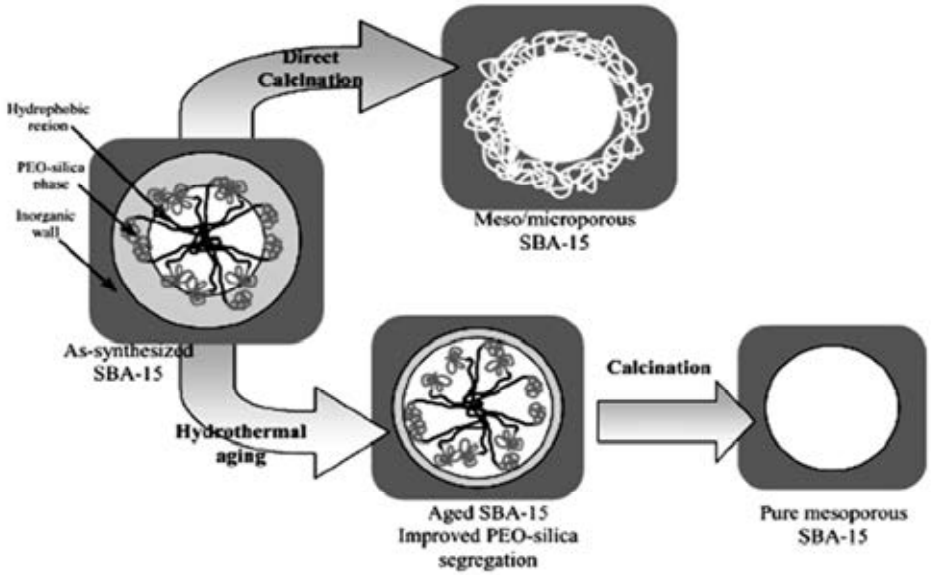

Figure 2.20 Pore evolution upon thermal treatment, depending on pre-treatment and aging [33].

Aging of an as-prepared precipitate at 80–100°C seems to help segregation of the PEO blocks and the inorganic framework, by promoting condensation of the latter. High temperatures also change the polymer behavior. It is known that for T >60°C, PEO blocks become less hydrophilic and expel water similar to PPO blocks when the temperature is higher than 40°C [30]. For a mechanism, firstly alkoxysilane species (TMOS or TEOS) are hydrolyzed as:

$$Si(OEt)_4 + nH_3O^{+} \xrightarrow[pH<2]{\text{hydrolysis}} Si(OEt)_{4-n}(H_2O^{+})_n + n\ EtOH$$

This is followed by partial oligomerization at the silica. Furthermore, at this condition, the PEO parts of surfactant associate with hydronium ions as followed:

$$-PEO_m- + yHX \xrightarrow{H_2O} -PEO_{m-y}[(EO)\cdot 3H_2O^{+}]_y\ ---X_y^{-}$$

Next, coordination sphere expansion around the silicon atom by anion coordination of the form $X^{-}SiO_2^{+}$ may play an important role. The hydrophilic PEO blocks are expected to interact with the protonated silica and thus be closely associated with the inorganic wall. During the hydrolysis and condensation of the silica species, intermediate mesophase is sometimes observed and further condensation of silica species and organization of the surfactant and inorganic species result in the formation of the lowest energy silica-surfactant mesophase structure allowed by solidifying network.

2.7 **Step in a heterogeneous catalytic reaction** [36]

In heterogeneous catalysis, the catalytic action involves the adsorption of reactant molecules on active sites on the surface of the solid catalysts; therefore, the transport of those molecules from the fluid phase to the surface, where the catalytic reaction effectively occurs, must be considered in the general mechanism. Similarly, the molecules of the reaction products are eventually desorbed and transferred in the opposite direction from inside the solid pores to the fluid phase.

Hougen and Watson and others have broken down the steps that occur on a molecular scale in the following manner.

1. Mass transfer of reactants from the main body of the fluid to the gross exterior surface of the catalyst particle.
2. Molecular diffusion and/or Knudsen flow of reactants from the exterior surface of the catalyst particle into the interior pore structure.

3. Chemisorptions of at least one of the reactants on the catalyst surface.
4. Reaction on the surface.
5. Desorption of (chemically) adsorbed species from the surface of the catalyst.
6. Transfer of products from the interior catalyst pores to the gross external surface of the catalyst by ordinary molecular diffusion and/or Knudsen diffusion.
7. Mass transfer of products from the exterior surface of the particle into particle into the bulk of the fluid.

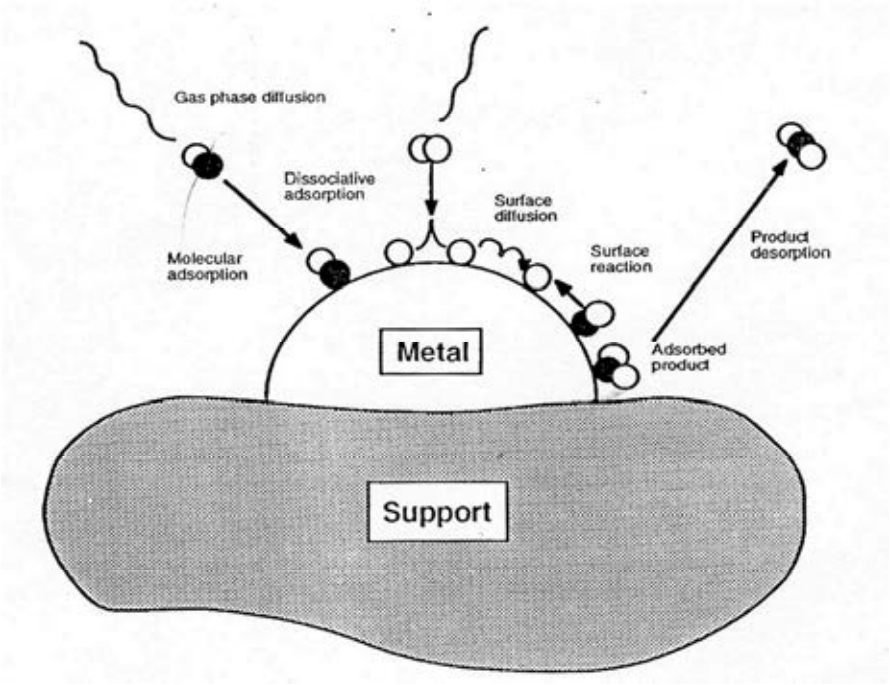

Figure 2.21 Steps in heterogenous catalysis [37].

Several of these steps are shown in Figure 2.13. Of course, if the catalyst is nonporous, steps 2 and 6 are absent. Steps 1, 2, 6, and 7 are obviously physical processes, while steps 3 to 5 are basically chemical in character. The rates of the various steps depend on a number of factors in addition to the concentration profiles of the reactant and product species.

Steps 1 and 7 are highly dependent on the fluid flow characteristics of the system. The mass velocity of the fluid steam, the particle size, and the diffusional characteristics of the various molecular species are the pertinent parameters on which the rates of these steps depend. These steps limit the observed rate only when the catalytic reaction is very rapid and the mass transfer is slow. Anything that tends to increase mass transfer coefficients will enhance the rates of these processes. Since the rate of these steps are only slightly influenced

by temperature, the influence of these processes on the overall conversion rate will vary as the temperature changes. Their influence is often negligible at low temperatures, but may be quite significant at higher temperatures.

2.8 Modification of catalysts

2.8.1 Incorporation of aluminum into SBA-15

Among the metal-substituted mesoporous materials, aluminum-incorporated mesoporius materials have great potentials in moderating acid-catalyzed reactions for large milecules. However, it is very difficult to introduce the metal ions directly in to SBA-15 due to the easy dissociation of metal-O-Si bonds under strong acidic conditions.

To date, only a few studies on the direct synthesis of Al-SBA-15 have been reported [37-39]. The comparison of direct and post syntheses of Al-SBA-15 is described in Table 2.7.

Table 2.7 Comparison of direct synthesis and post synthesis methods of Al-SBA-15 [37-41]

	Direct synthesis method	**Direct synthesis method**
Synthesis condition	Require complicated procedure	Simple method
Aluminum form in materials	Most of samples have both tetrahedral and octahedral aluminum	Most of samples have only tetrahedral aluminum
Catalyst activity	Lower activity due to extra-framework aluminum	Higher activity due to aluminum in framework

The direct synthesis of Al-SBA-15 is difficult and often not stoichiometric. From this viewpoint, therefore the development of a simple post synthesis method for the alumination of the mesoporous silicas that are synthesized under strongly acidic conditions becomes an appealing alternate choice.

Nowadays, several post synthesis method where aluminum was grafted onto the mesoporous wall with various aluminum source such as $Al(CH_3)_3$, $AlCl_3$ have been

developed without the mesoporous structure seriously destroyed [40]. In the case of zeolites, the introduction of Al into their framework will lead to the formation of bridging hydroxyl group(Brønsted acid sites). However, whether the similar situation occurs in mesoporous materials still keeps agument. Some researchers assigned the hydroxyl vibration at about 3606 cm^{-1} in IR spectrum to the acidic bridging hydroxyl groups, while others disagreed with the assignment. For example, Trombetta *et al.* [41] argued that the Brønsted acid sites in mesoporous materials or aluminosilicates resulted from terminal silanol groups in the vicinity of aluminum atoms. After the adsorption of a basic probe, such as pivalonitrile, the terminal silanol groups were induced to from the bridging hydroxyl groups (SiOHAl, shown in Figure 2.21)

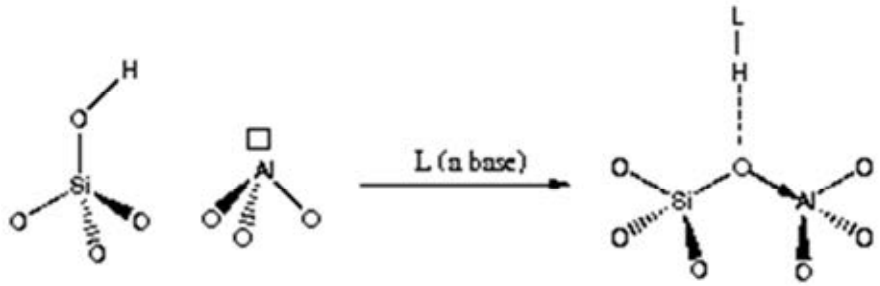

Figure 2.22 Alumination of mesoporous material using basic probe (L) inducing to form the bridging hydroxyl group [42].

2.8.2 **Impregnation** [43-44]

Supported metal catalysts may be prepared by three distinct methods (i) deposition, (ii) co-precipitation, and (iii) impregnation. All of these, the last mentioned is the most important. It consists of soaking the carrier with a solution of a suitable metal salt, followed by evaporation to dryness. The supported salt is then either reduced or, in certain case, calcined in air to convert the salt to the oxide which is then reduced to the metal. The main functions of carrier are to provide a structural framework for the catalytic component and increase the surface area per unit weight of metal. Other desirable effects may include such factors as increase stability due to small crystallites of metal being sufficiently separated to prevent sintering and a greater resistance to poisoning. The choice of carrier depends to a large extent upon the purpose for which the catalyst is required.

Properties of Al-SBA-15 material modified by the wet impregnation of metal such as nickel and ruthenium, the active metal precursor is dissolved in an aqueous solution.

Then the metal-containing solution is add to Al-SBA-15 in the same volume (10 wt.% of Al-SBA-15). Capillary action draws the solution into the pores. Then, the catalyst can be dried and calcined to drive off the volatile components within the solution, deposition the metal on the catalyst surface.

2.9 Characterization of materials

2.9.1 X-ray powder diffraction (XRD)

X-ray powder diffraction (XRD) is an instrumental technique used for identification of minerals, as well as other crystalline materials. XRD is a technique in which a collimated beams of nearly monochromatic. X-rays is directed onto the flat surface of a relatively thin layer of finely ground material. XRD can provide additional information beyond basic identification. If the sample is a mixture, XRD data can be analyzed to determine the proportion of the different minerals present. Other obtained information can include the degree of crystallinity of the minerals present, possible deviations of the minerals from their ideal compositions, the structural state of the minerals and the degree of hydration for minerals that contain water in their structure.

XRD is a reliable technique that can be used to identify mesoporous structure. Typically, the XRD pattern of hexagonal symmetry shows five well-resolved peaks corresponding to lattice planes of Miller indices (100), (110), (200), (210), and (300) [45]. These XRD peaks appear at low angle (2θ angle between 0.5 and 3 degree) because the materials are not crystalline at atomic level, diffraction at higher angles are not observed.

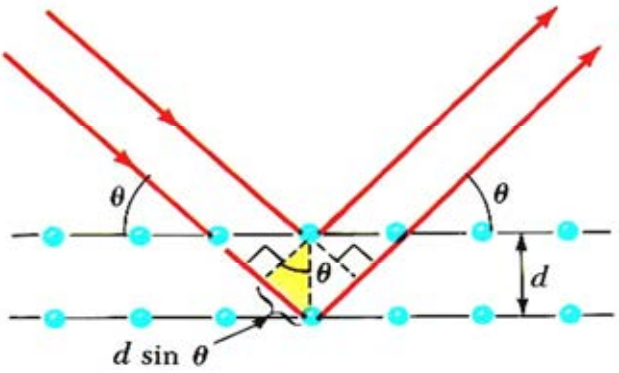

Figure 2.23 Diffraction of X-ray by regular planes of atoms [46].

Figure 2.22 shows a monochromatic beam of X-ray incident on the surface of crystal at an angle θ. The scattered intensity can be measured as a function of scattering angle 2θ. The resulting XRD pattern efficiently determines the different phases present in the sample. Using this method, Braggs' law is able to determine the interplanar spacing of the samples, from diffraction peak according to Bragg's angle.

$$n\lambda = 2\,d\sin\theta$$

Where the integer *n* is the order of the diffracted beam, λ is the wavelength; *d* is the distance between adjacent planes of the crystal (the *d*-spacings) and θ is the angle between the incident beam and these planes.

2.9.2 Nitrogen adsorption-desorption technique

The N_2 adsorption-desorption technique is used to classify the porous materials and its physical properties such as surface area, pore volume, pore diameter and pore-size distribution of solid catalysts. Adsorption of gas by a porous material is described by an adsorption isotherm, the amount of adsorbed gas by the material at a fixed temperature as a function of pressure. Porous materials are frequently characterized in terms of pore sizes derived from gas sorption data [47-48]. The IUPAC classification of adsorption isotherms is illustrated in Figure 2.23

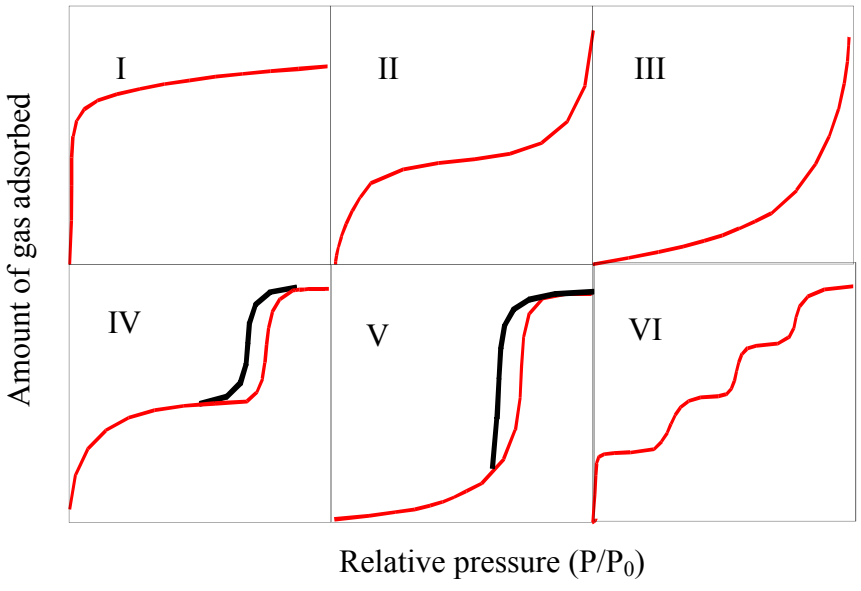

Figure 2.24 The IUPAC classification of adsorption isotherm [47].

As shown in Table 2.8, adsorption isotherms base on the strength of the interaction between the sample surface and adsorptive. Pore size distribution is measured by the use of nitrogen adsorption/desorption isotherm at liquid nitrogen temperature and relative pressures (P/P_o) ranging from 0.05-0.1. The large uptake of nitrogen at low P/P_o indicates filling of the micropores (<20 Å) in the adsorbent. The linear portion of the curve represents multilayer adsorption of nitrogen on the surface of the sample, and the concave upward portion of the curve represents filling of mesoporous and macropores. The multipoint Brunauer, Emmett and Teller (BET) method is commonly used to measure total surface area.

$$\frac{1}{W[(P_o/P)-1]} = \frac{1}{W_m C} + \frac{C-1}{W_m C}(P/P_o)$$

Where W is the weight of nitrogen adsorbed at a given P/P_o, W_m is the weight of gas to give monolayer coverage, and C is a constant that is related to the heat of adsorption. A slope and intercept are used to determine the quantity of nitrogen adsorbed in the monolayer and calculate the surface area. For a single point method, the intercept is taken as zero or a small positive value, and the slope from the BET plot is used to calculate the surface area. The surface area depends upon the method used, as well as the partial pressures at which the data are collected.

Table 2.8 Features of adsorption isotherms

Type	**Interaction between sample surface and gas adsorbate**	**Porosity**	**Example of sample-adsorbate**
I	relatively strong	Micropores	activated carbon-N_2
II	relatively strong	Nonporous	oxide-N_2
III	weak	Nonporous	carbon-water vapor
IV	relatively strong	Mesopore	silica-N_2
V	weak	Micropores	
		Mesopore	activated carbon-water vapor
VI	relatively strong sample surface has an even distribution of energy	Nonporous	graphite-Kr

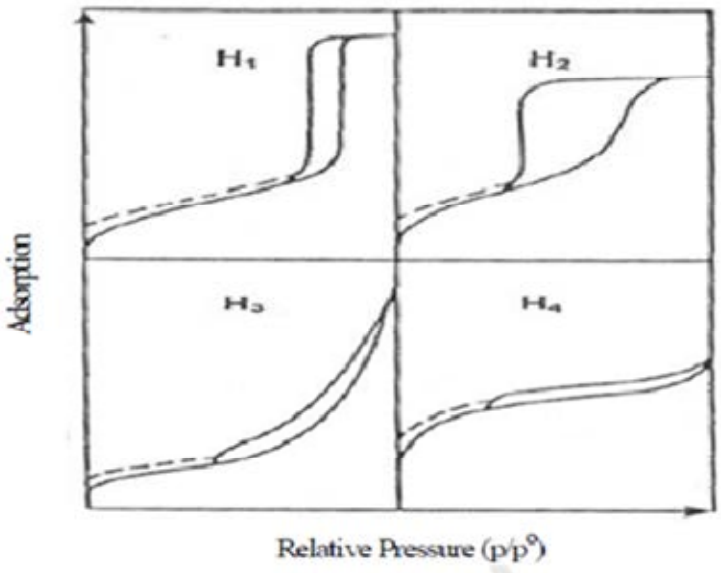

Figure 2.25 IUPAC classification of hysteresis loop.

1. Type H_1: the hysteresis loop associated with pores consisting of agglomerates or compacts of uniform spherical particles with regular array, whose pore size distribution are normally narrow.

2. Type H_2: the hysteresis loop associated with pores with ink-bottle shapes or more complicated net work structures.

3. Type H_3: the hysteresis loop associated with slit-shaped pores formed from aggregrates of plate-like particles.

4. Type H_4: the hysteresis loop associated slit-shaped pores with narrower sizes.

2.9.3 Scanning electron microscope (SEM)

The scanning electron microscope (SEM) has unique capabilities for analyzing surfaces and morphology of materials. It is analogous to the reflected light microscope, although different radiation sources serve to produce the required illumination. Whereas the reflected light microscope forms an image from light reflected from a sample surface, the SEM uses electrons for image formation. The different wavelength of these radiation sources result in different resolution levels: electron have much shorter wavelength than light photons, and shorter wavelength are capable of generating the higher resolution information. Enhanced resolution in turn permits higher magnification without loss of detail.

The maximum magnification of the light microscope is about 2,000 times; beyond this level is “empty magnification”, or the point where increased magnification does not provide additional information. This upper magnification limit is a function of the wavelength of visible light, 2000 Å, which equal the theoretical maximum resolution of conventional light microscope. In comparison, the wavelength of electron is less than 0.5 Å, and theoretically the maximum magnification of electron beam instrument is beyond 800,000 times. Because of instrumental parameters, practical magnification and resolution limits are about 75,000 times and 40 Å in a conventional SEM [49]. The SEM consists basically of four systems:

1. The *illuminating/imaging system* produces the electron beam and directs it onto the sample.

2. The *information system* includes the data released by the sample during electron bombardment and detectors which discriminate among analyze these information signals.

3. The *display system* consists of one or two cathode-ray tubes for observing and photographing the surface of interest.

4. The *vacuum system* removes gases from the microscope column which increase the mean free path of electron, hence the better image quality.

2.9.4 Transmission electron microscope (TEM)

TEM is a microscopy technique used for studying the size, Size dirtribution and morphology of particles. TEM involves a beam of accelerated electron, 50-200 keV, emitted by a tungsten filament cathode in vacuum. These electron are drflected in small angles by atoms in sample and transmitted through a thin sample. Then, these electrons are magnified by magnetic lenses and hotting a fluorescent screen coated with a phosphor to generate the bright field image. A schematic diagram of transmission electron microscopes is shown in Figure 2.25. The images from electron microscopes indicate the shape of a sample crystallite which can be used to determine size and morphology of solid nanoparticles [50].

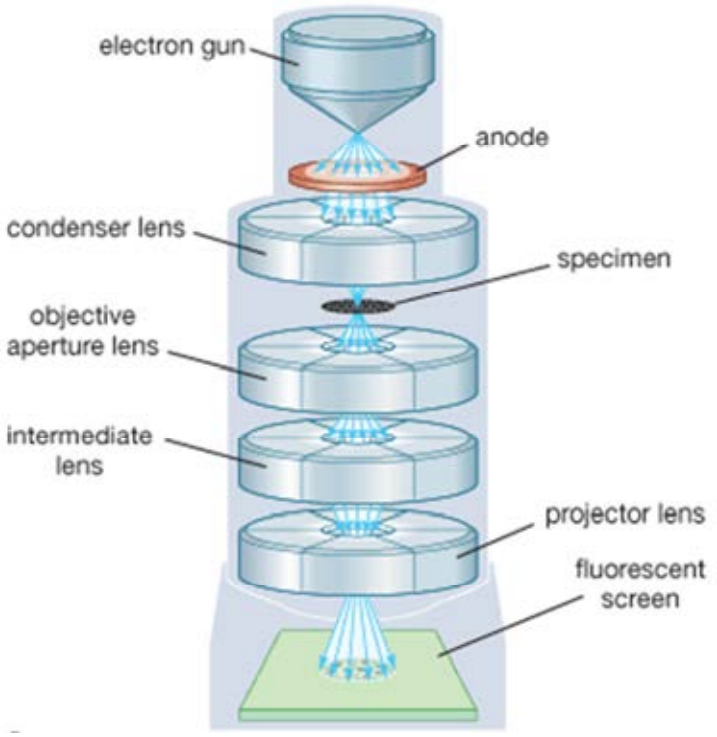

Figure 2.26 Schematic diagram of transmission electron microscope [51].

2.9.5 Energy-dispersive X-ray spectroscopy (EDX)

The Energy-dispersive X-ray spectroscopy (EDX or EDS) is an analytical technique used for the elemental analysis or chemical characterization of a sample. It relies on the investigation of an interaction of some source of X-ray excitation and a sample. Its characterization capabilities are due in large part to the fundamental principle that each element has a unique atomic structure allowing unique set of peaks on its X-ray spectrum To stimulate the emission of characteristic X-rays from a specimen, a high-energy beam of charged particles such as electrons or protons or a beam of X-rays, is focused into the sample being studied. At rest, an atom within the sample contains ground state (unexcited) electrons in discrete energy levels or electron shells bound to the nucleus. The incident beam may excite an electron in an inner shell, ejecting it from the shell while creating an electron hole where the electron was. An electron from an outer, higher-energy shell then fills the hole, and the difference in energy between the higher-energy shell and the lower energy shell may be released in the form of an X-ray (Figure 2.25). The number and energy of the X-rays emitted from a specimen can be measured by an energy-dispersive spectrometer. As the energy of the X-rays are characteristic of the difference in energy between the two shells, and of the atomic structure of the element from which they were emitted, this allows the elemental composition of the specimen to be measured [52].

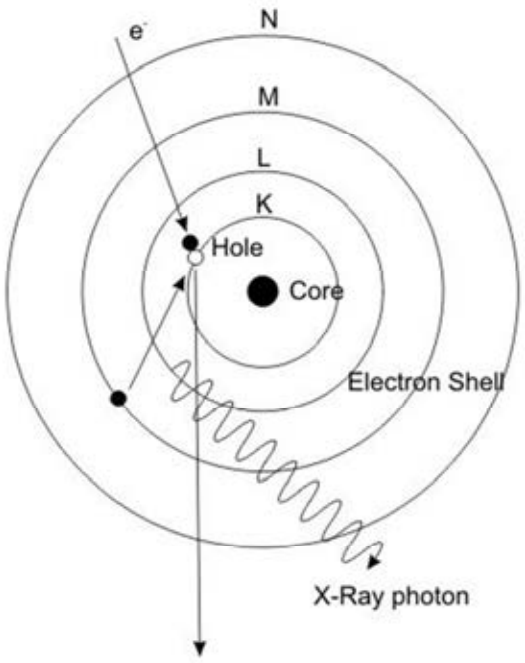

Figure 2.27 scheme of X-ray excitation [53]

2.9.6 Solid state ^{27}Al-magic angle spinning-nuclear magnetic resonance (^{27}Al-MAS-NMR)

NMR is a major and unique analytical tool in the characterization on the structure features of solid materials including zeolites and other aluminosilicates. Table 2.9 shows the relevant nuclei, the directly relevant nuclei in zeolite studies has been ^{29}Si and ^{27}Al-NMR which provide framework or structural information about zeolite or mesoporous molecular sieves.

Table 2.9 NMR properties of selected nuclei

Isotope	Spin	Natural abundance (%)
^{1}H	1/2	99.98
^{23}Na	3/2	100
^{27}Al	5/2	100
^{29}Si	1/2	4.70
^{129}Xe	1/2	26.44
^{205}Tl	1/2	70.50

An advantage in examining ^{27}Al-NMR spectra is that ^{27}Al has a 100 percent natural abundance with I = 5/2 and ranges in chemical shift about 450 ppm. Quadrupole coupling must be separated from chemical shift effect to render useful chemical information from^{27}Al-NMR spectrum. For the low Sl/Al molar ratio where the Si (Al) resonance is very weak in the ^{29}Si-NMR spectra, incorporation of Al in the framework can readily be demonstrated via ^{27}Al-NMR. The ^{27}Al-NMR has been used mainly for the detection of extra-framework aluminum, since the ^{27}Al-NMR chemical shifts depend primarily on the coordination of aluminum with respect to oxygen. For tetrahedral coordination, chemical shifts of 55 to 80 ppm from $Al(H_2O)_6{}^{3+}$ are observed. Octahedral Al appears at 0 to 22 ppm. Both the solid and solution spectra show similar ranges. The position of the signal in ^{27}Al-NMR spectra is also sensitive to the composition of material, i.e. the nature of counter ion, degree of hydration of sample. In dehydrated sample,quadrupolar effects are so strong that the tetrahedral Al line disappears, reappearing on dehydration. No effect is observed for the octahedrally bound aluminum with changing degrees of hydration [54-55].

2.10 Hydrothermolysis

Hydrothermolysis reaction involves applying heat under pressure to achieve reaction in an aqueous medium. The hydrothermolysis is one of the most promising liquefaction processes for the conversion of biomass feedstocks into chemical, because water at high temperatures and high pressures behaves as a reaction medium having outstanding properties which make it an excellent environment friendly solvent.

The reaction pathways of hydrothermolysis of carbohydrate change with acidic, neutral and alkaline condition. As shown in Figure 2.26, under acidic conditions, the main conversion compounds are 5-(Hydroxymethyl)fufural (HMF) and levulinic acids. Under alkaline conditions, they become carboxylic acids such as lactic and acetic acids. Under neutral conditions, both the acidic and alkaline conversion products are formed, due to the self-dissociation of H_2O to H^+ and OH^- at high temperature [56].

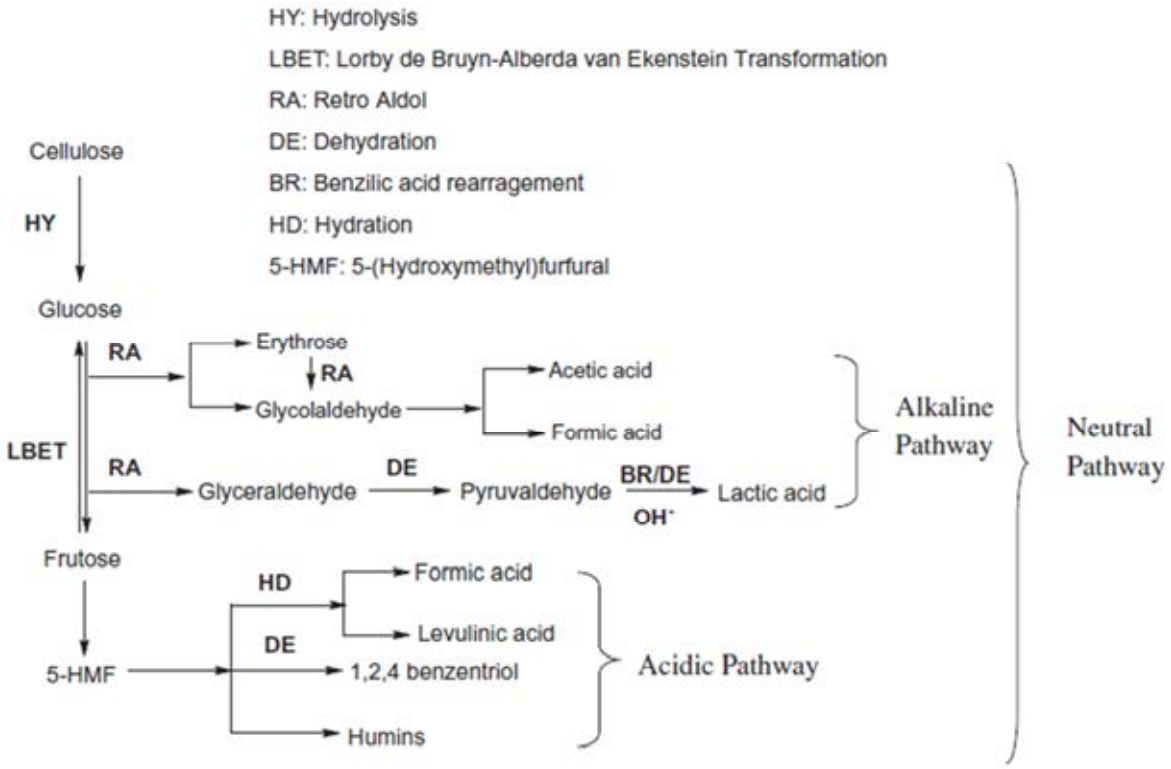

Figure 2.28 General pathways of hydrothermolysis [56].

The reaction pathways of glucose hydrothermolysis under acidic conditions with in a molecular-sieve catalyst is proposed in Figure 2.27. In the proposed reaction scheme, glucose molecules from the bulk phase enter the catalyst pores and adsorb onto vacant acid sites on the pore walls. The adsorbed glucose partially dehydrates to hydroxymethylfuraldehyde (HMF) or reversibly isomerizes to fructose. The adsorbed fructose can also dehydrate to HMF or desorb to the liquid phase. HMF is claved on acid sites and hydrolyze to yield levulinic acid (LA) and formic acid. HMF can also completely dehydrate to coke and deposite on the catalyst surface, or desorb to the liquid phase. The adsorbed LA and formic acid products can also completely dehydrate to coke or desorb to the liquid phase. The products exit out of the pores and into the bulk liquid phase [8]. The proposed mechanism of glucose hydrothermolysis was showed in Figure 2.30, which composed of tautomerization, dehydration and hydration reactions.

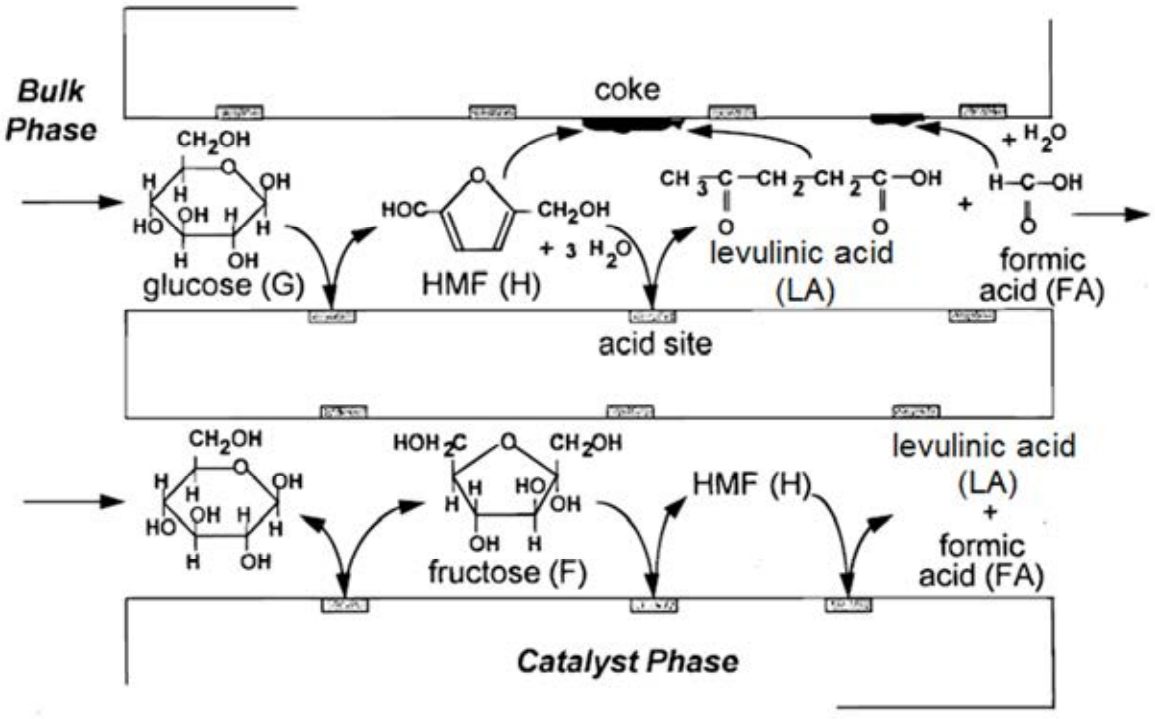

Figure 2.29 Overall reaction pathways of hydrothermolysis of glucose to LA within the porous matrix of the solid-acid molecular-sieve catalyst [8].

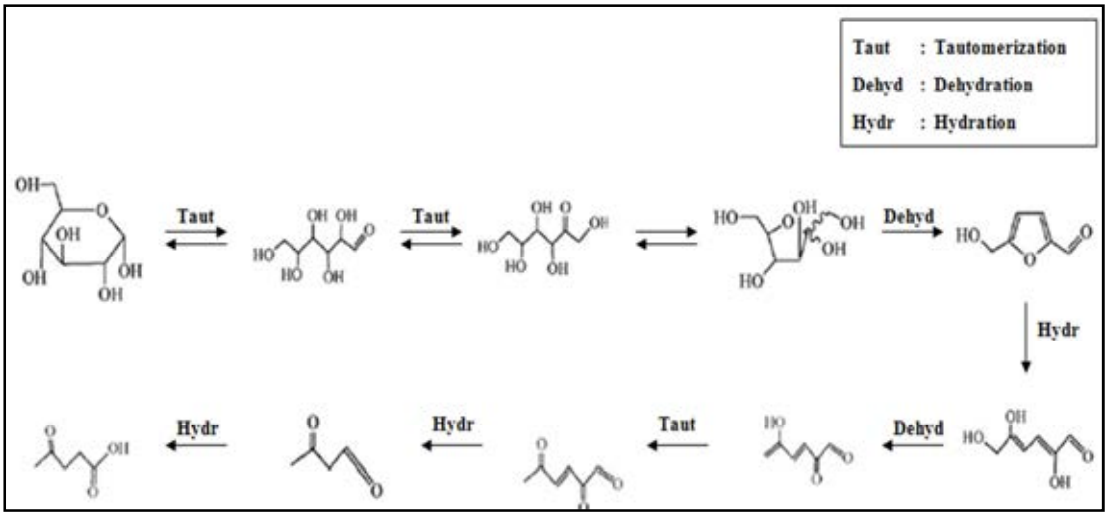

Figure 2.30 Schematic of proposed mechanism of hydrothermolysis of glucose to LA [57].

2.11 Levulinic acid (LA)

LA contains a ketone group and a carboxylic acid group. These two functional groups make levulinic acid a potentially very versatile building block for the synthesis of various organic (bulk)-chemicals [58] as shown in Figure 2.28.

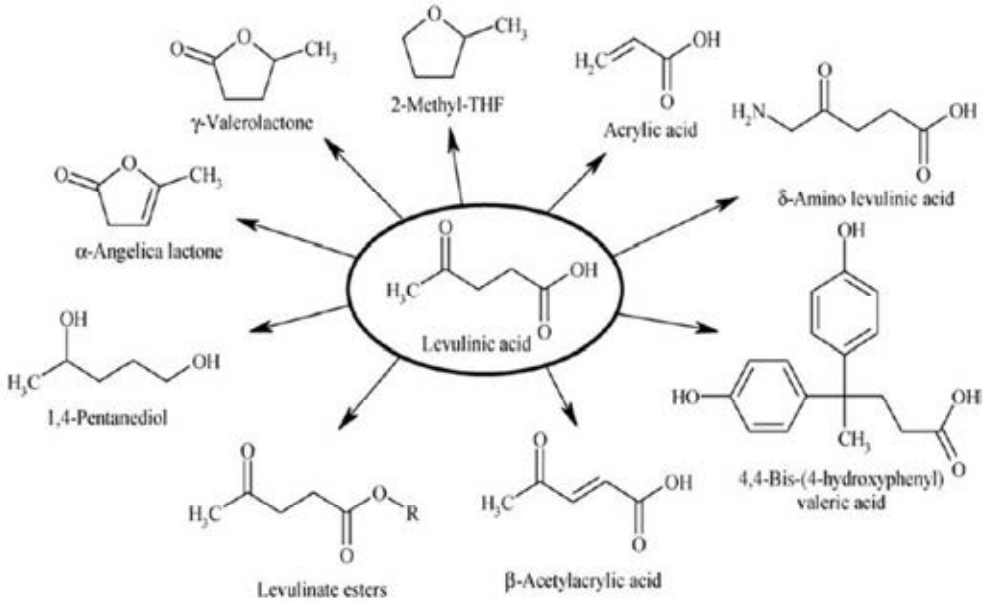

Figure 2.31 Potentially interesting derivatives of levulinic acid [58].

The combination of low cost source of LA with new technology has opened up new opportunities for LA as platform chemical feedstock. LA and its derivatives have found use in highly diverse areas. For example of these application are chiral reagent, lubricants, adsorbents, printing, coating, drug delivery, and corrosion inhibitors ,etc. Consequently, it is an attractive starting material for the production of many useful compounds such as methyltetrahydrofuran (MTHF), Δ-aminolevulinic acid (DALA), diphenolic acid (DPA), tetrahydrofuran (THF), and butanediol (BDO) as shown in Table 10 [59].

Table 2.10 Products from LA and potential LA markets demand [59].

Product	**Use**	**Potential LA market (million lb/year)**
MTHF	Fuel extender	10,000-100,000
DALA	Biodegradable herbicide	175-350
DPA	Monomer	35
THF	Solvent	200
BDO	Monomers	200

CHAPTER III

EXPERIMENTS

3.1 Instruments and apparatus

3.1.1 Oven and furnace

Crystallization of SBA-15 during the synthesis was carried out at a temperature of 100^{o}C in static condition using UM-500 oven as heater. The calcination was performed on a Carbolite RHF 1600 muffle furnace in air with programmable heating rate of 1^{o}C/min. Calcination of the solid catalysts was conducted in order to remove moisture and organic template from the catalyst. The temperature program used for the calcination of SBA-15 was shown in Figure 3.1.

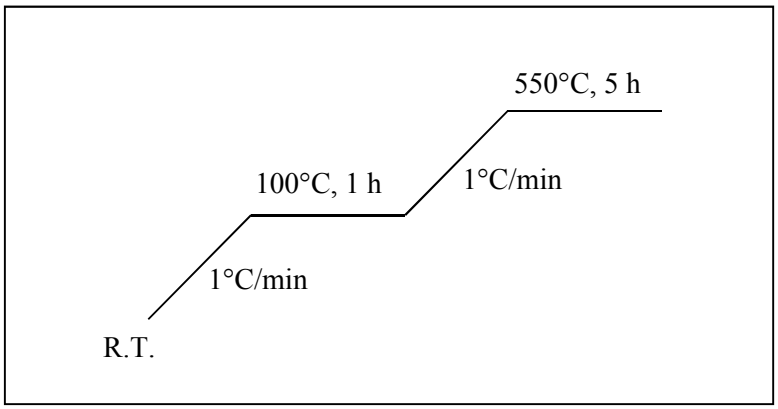

Figure 3.1 The temperature program for the calcination of SBA-15

3.1.2 X-ray powder diffractometer (XRD)

The structure of synthesized SBA-15 was identified using a Rigaku D/MAX-2200 Ultima^{+} X-ray diffractometer equipped with Cu target X-ray tube (40 kV, 30mA) at 2 Theta angle between 0.5 to 3.0 degree with a scan speed of 1.00 degree/min and sampling width of 0.02 degree. The scattering slit, divergent slit and receiving slit were fixed at 0.5 degree, 0.5 degree, and 0.15 mm, respectively. The measured diffractograms were analyzed by MDI software (Jade 6.5).

3.1.3 Nitrogen adsorption-desorption technique

Characterization of catalyst porosity in terms of nitrogen adsorption-desorption isotherms, BET specific surface area, and pore size distribution of the catalysts were carried out using a BEL Japan, BELSORP-mini instrument. The pure materials weights were nearly 40 mg and weighted exactly after pretreatment at 400^{o}C for 3 h before each measurement.

3.1.4 Scanning electron microscope (SEM)

The morphology and particle size of the catalysts were observed using a Hitachi S-4800 field emission scanning electron microscope. All samples were coated with platinum under vacuum.

3.1.5 Transmission electron microscope (TEM)

The microstructure of synthesized materials were investigated by JEOL; JEM-2100 transmission electron microscopy.

3.1.6 Energy dispersive spectrometer (EDX)

The energy dispersive spectrometer with Horiba detector calibrated with Cu, was used to measure the amount of metal loaded on the support.

3.1.7 ^{27}Al-NMR Spectrometer

Solid state ^{27}Al-NMR spectra were performed using the ^{UNITY}INOVA Varian 500 MHz NMR spectrometer.

3.1.8 Gas chromatograph (GC)

Liquid products from carbohydrate hydrothermolysis were analyzed using a Varian CP 3800 gas chromatograph equipped with a 30 m length × 0.25 mm inner diameter of CP-Sil 8 capillary column (equivalent to DB-5 and HP-5 column). The detector was a flame ionization detector (FID). The sample volumes were 1 μL. The column oven heating program was illustrated in Figure 3.2.

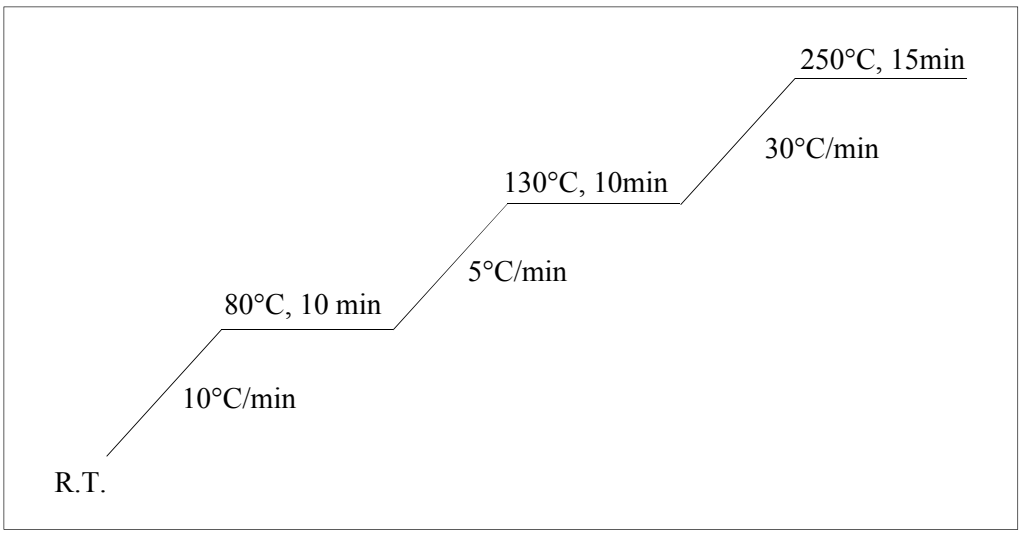

Figure 3.2 The GC heating condition liquid products analysis.

3.1.9 Gas chromatograph-mass spectrometer (GC-MS)

Qualitative analysis of liquid sample was confirmed with GC-MS technique. GC system network of Agilent model 6890N, mass selective detector network of Agilent model 5973N and injector of Agilent 7683 Series were used.

3.1.10 Parr reactor

The hydrothermolysis reaction of carbohydrates (glucose, sucrose, and starch) was performed in 300 ml PARR reactor. The temperature program for the reaction was shown in Figure 3.3.

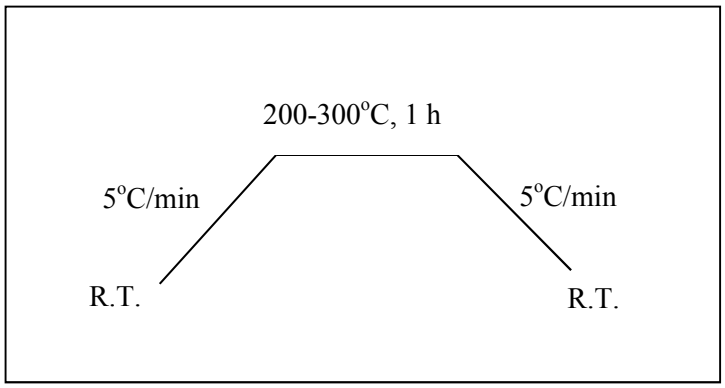

Figure 3.3 The temperature program for hydrothermolysis reaction.

3.2 Chemicals

3.2.1 Chemicals for synthesis catalysts

1. Triblock copolymer pluronic P123 (PEO_{20}-PPO_{70}-PEO_{20}, average molecular weight = 5800) (Aldrich)
2. Tetraethylorthosilicate, TEOS (Fluka, 98 %)
3. Sodium aluminate, $NaAlO_2$ (Riedel-deHaen)
4. Hydrochloric acid, HCl (Fluka, 37 %)
5. Nickel nitrate hexahydrate, $Ni(NO_3).6H_2O$ (Merck)
6. Ruthenium chloride hydrate, $RuCl_3.xH_2O$ (Aldrich)
7. Deionized Water

3.2.2 Chemicals for hydrothermolysis of carbohydrate

1. Glucose (Merck)
2. Sucrose (Wangkanai Demerara sugar)
3. Starch (Sigma-Aldrich)
4. Nitrogen gas, N_2 (Thai Industrial Gases (TIG), highly pure grade)
5. Deionized Water

3.3 Synthesis procedure of SBA-15 by hydrothermal method

Pure silica SBA-15, a mesoporous material was synthesized using gel mole composition of 1.0TEOS: 0.0165 P123: 6.95 HCl: 140 H_2O reported by Stucky *et al*. [34]. In a typical procedure, triblock copolymer Pluronic P123 as template was dissolved in 1.9 M HCl solution at room temperature under stirring. Subsequently, TEOS was added dropwise and stirred for 30 min and then, aged at 40^oC for 24 h with stirring. The resulting gel was transferred to a Teflon-lined autoclave for hydrothermal crystallization at 100^oC for 48 h without stirring. As-synthesized SBA-15 was separated by filtration, washed with deionized water for several times, and dried in the air overnight. The white powder material was obtained and then, the template was removed by calcination at 550^oC for 5 h in a muffle furnace as shown in Figure 3.4. The procedure for synthesizing the SBA-15 was illustrated in Figure 3.5.

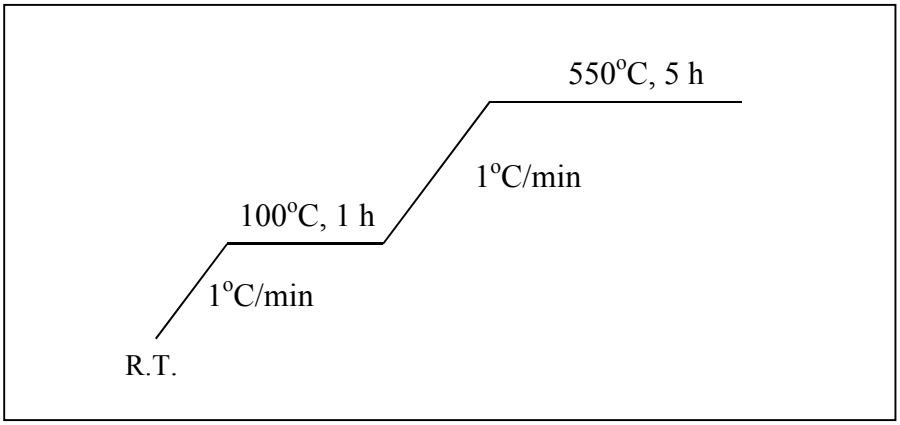

Figure 3.4 Calcination temperature program for Si-SBA-15.

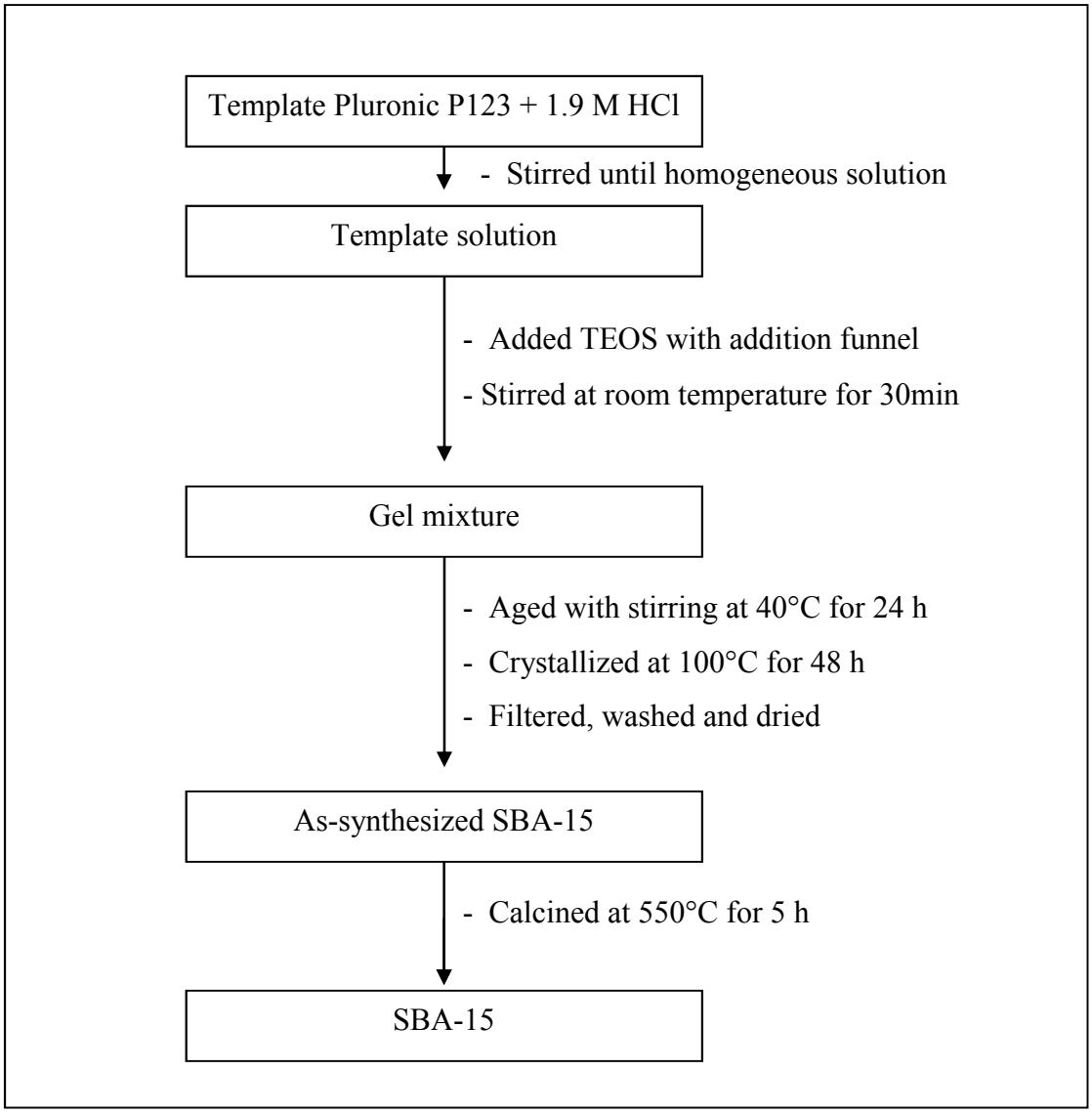

Scheme 3.1 Preparation diagram for SBA-15 by hydrothermal method

3.4 Aluminium functionalized mesoporous materials

In this work, mesoporous SBA-15 was incorporated with aluminium via post synthesis. Alumination of calcined mesoporous was conducted by stirring 0.5 g of calcined SBA-15 in 50 mL of water containing exact amounts of sodium aluminate at room temperature (RT) for 12 h. The Al-containing mesoporous material was filtered and washed with deionized water and then, dried at room temperature. After that, sodium ion in post-synthesized sample was removed by ion exchange with 0.01M NH_4Cl for 24 h [59]. Then material was calcined at 550°C for 5 h. The solid was designated as Al-SBA-15 at Si/Al mole ratio 30. The procedure for preparing Al-SBA-15 was shown in Figure 3.6.

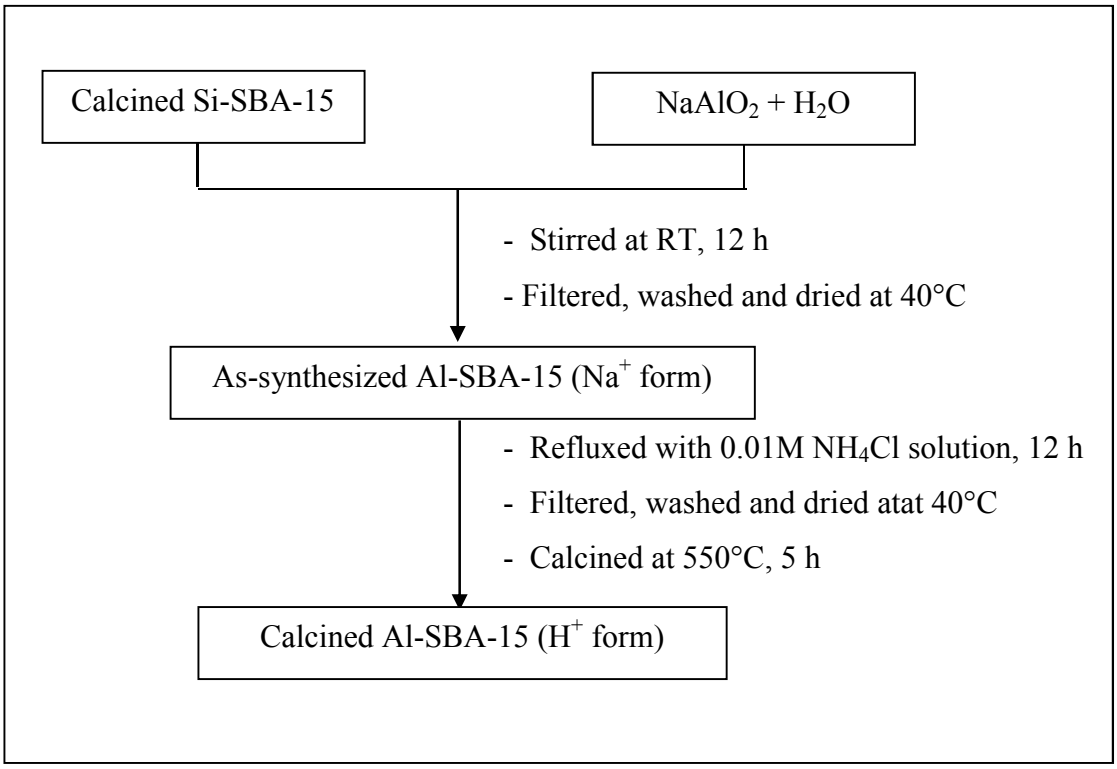

Scheme 3.2 Alumination of Al-SBA-15.

3.5 Preparation of metal supported on SBA-15, Al-SBA-15 and ZSM-5.

The Ni and Ru metal was supported on SBA-15, Al-SBA-15, and ZSM-5. Supported metal catalysts were also prepared by aqueous wet impregnation method using metal salt aqueous solution ($Ni(NO_3).6H_2O$ and $RuCl_3.xH_2O$), the amount of metal loading was 10 wt.%. Special attention was given to the Ru supported on Al-SBA-15 and ZSM-5 with 20 wt.%Ru loading. After impregnation, the materials were dried at 120°C followed by

calcination at 500°C for 4 h as shown in Figure 3.7. The sample was denoted as (x)%(metal)-(catalyst support) where x was percent of metal loaded on catalyst support, metal was Ni, or Ru, and catalyst support was SBA-15, Al-SBA-15, or ZSM-5.

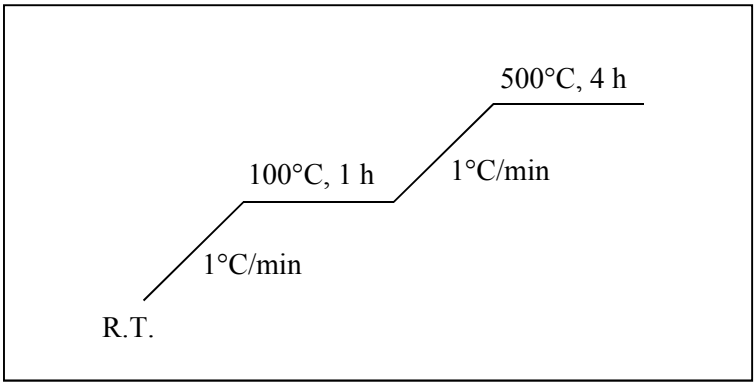

Figure 3.5 The temperature program for the calcination of metal supported mesoporous materials

3.6 Acid-base titration

The acid capacities of metal and aluminium functionalized mesoporous materials were quantified using 2M NaCl solution as the ion-exchange agent (Figure 3.8). Approximately 0.05xx g of the catalyst was exchanged with 15 ml of NaCl solution for 30 min under constant agitation at room temperature and titration with 0.01 M NaOH by used phenolphthalein as indicator [60].

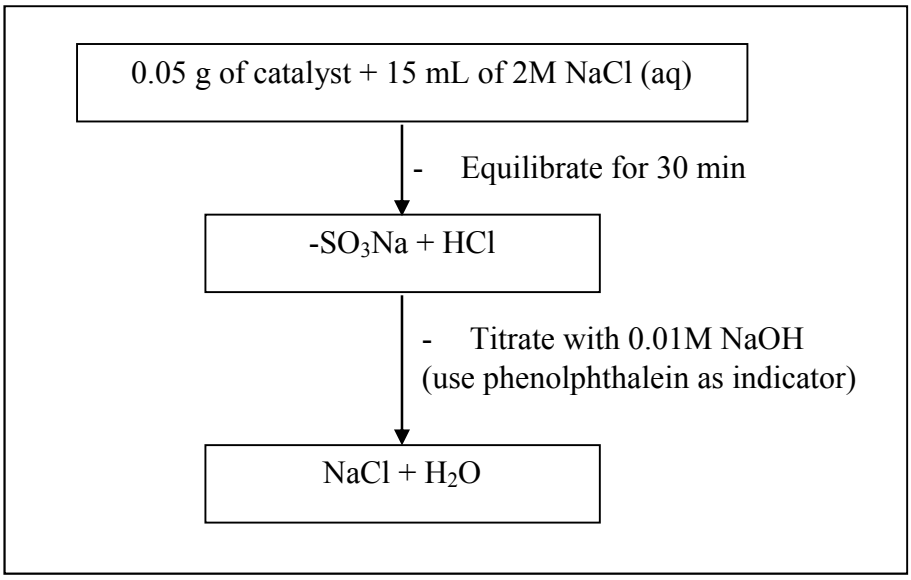

Scheme 3.3 Diagram for acid-base titration

3.7 Procedure in carbohydrates hydrothermolysis

The hydrothermolysis used carbohydrates (glucose, sucrose, or starch) as starting material were carried out in stainless steel batch reactor. Initially, 30 ml of water, 0.50 g of catalyst and 5.00 g of starting material were loaded into the PARR reactor (Figure 3.9) and mixed thoroughly. Afterward, the reactor was set up, purged with N_2 at 145 psi and heat up to the desired temperature and keeping to constant for 1 h. After the reaction complete, the reactor was cooled down to room temperature. The alternative products were classified into three groups that were gas products, liquid products, and residue. The liquid products were confirmed using GC-MS technique and compared to the authentic samples. Likewise, the liquid products were quantitatively analyzed by gas chromatography.

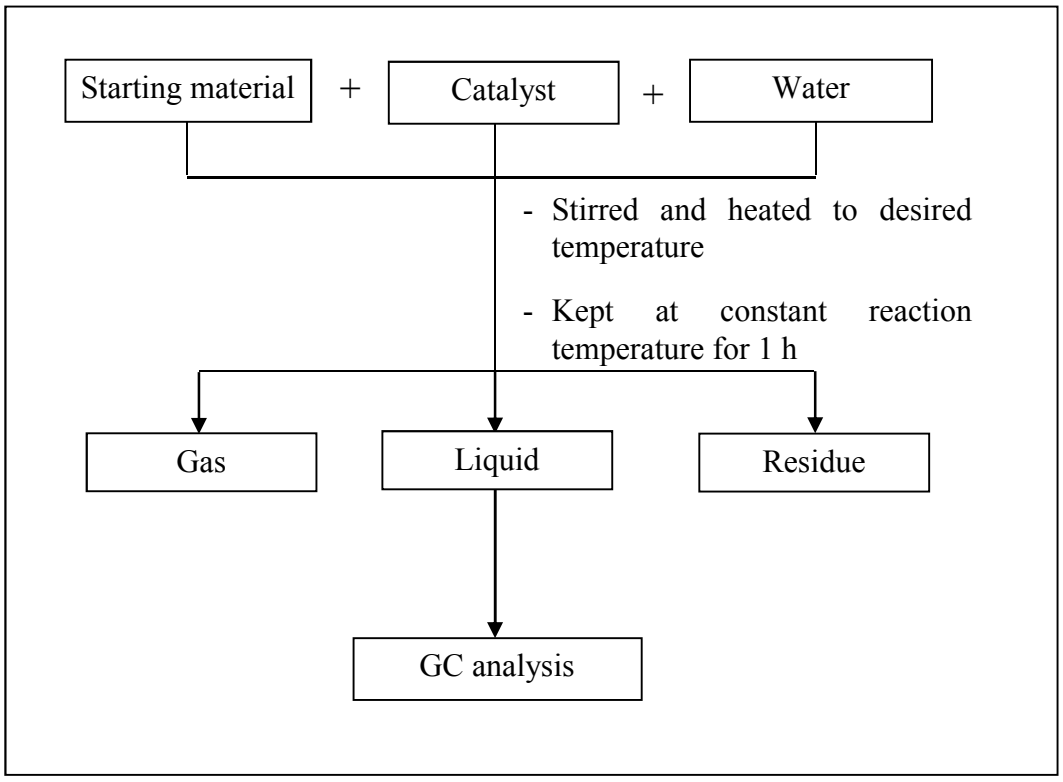

Scheme 3.4 Diagram for carbohydrate hydrothermolysis and analysis.

3.8 Parameters affecting carbohydrate hydrothermolysis

3.8.1 Effect of temperature

The reaction temperature was varied to 200, 250, and 300°C.

3.8.2 Effect of catalytic amount

In this work, the amount of catalyst was changed to 0 wt.%,5 wt.%, 10 wt.% and 15 wt.% of starting material.

3.8.3 Effect of various catalysts

Catalytic activities of ZSM-5, Al-SBA-15, and metal (Ni and Ru) supported on SBA-15, Al-SBA-15, and ZSM-5 were tested in hydrothermolysis compared to non catalytic reaction.

3.8.4 Effect of molecular size of starting material

Hydrothermolysis of various carbohydrates was carried out using glucose, sucrose, and starch as starting material for molecular size of starting materials comparison.

CHAPTER IV

RESULTS AND DISCUSSION

4.1 Synthesis of SBA-15 catalysts

4.1.1 The physico-chemical properties of aluminium functionalized SBA-15

4.1.1.1 XRD results

The XRD patterns of SBA-15 materials and Al-SBA-15 with Si/Al ratio in gel composition of 30 were shown in Figure 4.1. SBA-15 exhibited the peak positions consist of three well-resolved peaks corresponding to the reflection (100), (110), and (200) associated with hexagonal symmetry of SBA-15. Al-SBA-15 was synthesized by alumination method following Kevan *et al.* [59] retained the ordered structure of SBA-15 during the post synthesis process and exhibited increasing intensity of the (100) reflection plane and slightly shifted to higher value of 2-Theta as 0.90^{o} comparing to pure silica SBA-15 (0.88^{o}) meaning to lower d-spacing in pores structure, resulting from the shrinkage during the recalcination process [61].

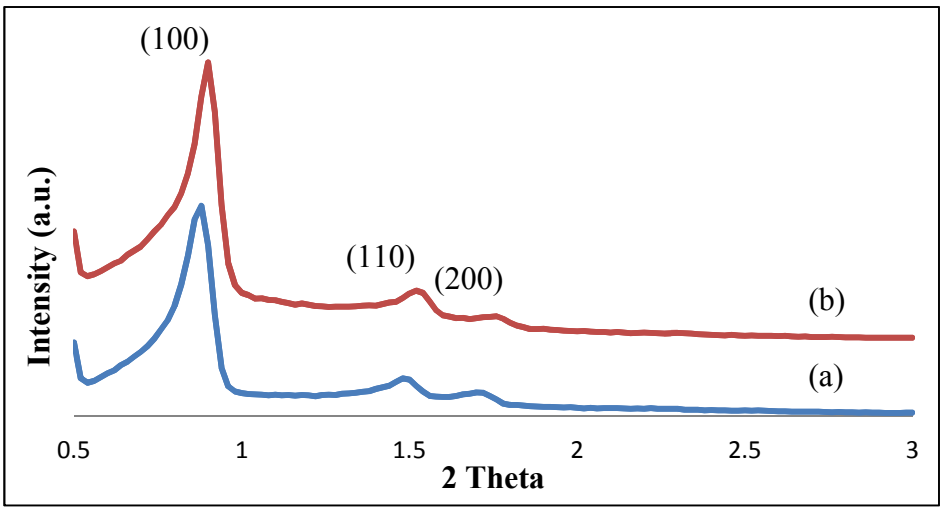

Figure 4.1 X-ray powder diffraction patterns of (a) SBA-15, (b) Al-SBA-15.

4.1.1.2 Sorption properties

The N_2 adsorption-desorption isotherm of aluminated SBA-15 catalyst with Si/Al mole ratio of 30 compared with that of pure silica SBA-15 were shown in Figure 4.2. Although, modified material were inserted Al ion in the framework, the isotherms were classified as type IV isotherm with H1 hysteresis loop, similar to the pure silica SBA-15. They were characteristic pattern of mesoporous materials.

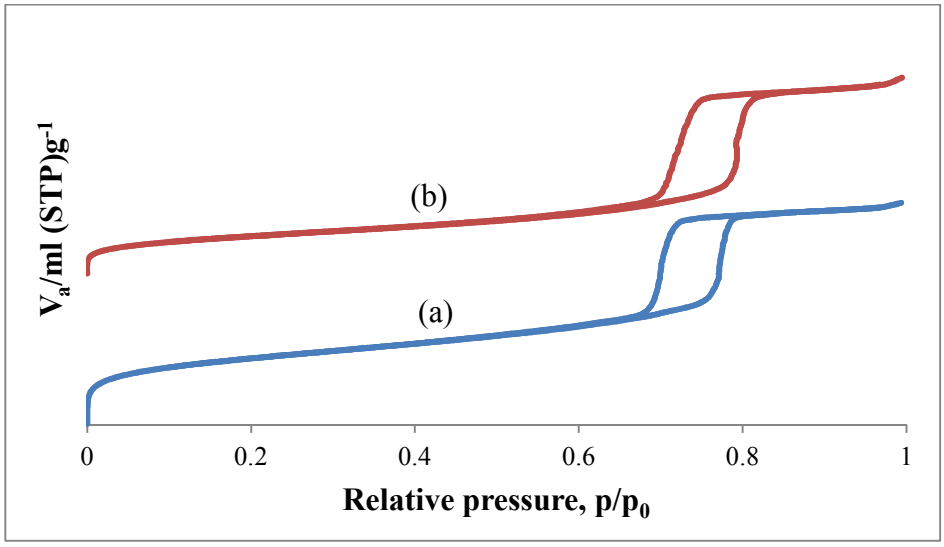

Figure 4.2 N_2 adsorption-desorption isotherms of (a) SBA-15, (b) Al-SBA-15.

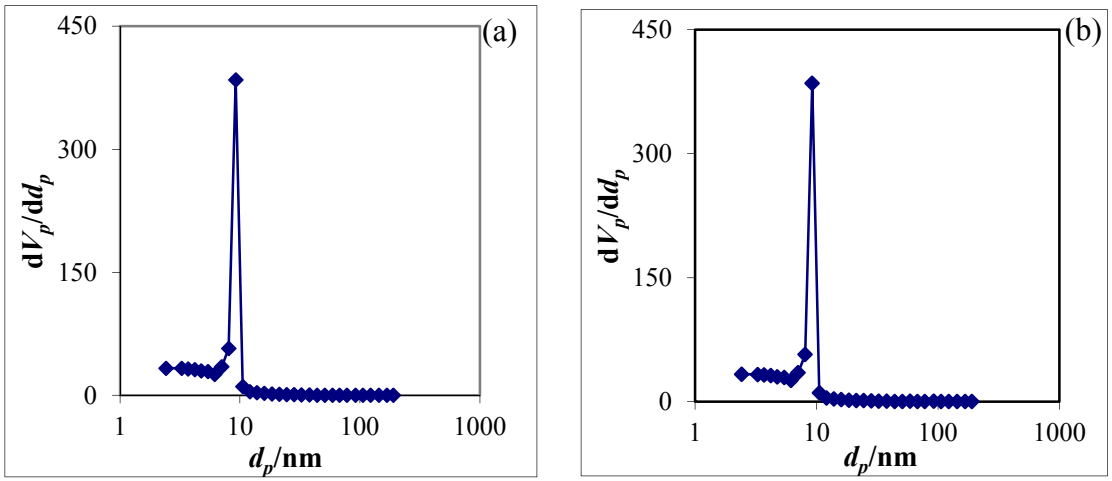

Figure 4.3 BJH-Pore size distributions of (a) SBA-15, (b) Al-SBA-15.

The pore size distribution obtained from Barrett-Joiner-Halenda (BJH) method was shown in Figure 4.3. The data showed that SBA-15 and Al-SBA-15 had a narrow distribution of mesopores with the pore size of 9.23 nm. The pore size of Al-SBA-15 sample still unchanged, demonstrated that the original pore structure of the pure silica SBA-15 sample was preserved intact after Al incorporation. Textural properties of calcined catalysts were showed in Table 4.1.

Table 4.1 Textural properties of SBA-15 and Al-SBA-15.

Catalyst	**Total specific surface area[a] ($m^2 \cdot g^{-1}$)**	**Pore size distribution[b] (nm)**	**Mesopore volume[b] ($cm^3 \cdot g^{-1}$)**	**$d_{(100)}$[c] (nm)**	**Wall thickness[d] (nm)**
SBA-15	809.30	9.23	1.0270	9.82	2.11
Al-SBA-15	464.84	9.23	0.9812	9.80	2.08

[a]Calculated using the BET plot method,
[b]Calculated using the BJH method,
[c]Calculated using XRD, Jade5.6,
[d]Calculated as: a_0-pore size ($a_0 = 2 \times d_{(100)} / \sqrt{3}$)

From the *d*-spacing of the (100) reflection plane and the pore size distribution determined by N_2 adsorption, the estimated mean thickness of the pore walls of the mesoporous silica materials could be calculated based on the equation as following [62]:

Wall thickness = a_0-pore size

Where; $a_0 = 2 \times d_{(100)} / \sqrt{3}$

$d_{(100)}$ = *d*-spacing of the (100) reflection plane from XRD method

The total surface area was calculated using Brunauer, Emmett and Teller (BET) equation. Incorporated Al in the SBA-15 framework leads to a reduction in the amount of nitrogen up taken in SBA-15 due to the decreasing of mesoporous volume. In addition, the d-spacing of Al-SBA-15 was decreased, indicating that the distance from each plane was reduced. Considering the effect of aluminum content in catalysts, wall thickness was calculated in the same method as Stucky *et al*. [35]. The wall thickness decreased corresponding to the decrease of d-spacing as $d_{(100)}$ in the equation.

4.1.1.3 SEM images

The SEM images of SBA-15 and Al-SBA-15 are illustrated in Figure 4.4. Morphology of SBA-15 was uniform rope-like particle shape aggregated particles as presented in Figure 4.4 (a). From aluminum additions, the small rod particles were broken out of the rope-like agglomeration. However the rod shape of individual particle remained the same as precursor.

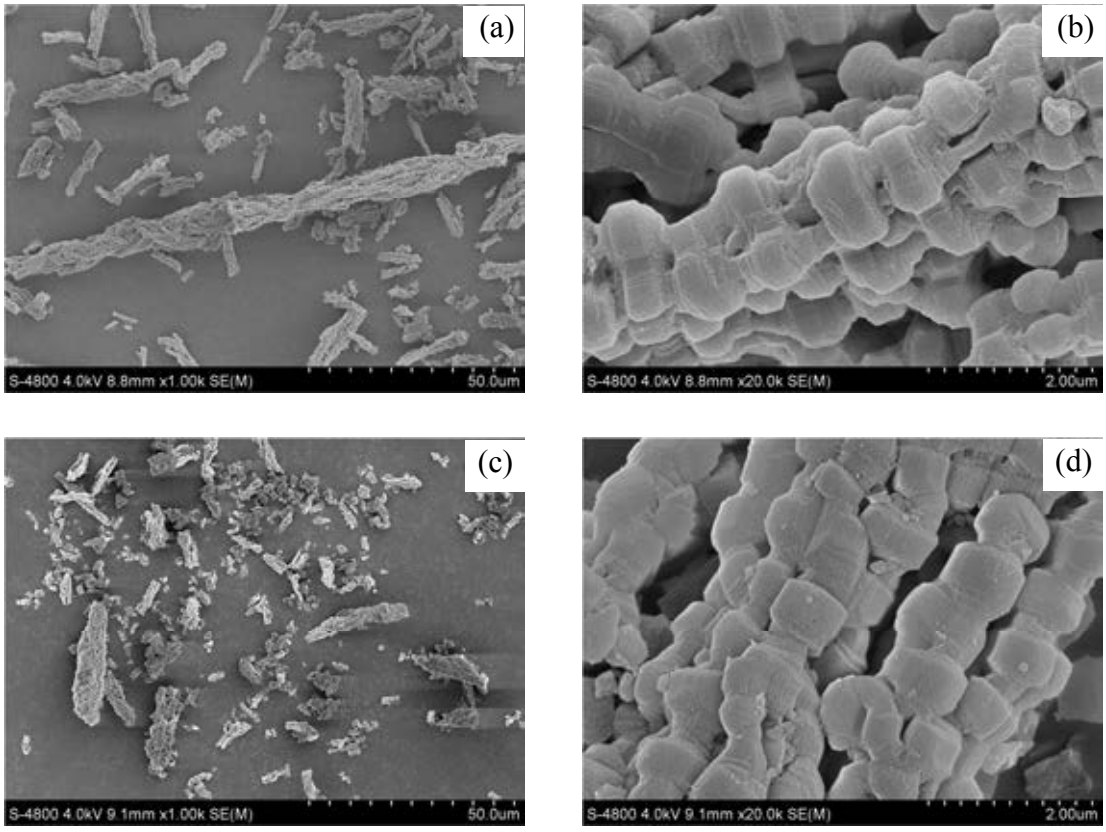

Figure 4.4 SEM images of (a) SBA-15 x5000, (b) SBA-15 x20000, (c) Al-SBA-15 x5000, and (d) Al-SBA-15 x20000.

4.1.1.4 TEM images

The microstructure of SBA-15 and Al-SBA-15 powder were examined by TEM micrograph as shown in Figure 4.5. The TEM images of SBA-15 exhibited the well-ordered hexagonal arrays of one dimensional mesoporous channels. The incoporation of Al into porous material framework was leaded to the formation of Al in tetrahedral site which expresses the acidity of Al-SBA-15 structure and remained exhibited the well-ordered hexagonal arrays of mesoporous channels.

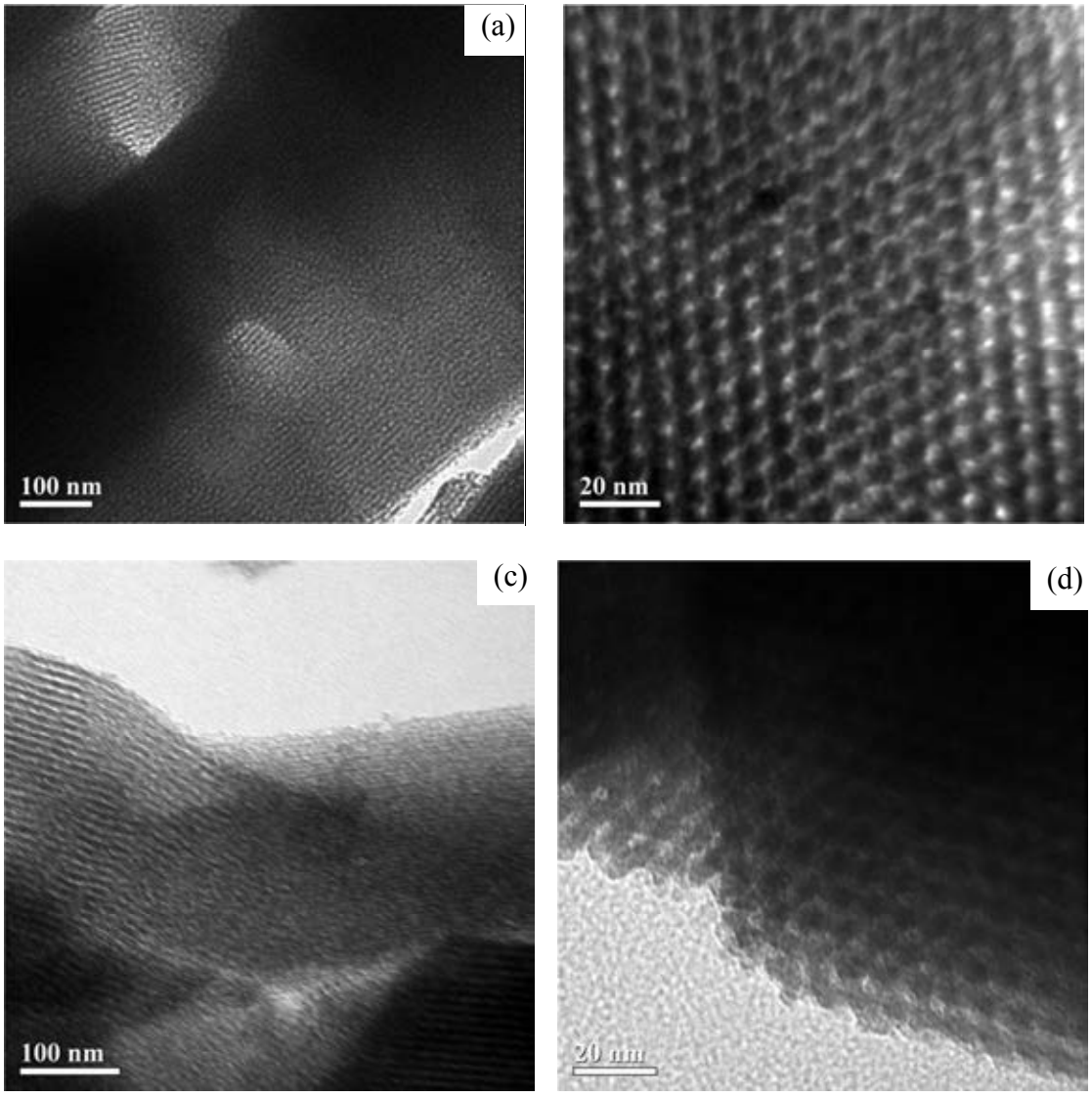

Figure 4.5 TEM images of (a) SBA-15 ×40000, (b) SBA-15 ×250000, (c) Al-SBA-15 ×40000, (d) Al-SBA-15 ×250000.

4.1.1.5 Elemental analysis and acid-base titration

The EDX methode was used to measure percent of elemental in materials and the number of proton in the mesoporous materials (SBA-15 and Al-SBA-15) were measured quantitatively by acid-base titration using sodium chloride as ion-exchange agent, the results were shown in Table 4.2. The Si/Al molar ratio in the gel of Al-SBA-15 in preparation step (Si/Al 30) was higher than found in synthetic matter (Si/Al 20.13). That may be caused by the structural framework of pure silica SBA-15 was collapsed, thus the silica in the framework was substituted by aluminium via acid strong condition of alumination. The Al-SBA-15 (0.45 mmol/g) attained about two times more acidic value than SBA-15 (0.23 mmol/g), by alumina incorporation via post synthesis.

Table 4.2 EDX analysis and acid value of SBA-15 and Al-SBA-15.

Catalysts	Si (wt.%) [a]	Al (wt.%)[a]	Si/Al mole ratios		H^+ content[c] (mmol/g)
			in gel composition[b]	in catalysts[a]	
SBA-15	32.44	-	-	-	0.23
Al-SBA-15	26.16	1.26	30	20.13	0.45

[a]EDX measurements,
[b]Calculated from reagent quantities,
[c]Acid capacity defined as millimole of acid centers per gram of catalyst, obtained directly by titration (mmol H^+/g).

4.1.1.6 ^{27}Al-MAS-NMR spectra of Al-SBA-15

Solid state ^{27}Al-MAS-NMR provided the information of the aluminum atoms, located at the framework or non-framework site, two resonance signals were observed. The intense peak at 50 ppm could be assigned to aluminum atoms in tetrahedral surroundings (AlO_4 structural unit). The appearance of this peak meant that aluminum atoms have been incorporated into the framework of SBA-15. The other signal at 0 ppm was due to the octahedral coordinated, located at non-framework site (AlO_6 structural unit) [63]. The ^{27}Al-MAS-NMR spectrum of calcined Al-SBA-15 sample was presented in Figure 4.7. It exhibited two intense signals of framework site at 50 and 0 ppm. Indicating Al atoms were incorporated into the SBA-15 at both of tetrahedral and octahedral as ratio 1.00 : 0.20.

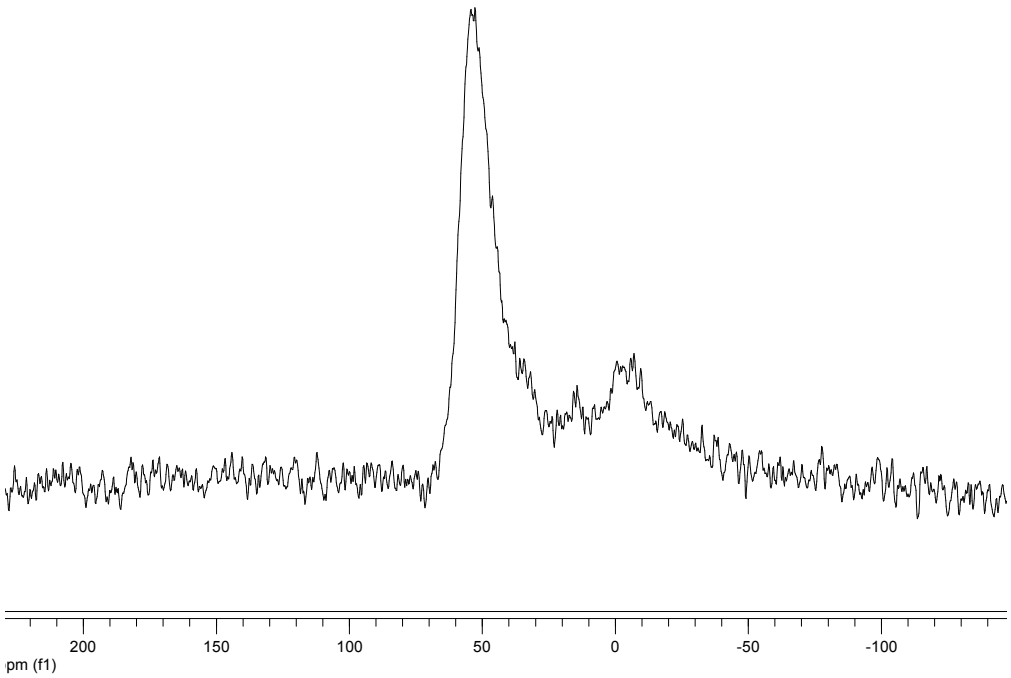

Figure 4.6 ^{27}Al-MAS-NMR spectrum of Al-SBA-15**.**

4.1.2 The physico-chemical properties of metal (Ni and Ru) supported on SBA-15

4.1.2.1 XRD results

The XRD patterns of metal-SBA-15 samples that prepared by wet impregnation method were compared with SBA-15 shown in Figure 4.7. For 10%Ni-SBA-15 and 10%Ru-SBA-15 materials, similar three well-resolved peaks were observed, exhibited the materials retained the ordered structure of SBA-15 after wet impregnation method. From XRD patterns, both of metal-SBA-15 samples were decreased the intensity of the (100) reflection and slightly shifted towards a lower angle (higher d-spacing) was observed that may be due to the metal atoms with different diameter (Ni = 0.144 nm, Ru = 0.164 nm, and Si = 0.082 nm) entered into the lattice of SBA-15 [64]. However, there was not much significant change in hexagonal structure after loading metal on SBA-15.

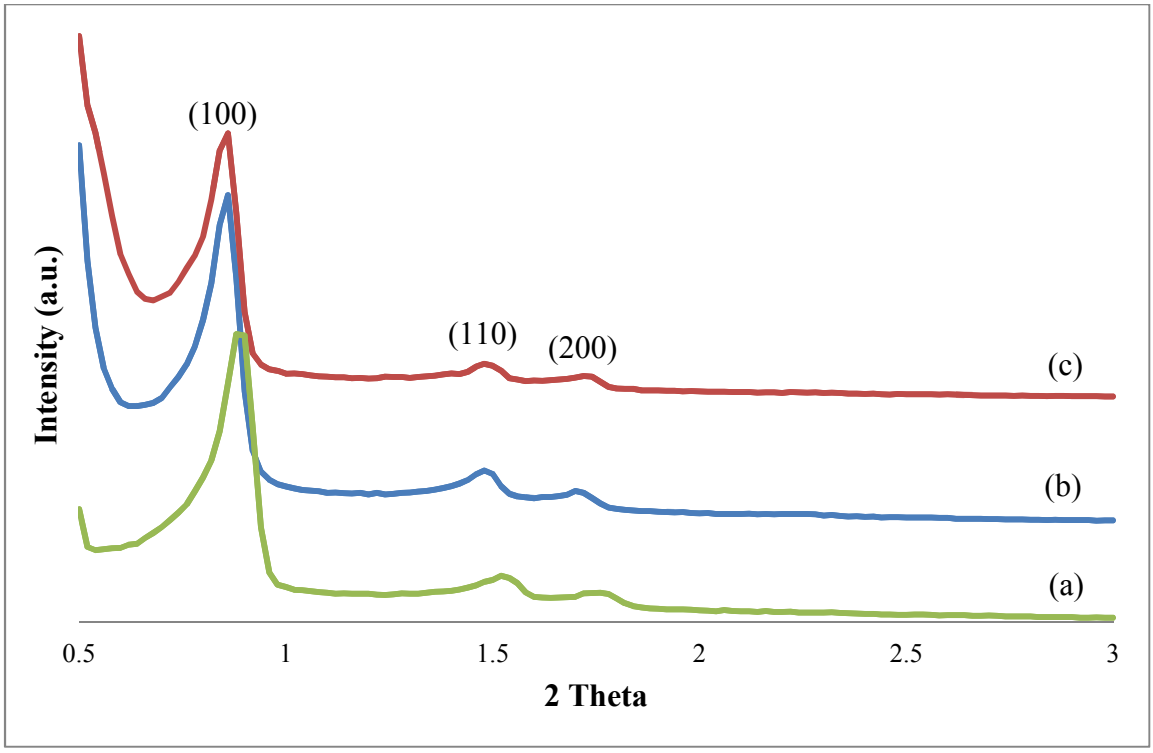

Figure 4.7 X-ray powder diffraction patterns of (a) SBA-15, (b) 10%Ni-SBA-15, and (c) 10%Ru-SBA-15.

4.1.2.2 Sorption properties of metal-SBA-15

The N_2 adsorption-desorption isotherm of SBA-15, 10%Ni-SBA-15, and 10%Ru-SBA-15 were shown in Figure 4.8. All samples exhibited type IV isotherm which was typical for mesoporous material. Furthermore, the shape of the adsorption-desorption isotherm of 10%Ni-SBA-15 and 10%Ru-SBA-15 were similar to SBA-15. This result indicated that uniform pore structure of SBA-15 was maintained even after impregnation.

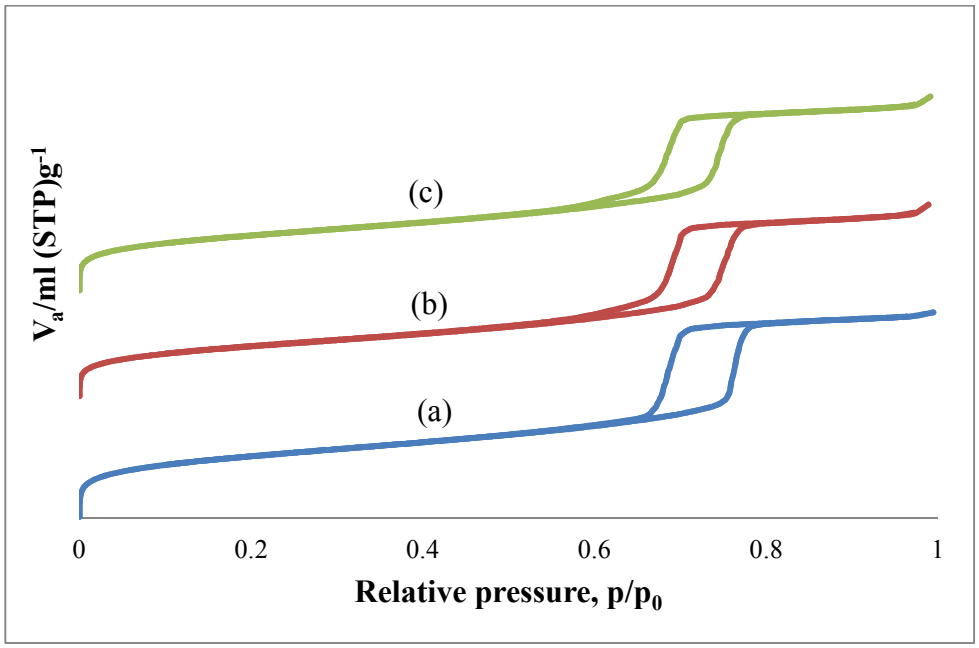

Figure 4.8 N_2 adsorption-desorption isotherm of (a) SBA-15, (b) 10%Ni-SBA-15 and (c) 10%Ru-SBA-15

Pore size distribution of 10%Ni-SBA-15 and 10%Ru-SBA-15 were shown in Figure 4.9 (b) and Figure 4.9 (c), respectively. Both of samples performed a narrow distribution with the pore size of 9.23 nm. By comparing to the pore size distribution of pure silica SBA-15 as shown in Figure 4.9 (a), the pore size of 10%Ni-SBA-15 and 10%Ru-SBA-15 samples still remained unchanged, indicating the stability of metal-SBA-15.

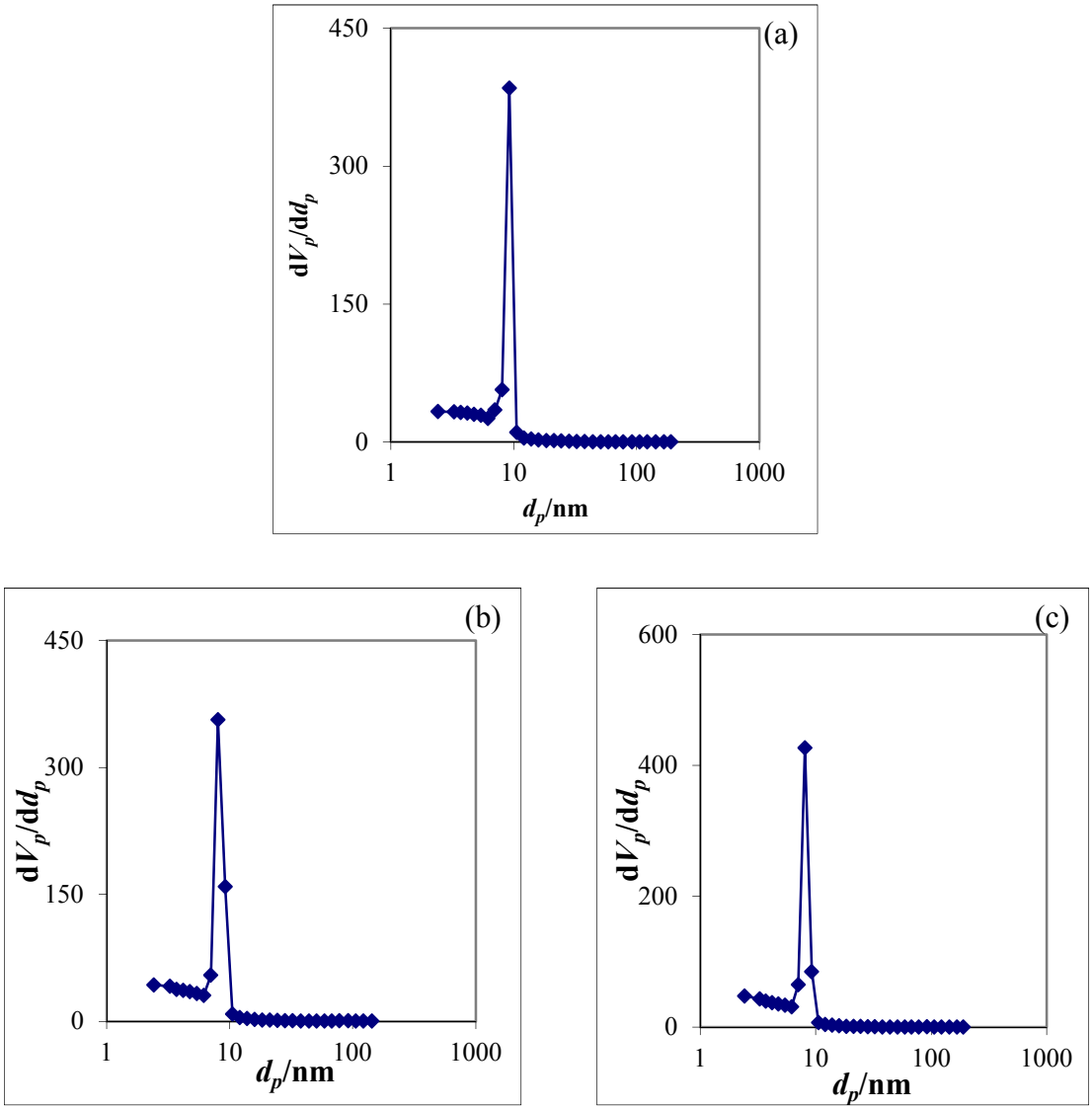

Figure 4.9 BJH-Pore size distributions of (a) SBA-15, (b) 10%Ni-SBA-15, and (c) 10%Ru-SBA-15.

Textural properties of SBA-15, 10%Ni-SBA-15, and 10%Ru-SBA-15 samples were shown in Table 4.3. The data showed $d_{(100)}$ spacing of metal-SBA-15 close to that of pure silica SBA-15. Then the additional of Ni and Ru did not disrupt the mesoscopic hexagonal ordering classical of SBA-15. As observed, the wall thickness increased when metal was added, related to mesopore volume and specific surface area were decreased. The surface area of the Ni supported catalyst was slightly lower than that of corresponding Ru supported catalyst, it may be the dispersions of Ru particles greater than Ni particles.

Table 4.3 Textural properties of SBA-15 and metal-SBA-15.

Catalyst	Total specific surface area[a] ($m^2 \cdot g^{-1}$)	Pore size distribution[b] (nm)	Mesopore volume[b] ($cm^3 \cdot g^{-1}$)	$d_{(100)}$[c] (nm)	Wall thickness[d] (nm)
SBA-15	809.30	9.23	1.0270	9.82	2.11
10%Ni-SBA-15	598.68	9.23	0.9247	10.32	2.68
10%Ru-SBA-15	656.50	9.23	0.9175	10.34	2.71

[a]Calculated using the BET plot method,
[b]Calculated using the BJH method,
[c]Calculated using XRD, Jade5.6,
[d]Calculated as: a_0-pore size ($a_0 = 2 \times d_{(100)} / \sqrt{3}$)

4.1.2.3 SEM images

The SEM images of metal-SBA-15 catalysts were shown in Figure 4.10. When compared to the pure silica SBA-15, both 10%Ni-SBA-15 and 10%Ru-SBA-15 performed small rod aggregated particles. From metal addition, rope-liked agglomerates of SBA-15 were separated as small rod particles in metal-SBA-15. Nevertheless, the rod shape of individual particle remained the same as pure silica SBA-15.

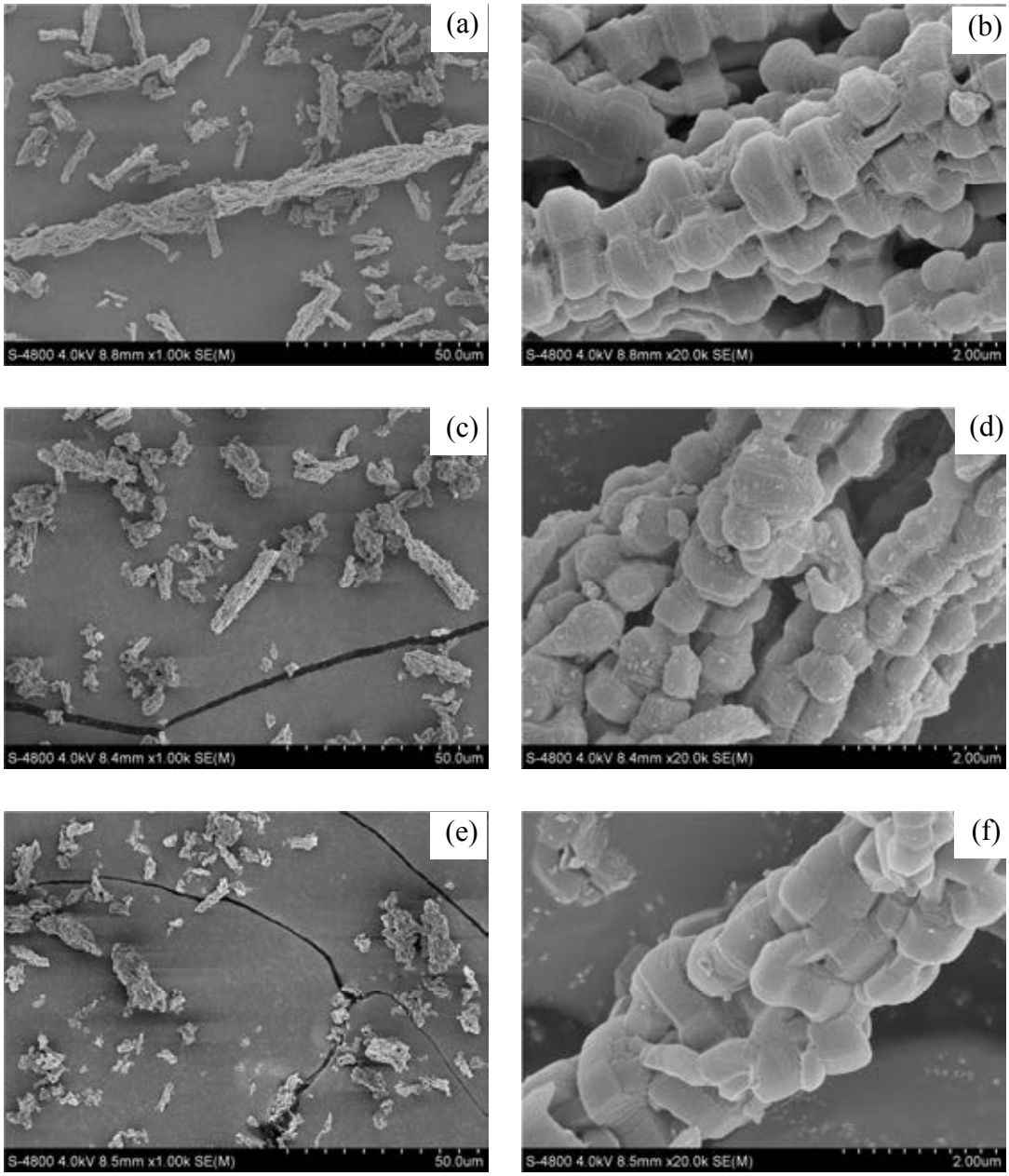

Figure 4.10 SEM images of (a) SBA-15 ×5000, (b) SBA-15 ×20000, (c) 10%Ni-SBA-15 ×5000, (d) 10%Ni-SBA-15 ×20000, (e) 10%Ru-SBA-15 ×5000, and (f) 10%Ru-SBA-15 ×20000

4.1.2.4 TEM images

All the presented microstructure of metal-SBA-15 were examined by TEM as shown in Figure 4.11. The TEM images proved that the location of metallic particles where placing outside the channels of the SBA-15 [11, 15]. TEM images suggested that metal impregnation method could not bring all of metal particles into the pores of SBA-15, most of them existed on the external surface where minority of the silanol groups locates, could observe from dark spots of metal particles on catalyst surface. In comparison Figure 4.11(b) and 4.11(c), observed that the fine Ru particles greater extended as tiny particles than Ni particles.

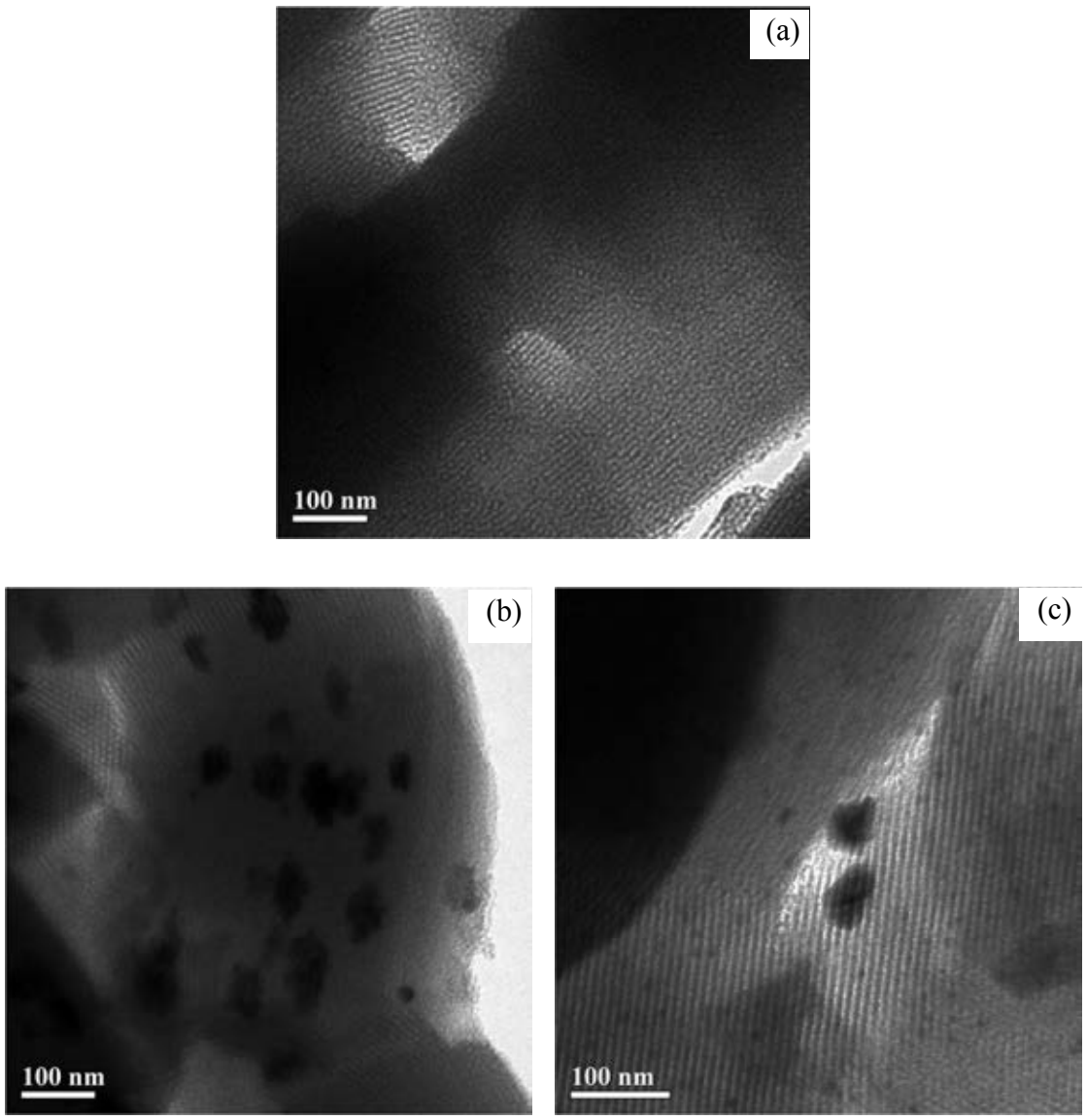

Figure 4.11 TEM images of (a) SBA-15 ×40000, (b) 10%Ni-SBA-15 ×40000, and (c) 10%Ru-SBA-15 ×40000.

4.1.2.5 Elemental analysis and acid-base titration

The percentage of Ni and Ru loaded in the SBA-15 after calcination were measured by EDX method and the number of proton in the mesoporous silica were measured quantitatively by acid-base titration, the results were shown in Table 4.4. The value from EDX showed metal containing in SBA-15 less than amount of metal in loading solution (10 wt.%) for both of Ni and Ru as 4.87% and 5.21%, respectively due to limitation of EDX analysis method indicated the metal particles had not well dispersion on catalyst surface. From metal loading result, the acid value of metal-SBA-15 were higher than SBA-15. In addition, the 10%Ru-SBA-15 presented more acidic than 10%Ni-SBA-15 because have more metal particles on catalyst.

Table 4.4 EDX analysis and acid value of SBA-15 and Al-SBA-15.

Catalysts	Ni [a] (wt.%)	Ru [a] (wt.%)	H^+ content[b] (mmol/g)
SBA-15	-	-	0.23
10%Ni-SBA-15	4.87	-	0.30
10%Ru-SBA-15	-	5.21	0.34

[a]EDX measurements,
[b]Acid capacity defined as millimole of acid centers per gram of catalyst, obtained directly by titration (mmol H^+/g).

4.1.3 The physico-chemical properties of metal (Ni and Ru) supported on aluminium functionalized SBA-15 (metal-Al-SBA-15)

4.1.3.1 XRD results

The metal loaded Al-SBA-15 samples were prepared by wet impregnation method. The XRD patterns of Al-SBA-15, 10%Ni-Al-SBA-15, 10%Ru-Al-SBA-15, and 20%Ru-Al-SBA-15 were shown in Figure 4.12. All of materials suggesting that the long-range periodicity order of the SBA-15 pore structure was maintained. The metal-Al-SBA-15 materials exhibited decreasing intensity of the (100) reflection plane when comparing to Al-SBA-15 indicated that the crystallinity was lower which may be cause by the metal particles located on the Al-SBA-15 and some Si or Al atoms were leached from

framework. The peak intensity of 20%Ru-Al-SBA-15 was much weaker than those of the other samples. It could deduce that the long-range order of the hexagonally ordered porosity may be significantly lowered [64].

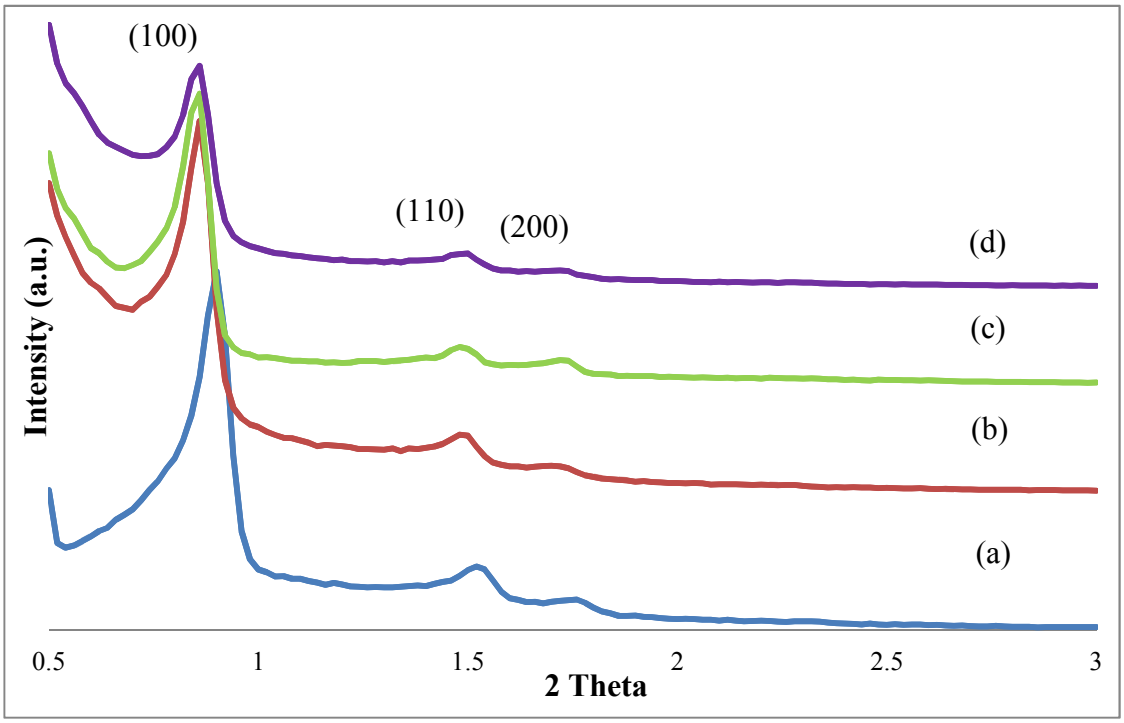

Figure 4.12 X-ray powder diffraction patterns of (a) Al-SBA-15, (b) 10%Ni-Al-SBA-15, (c) 10%Ru-Al-SBA-15, and (d) 20%Ru-Al-SBA-15.

4.1.3.2 Sorption properties of metal-Al-SBA-15

Figure 4.13 depicted the N_2 adsorption-desorption isotherm of Al-SBA-15 support after successive addition of Ni and Ru. No changes were detected in the form of the isotherms or in the shape of the hysteresis loop indicating the preservation of the support pore structure after Ni and Ru deposition.

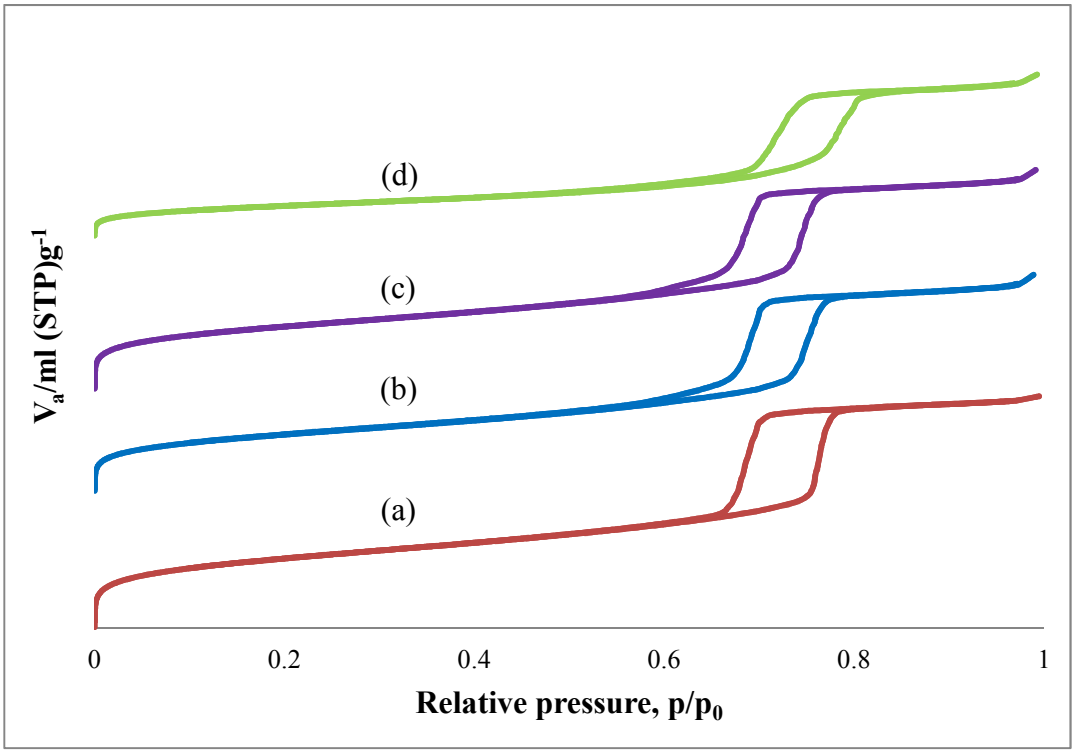

Figure 4.13 N_2 adsorption-desorption isotherm of (a) Al-SBA-15, (b) 10%Ni-Al-SBA-15, (c) 10%Ru-Al-SBA-15, and (c) 20%Ru-Al-SBA-15.

Pore size distribution of Al-SBA-15 and metal-Al-SBA-15 were shown in Figure 4.14. All of samples performed a narrow distribution with the pore size of 9.23 nm. The pore size of all metal-Al-SBA-15 samples still remained unchanged, indicating the stability of metal-Al-SBA-15.

Textural properties of Al-SBA-15, and metal-Al-SBA-15 were shown in Table 4.5. The data showed that mesopore volume and specific surface area were decreased in all of metal loaded materials, and greatly decrease in case of 20%Ru-Al-SBA-15 due to high amount of Ru particles loading in the Al-SBA-15.

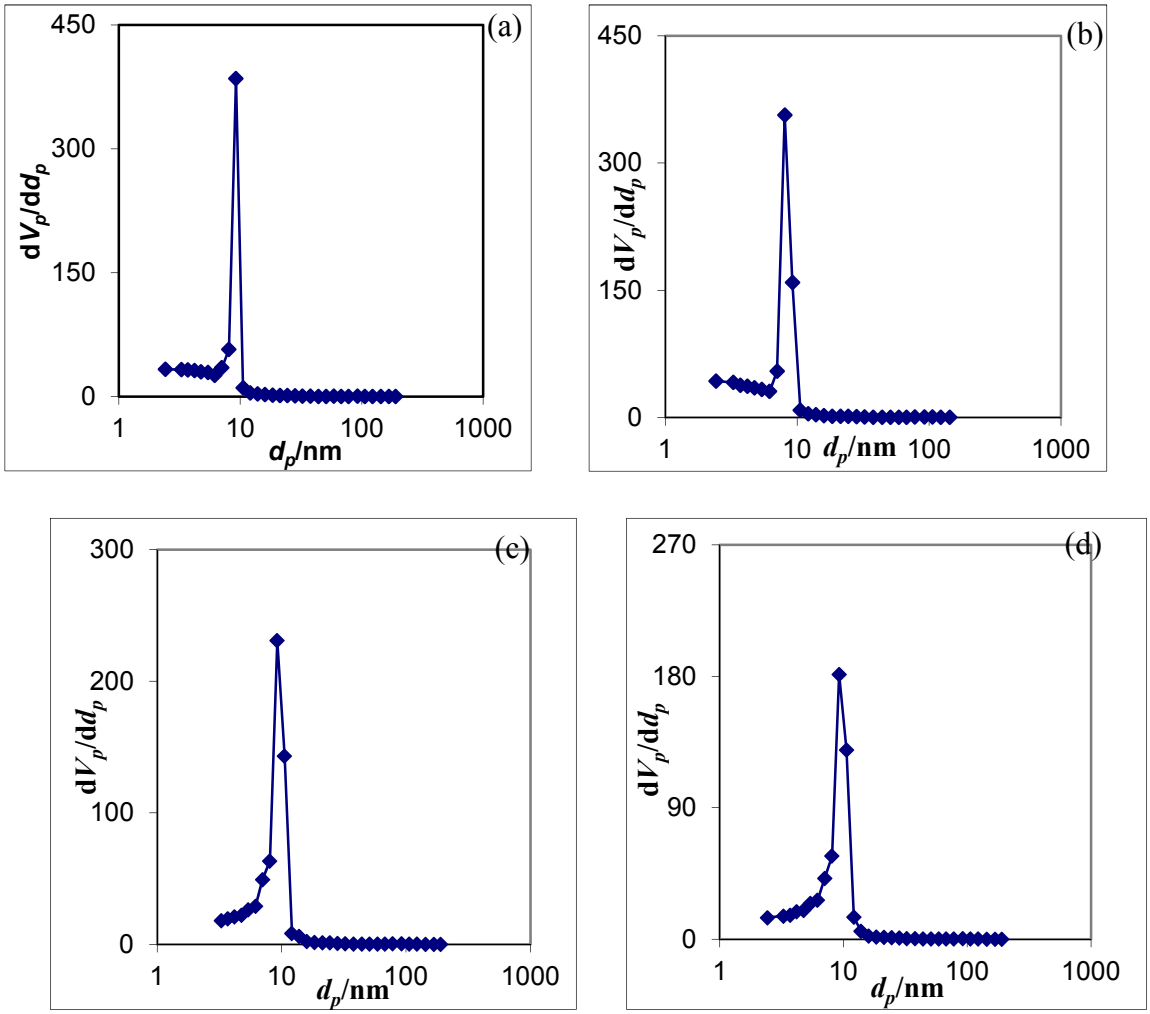

Figure 4.14 BJH-Pore size distributions of (a) Al-SBA-15, (b) 10%Ni-Al-SBA-15, (c) 10%Ru-Al-SBA-15, and (c) 20%Ru-Al-SBA-15.

Table 4.5 Textural properties of Al-SBA-15 and metal-Al-SBA-15.

Catalyst	Total specific surface area[a] ($m^2 \cdot g^{-1}$)	Pore size distribution[b] (nm)	Mesopore volume[b] ($cm^3 \cdot g^{-1}$)	$d_{(100)}$[c] (nm)	Wall thickness[d] (nm)
Al-SBA-15	464.84	9.23	0.9812	9.80	2.08
10%Ni-Al-SBA-15	367.78	9.23	0.8775	10.07	2.40
10%Ru-Al-SBA-15	377.54	9.23	0.8244	10.08	2.41
20%Ru-Al-SBA-15	327.73	9.23	0.7225	10.31	2.67

[a]Calculated using the BET plot method,
[b]Calculated using the BJH method,
[c]Calculated using XRD, Jade5.6,
[d]Calculated as: a_0-pore size ($a_0 = 2 \times d_{(100)} / \sqrt{3}$)

4.1.3.3 SEM images

The SEM images of metal-Al-SBA-15 catalysts were showed in Figure 4.15. When compared to the Al-SBA-15 (Figure 4.4(c-d)), all of metal-Al-SBA-15 catalysts performed smaller rod aggregated particles in range of 10 - 15 μm. From metal addition, the small rod particles were separated from the rod-liked agglomeration. Nevertheless, the rod shape of individual particle remained the same as pure silica SBA-15 and Al-SBA-15.

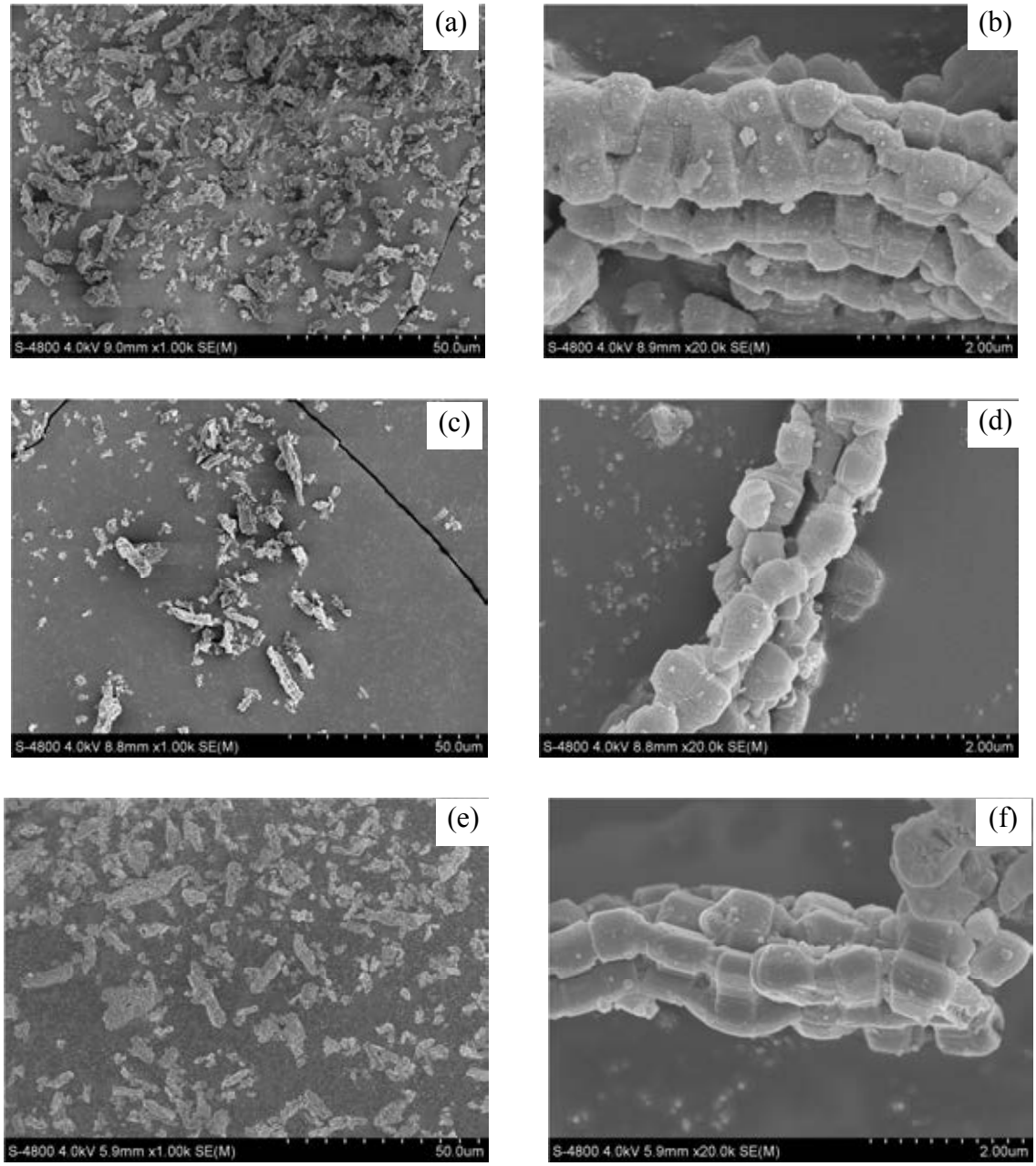

Figure 4.15 SEM images of (a) 10%Ni-Al-SBA-15 ×5000, (b) 10%Ni-Al-SBA-15 ×20000, (c) 10%Ru-Al-SBA-15 ×5000, (d) 10%Ru-Al-SBA-15 ×20000, (e) 20%Ru-Al-SBA-15 ×5000, and (f) 20%Ru-Al-SBA-15 ×20000.

4.1.3.4 TEM images

The TEM technique was used to investigate the effects of metal loading and microstructure of metal-Al-SBA-15 as shown in Figure 4.16, an additional TEM images of Al-SBA-15 were also included for comparison purpose. In comparison, observed that Ru metal shown fine particles that greater dispersion than Ni particles. Figure 4.16(c) showed the dispersion of 10%Ru particles on Al-SBA-15 was rather higher than that of 10%Ni particles (Figure 4.16(b)) and 20%Ru particle on Al-SBA-15 (Figure 4.16(d)). The 20%Ru-Al-SBA-15 was lower dispersion than 10%Ru-Al-SBA-15 because contained more metal particles. However, 20%Ru-Al-SBA-15 was higher dispersion than 10%Ni-Al-SBA-15 althought contained the higher percentage of metal particles.

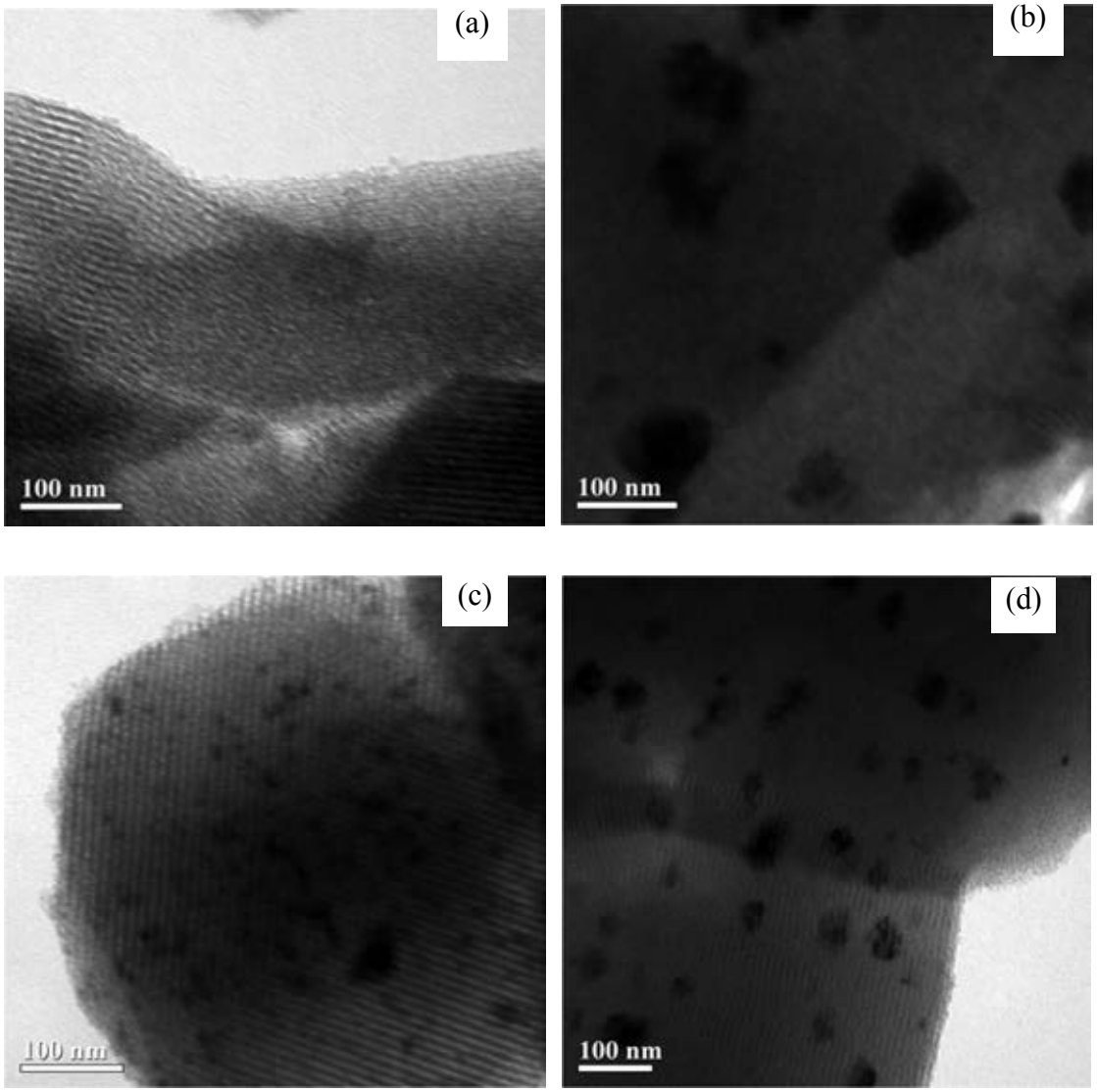

Figure 4.16 TEM images of (a) Al-SBA-15 ×60000, (b) 10%Ni-Al-SBA-15 ×60000, (c) 10%Ru-Al-SBA-15 ×60000, and (d) 20%Ru-Al-SBA-15 ×60000.

4.1.3.5 Elemental analysis and acid-base titration

In EDX method was used to measure percent of Ni and Ru in Al-SBA-15 and metal-Al-SBA-15 materials and the number of proton were measured quantitatively by acid-base titration, the results were shown in Table 4.6. It might be cause by aluminium incoporation in the SBA-15 material resulted in a better dispersion of Ru due to the strong interaction of Ru species with aluminium atoms serve as anchoring sites on the support surface. The amount of Ru loaded on Al-SBA-15 was higher than that of Ni amount as 5.42 and 3.88%, respectively. When increase the amount of Ru in solution as 20 wt.%, the Ru matal on Al-SBA-15 was increasing as 8.46%. Therefore, the highest acidity was obtained as 0.81 mmol/g of 20%Ru-Al-SBA-15 and decresed as in the order of 10%Ru-Al-SBA-15 (0.64 mmol/g) > 10%Ni-Al-SBA-15 (0.53 mmol/g) > Al-SBA-15 (0.45 mmol/g).

Table 4.6 EDX analysis and acid value of Al-SBA-15 and metal-Al-SBA-15.

Catalyst	Ni [a] (wt.%)	Ru [a] (wt.%)	H^+ content[b] (mmol/g)
Al-SBA-15	-	-	0.45
10%Ni-Al-SBA-15	3.88	-	0.53
10%Ru-Al-SBA-15	-	5.42	0.64
20%Ru-Al-SBA-15	-	8.46	0.81

[a]EDX measurement,
[b]Acid capacity defined as millimole of acid centers per gram of catalyst, obtained directly by titration (mmol H^+/g).

4.1.3.6 ^{27}Al-MAS-NMR spectra of metal-Al-SBA-15

Figure 4.17 showed ^{27}Al-MAS-NMR spectra of the metal-Al-SBA-15 materials. The results clearly showed the simultaneous presence of both tetrahedral and octahedral coordinated aluminium species. Tetrahedral Al species were more abundant in all metal-Al-SBA-15 materials, it revealed the ratio of tetrahedral : octahedral decreased in order of Al-SBA-15 (1.00 : 0.20) > 10%Ni-Al-SBA-15 (1.00 : 0.23) > 10%Ru-Al-SBA-15 (1.00 : 0.27) > 20%Ru-Al-SBA-15 (1.00 : 0.40), indicated that the proportion of tetrahedral aluminium species decreased when amount of metal loading was increased.

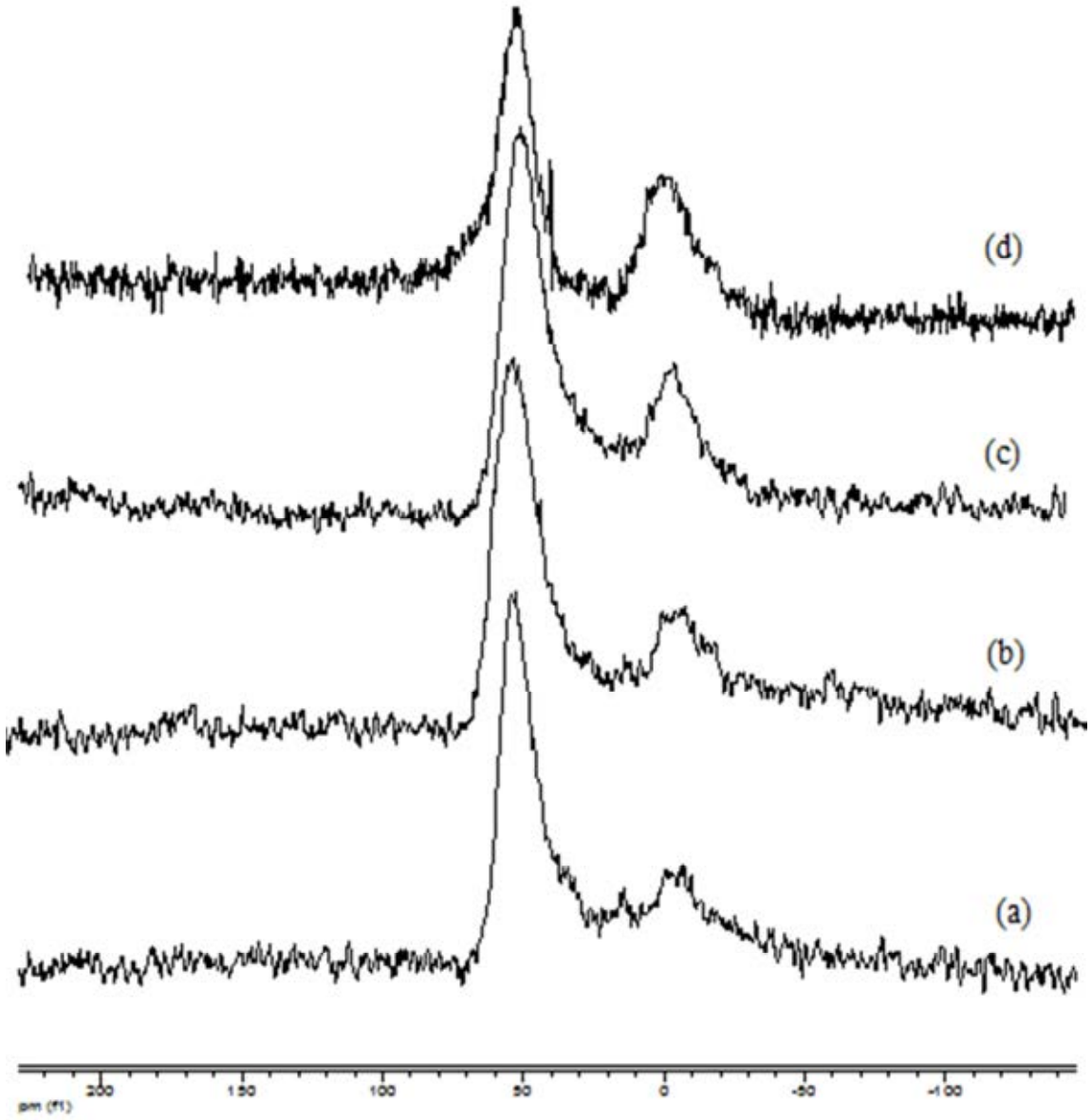

Figure 4.17 ^{27}Al-MAS-NMR spectra of (a) Al-SBA-15, (b) 10%Ni-Al-SBA-15, (c) 10%Ru-Al-SBA-15, and (d) 20%Ru-Al-SBA-15.

4.2 Modification of ZSM-5

4.2.1 The physico-chemical properties of metal supported ZSM-5 (20%Ru-ZSM-5)

4.2.1.1 XRD results

Figure 4.18 showed the XRD spectra of two different catalysts, ZSM-5 and 20%Ru-ZSM-5. Both samples showed the typical characteristic pattern of MFI structure [65]. The intensity of 20%Ru-ZSM-5 diffraction peaks was decreased by comparison with that of ZSM-5 indicating that the crystallinity was decreased because there were Ru particles located on ZSM-5 framework but the MFI structure still remained after loading the Ru particles on the ZSM-5.

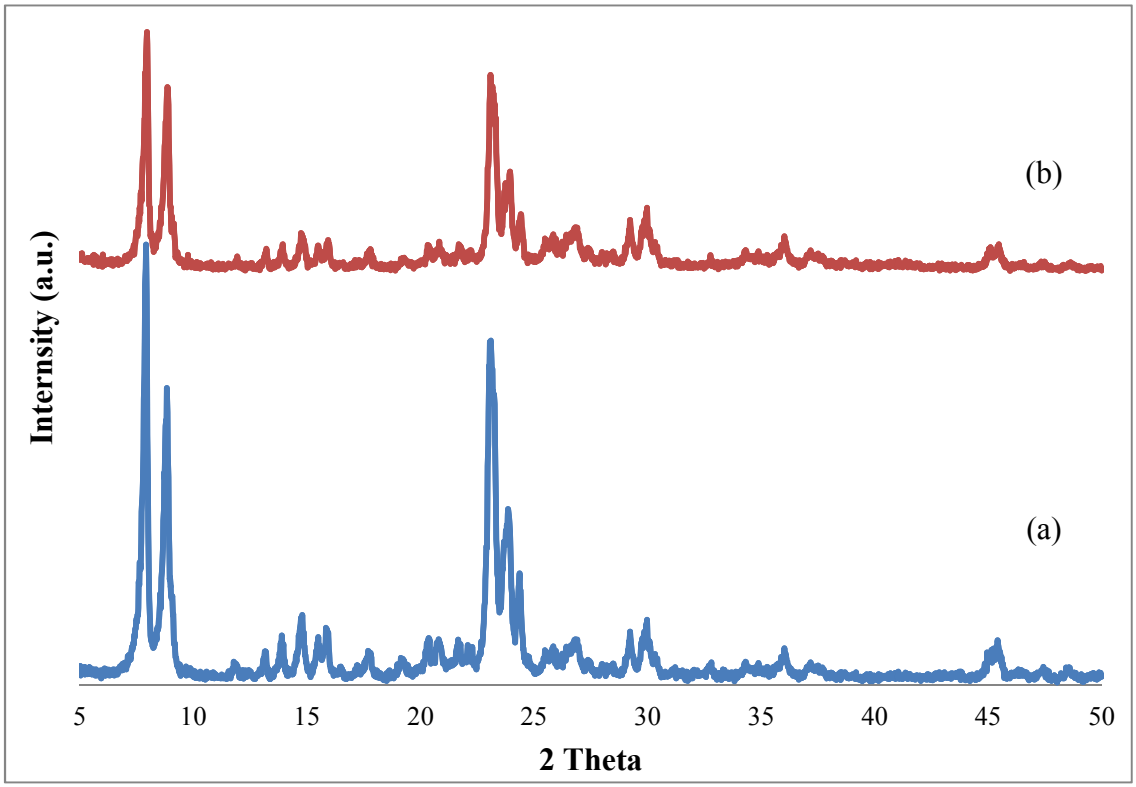

Figure 4.18 X-ray powder diffraction patterns of (a) ZSM-5, and (b) 20%Ru-ZSM-5.

4.2.1.2 Sorption properties of ZSM-5 and 20% Ru-ZSM-5

The N_2 adsorption-desorption isotherms of the calcined ZSM-5 and 20%Ru-ZSM-5 were shown in Figure 4.19. The samples exhibited a type I isotherm, characteristic of microporous material [67]. Both of isotherm exhibited the same three adsorption zones. The first zone observed at very low partial pressures, corresponds to the N_2 adsorption in the ZSM-5 micropore system. The second zone at medium partial pressures was the saturation indicating the completion of pore filling with N_2 molecules. The third zone at high relative pressure ($P/P_0 > 0.8$), was the adsorption on the external surface. The textural properties of both samples were listed in Table 4.7. The internal and external surface area of 20%Ru-ZSM-5 were lower than parent ZSM-5 because there were Ru particles loaded on zeolite surface and blocked pore, the total specific surface area of 20%Ru-ZSM-5 was also lower than ZSM-5. However, both samples showed the same pore size of 0.6 nm which was the average size of the ZSM-5 structure.

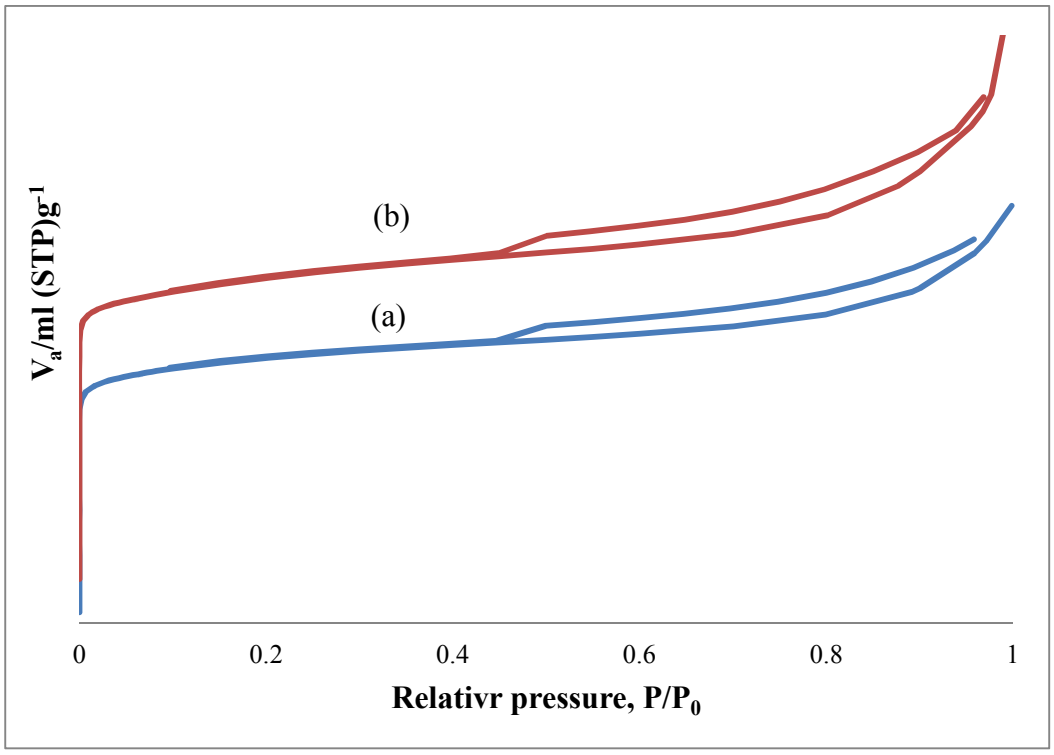

Figure 4.19 N_2 adsorption-desorption isotherms of (a) ZSM-5, (b) 20%Ru-ZSM-5.

Table 4.7 Textural properties of ZSM-5 and 20%Ru-ZSM-5.

Catalyst	Total specific surface area[a] ($m^2 \cdot g^{-1}$)	Pore size distribution[b] (nm)	External surface area[c] ($m^2 \cdot g^{-1}$)	Internal surface area ($m^2 \cdot g^{-1}$)
ZSM-5	370	0.6	72	298
20%Ru-ZSM-5	312	0.6	46	266

[a]Calculated using the BET plot method,
[b]Calculated using the MP-plot method,
[c]Calculated using t-plot method

4.2.1.3 SEM images

SEM images of ZSM-5 and 20%Ru-ZSM-5 were shown in Figure 4.20. The 20%Ru-ZSM-5 particle was aggregated to the bigger crystal size after Ru metal doping (Figure 4.20(c)). At high magnification, it could be observed that there was no effect of metal impregnation on morphology of the zeolite sample.

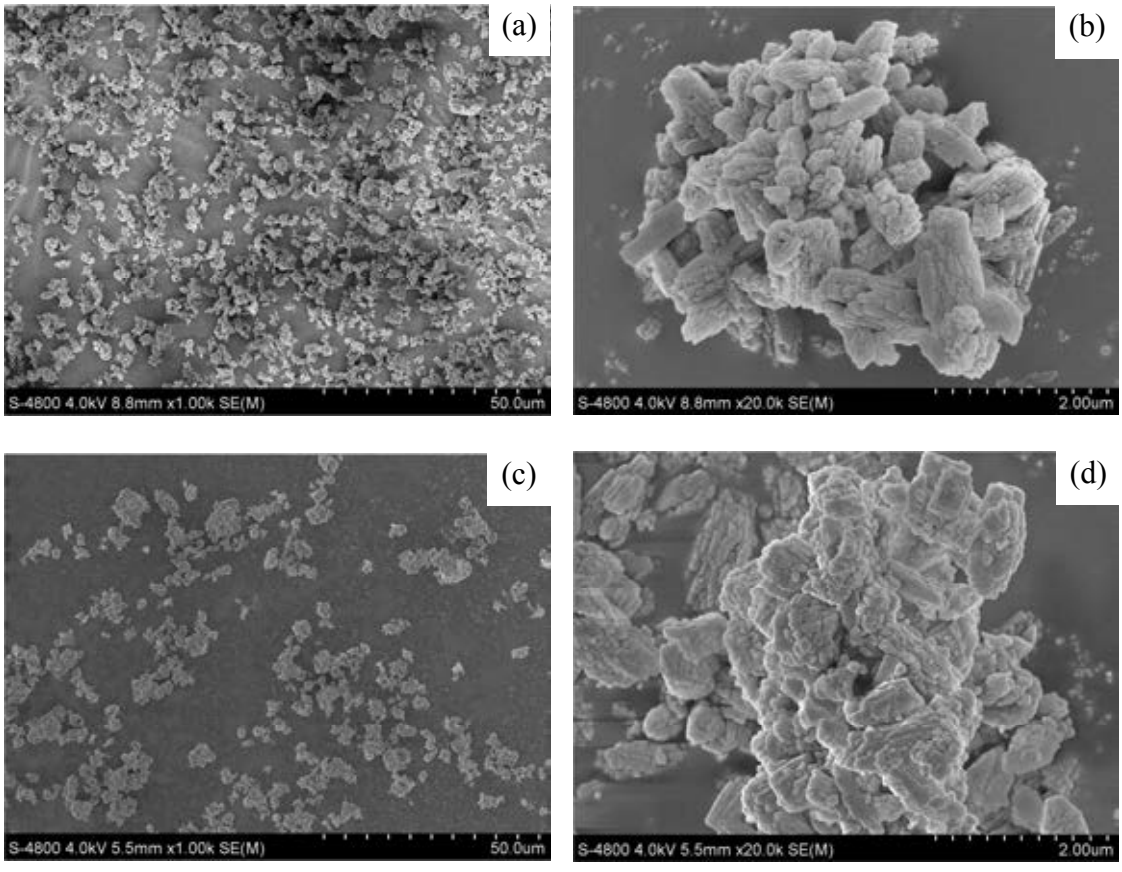

Figure 4.20 SEM images of (a) ZSM-5 ×5000, (b) ZSM-5 ×20000, (c) 20%Ru-ZSM-5 ×5000, (d) 20%Ru-ZSM-5 ×20000.

4.2.1.4 Elemental analysis and acid-base titration

The EDX method was used to measure content of Ru metal on 20%Ru-ZSM-5 as percentage and the number of proton was measured quantitatively by acid-base titration, the results were shown in Table 4.8. The Ru particles were located on ZSM-5 equal to 7.05 wt.%, less than amount of metal solution loading (20 wt.%) due to limitation of EDX analysis method indicated the metal particles had not well dispersion on catalyst surface. The Ru loaded on ZSM-5 increased acidic property of ZSM-5 from 0.51 to 0.71 mmol/g.

Table 4.8 EDX analysis and acid value of ZSM-5 and 20%Ru-ZSM-5.

Catalysts	**Ru** [a] **(wt.%)**	**H^+ content**[b] **(mmol/g)**
ZSM-5	-	0.51
20%Ru-ZSM-5	7.05	0.71

[a]EDX measurements,
[b]Acid capacity defined as millimole of acid centers per gram of catalyst, obtained directly by titration (mmol H^+/g).

4.2.1.5 ^{27}Al-MAS-NMR spectra of ZSM-5 and 20% Ru-ZSM-5

Figure 4.17 showed ^{27}Al-MAS-NMR spectra of 20%Ru-ZSM-5 compared with ZSM-5. The results showed the simultaneous presence of both tetrahedral and octahedral coordinated aluminium species. Tetrahedral Al species were more abundant in both of them but the ratio of tetrahedral : octahedral in ZSM-5 (1.00 : 0.17) was higher than 20%Ru-ZSM-5 (1.00 : 0.37), indicated that the proportion of tetrahedral coordinated decreased when obtained the amount of Ru metal loading on ZSM-5, same as the results of metal-Al-SBA-15.

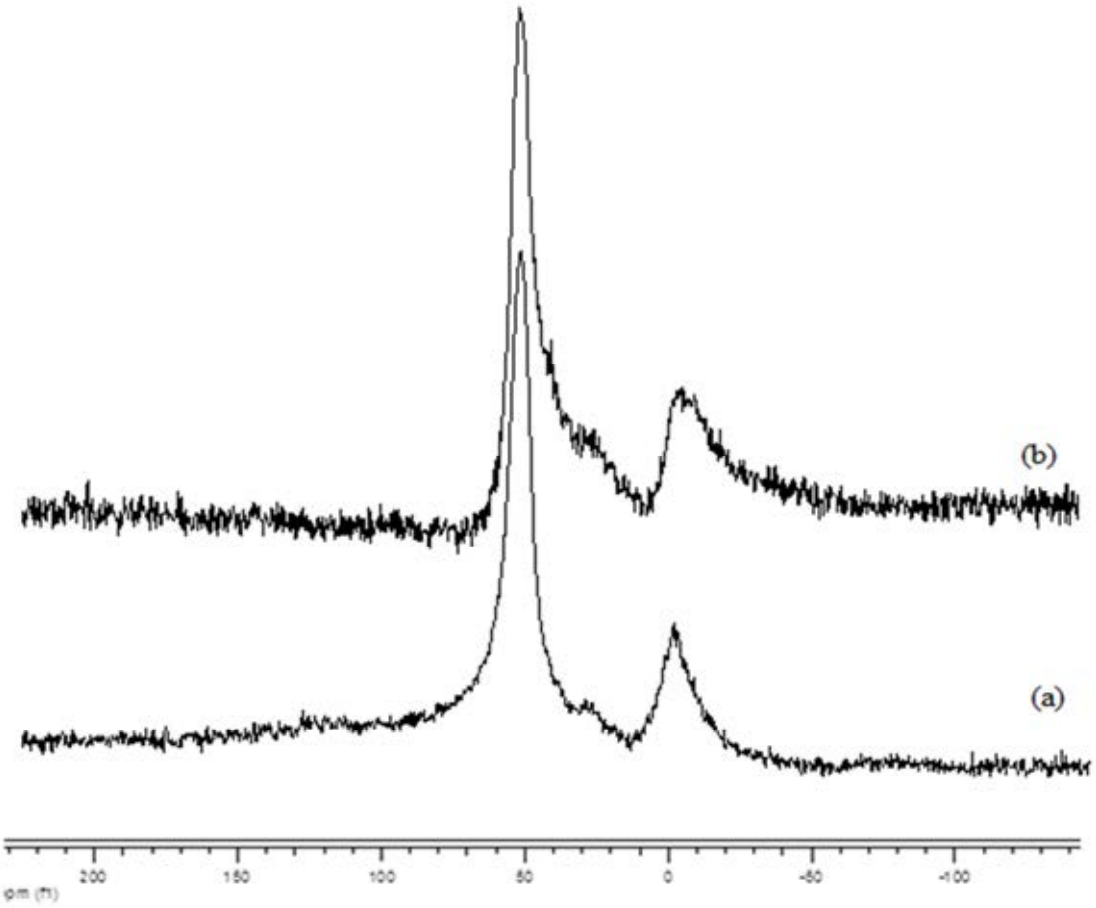

Figure 4.21 ^{27}Al-MAS-NMR spectrum of (a) ZSM-5, and (b) 20%Ru-ZSM-5.

4.3 Catalytic activities of ZSM-5 and SBA-15 derivatives in hydrothermolysis of carbohydrates

The obtained catalysts were tested in the hydrothermolysis of carbohydrates in order to determine their catalytic properties in terms of both activity and selectivity. In this work, the 10 wt.% of ZSM-5 was used as a model catalyst to investigate an optimal reaction temperature that gave the highest yield of LA in liquid product of each starting material. The catalytic performances of metal-Al-SBA-15 were evaluated in the optimum conditions of carbohydrate hydrothermolysis.

4.3.1 Effect of reaction temperature

The prime attention was put on reaction temperature. The 10 wt.% of ZSM-5 was selected to determine the effect of reaction temperature. The experiments were conducted at three reaction temperatures of 200, 250, and 300°C.

4.3.1.1 Glucose reaction

The product yields of glucose hydrothermolysis at various reaction temperatures were in Table 4.9. All of the reaction temperatures exhibited high yield of liquid product (85-88%) with low yield of residue (4-6%). The liquid product yield of glucose was insignificantly affected by the reaction temperatures in the range 200-300°C. Figure 4.22 showed the influence of reaction temperature on the selectivity of liquid product. When the temperature was raised from 200 to 300°C in catalytic reaction, the LA selectivity was decreased from 34.2 to 12.5%. It was probably due to LA conversion to other products. Hence, the highest LA yield was obtained at a reaction temperature of 200°C then this temperature was selected to be used in glucose reaction for other reaction parameter effects.

Table 4.9 Product yields from glucose hydrothermolysis at various reaction temperatures (Condition: 10 wt.% ZSM-5 of starting material, reaction time 1 h, 10 bar N_2)

Yield (%)	200°C		250°C		300°C	
	Non catalyst	ZSM-5	Non catalyst	ZSM-5	Non catalyst	ZSM-5
[a]Gas	6.1	7.6	7.1	8.8	7.8	10.3
[b]Liquid	87.9	87.4	87.3	87.0	87.7	85.8
[c]Residue	6.0	5.0	5.6	4.2	4.5	3.9

[a]Deviation within 1.00%
[b]Deviation within 1.17%
[c]Deviation within 0.93%

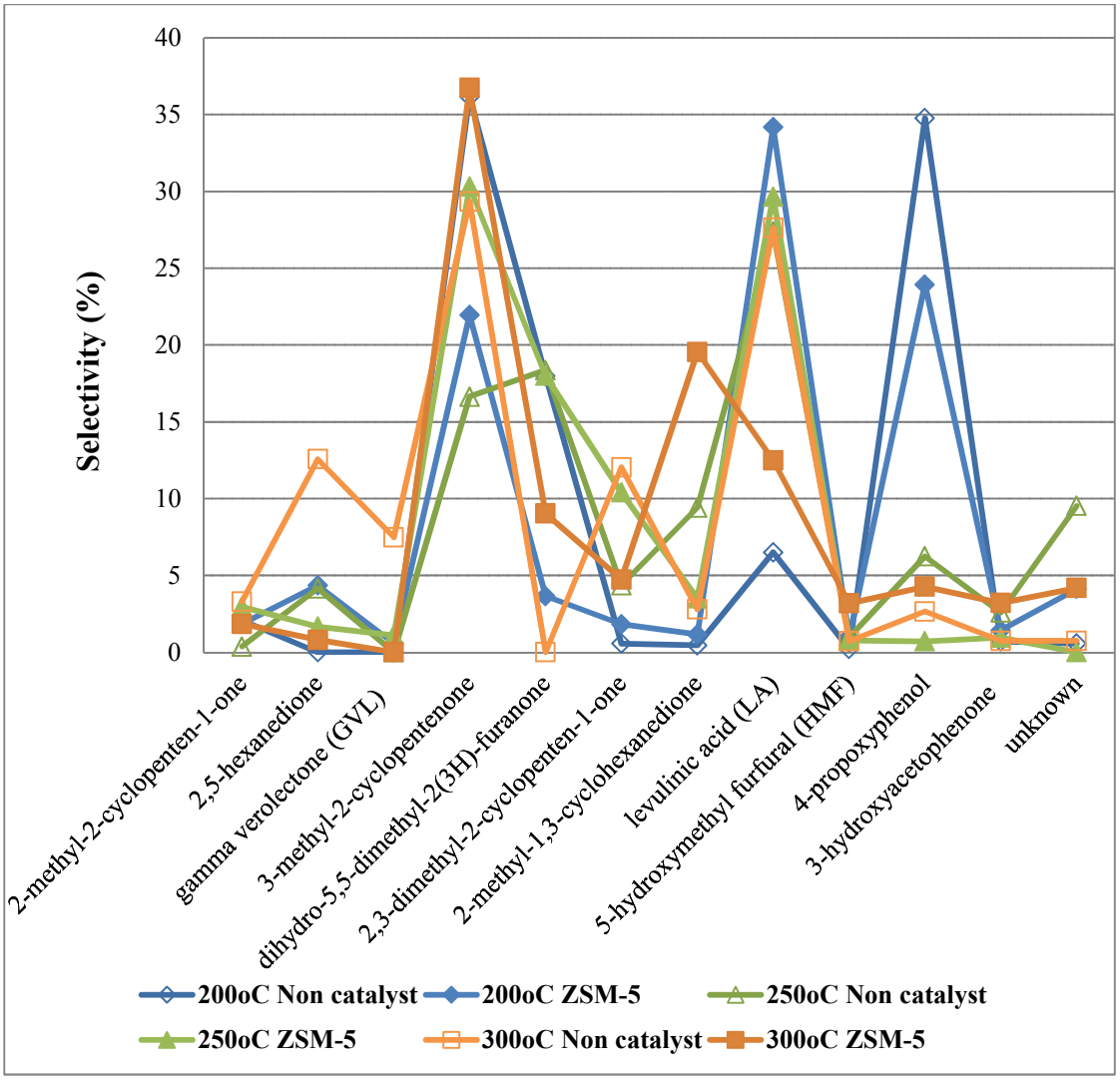

Figure 4.22 Liquid product selectivity of glucose hydrothermolysis at various reaction temperatures (Condition: 10 wt.% ZSM-5 of starting material, reaction time 1 h, 10 bar N_2)

4.3.1.2 Sucrose reaction

Figure 4.22 showed the influence of reaction temperature on selectivity of liquid product from sucrose hydrothermolysis over ZSM-5. The LA selectivity from sucrose was approximately 26% at all temperatures for catalytic reactions. Indicate that the reaction temperature in range 200-300°C had no influence on LA yield from sucrose reaction. The product yields of sucrose hydrothermolysis at various reaction temperatures were in Table 4.10. For all cases, the products were mainly in liquid product at the yield above 87% with less residue in range 4-8%. Consequently, a reaction temperature of 200°C was selected for sucrose hydrothermolysis.

Table 4.10 Product yields from sucrose hydrothermolysis at various reaction temperatures (Condition: 10 wt.% ZSM-5 of starting material, reaction time 1 h, 10 bar N_2)

Yield (%)	200°C		250°C		300°C	
	Non catalyst	ZSM-5	Non catalyst	ZSM-5	Non catalyst	ZSM-5
[a]Gas	4.8	6.6	2.7	5.1	6.6	7.2
[b]Liquid	89.1	87.4	91.5	89.7	87.6	88.4
[c]Residue	6.1	6.0	5.8	5.2	5.8	4.4

[a]Deviation within 1.03%
[b]Deviation within 1.07%
[c]Deviation within 1.03%

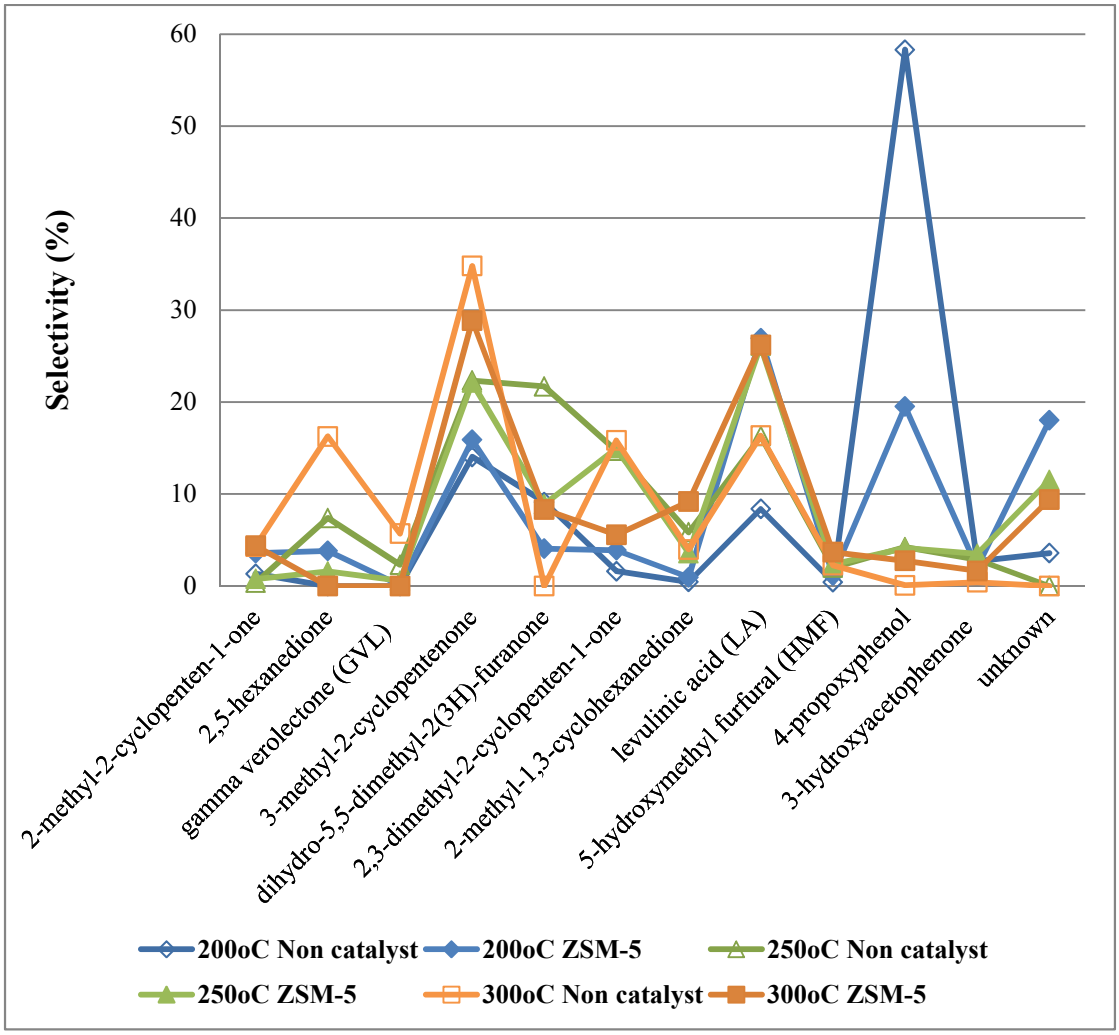

Figure 4.23 Liquid product selectivity of sucrose hydrothermolysis at various reaction temperatures (Condition: 10 wt.% ZSM-5 of starting material, reaction time 1 h, 10 bar N_2)

4.3.1.3 Starch reaction

Table 4.11 showed the product yields of starch hydrothermolysis with various reaction temperatures. All reactions obtained high liquid product yield over 85%. At reaction temperature 250°C, the liquid product yield was highest as 90.8% but produced LA selectivity (29.1%) lower than using reaction temperature at 300°C (35.0%) as showed in Figure 4.23, liquid product selectivity of starch hydrothermolysis at various reaction temperatures. This might be due to the large molecule of starch relied on high temperature to break down its to smaller molecular products. According to these results, the reaction temperature at 300°C was selected to use in starch reaction for the next experiments.

Table 4.11 Product yields from starch hydrothermolysis at various reaction temperatures (Condition: 10 wt.% ZSM-5 of starting material, reaction time 1 h, 10 bar N_2)

[a]Yield (%)	200°C		250°C		300°C	
	Non catalyst	ZSM-5	Non catalyst	ZSM-5	Non catalyst	ZSM-5
[a]Gas	3.8	4.1	5.1	5.3	8.90	9.1
[b]Liquid	90.2	90.5	89.2	90.8	85.7	86.8
[c]Residue	6.0	5.4	5.7	3.9	5.4	4.1

[a]Deviation within 0.96%
[b]Deviation within 0.91%
[c]Deviation within 1.01%

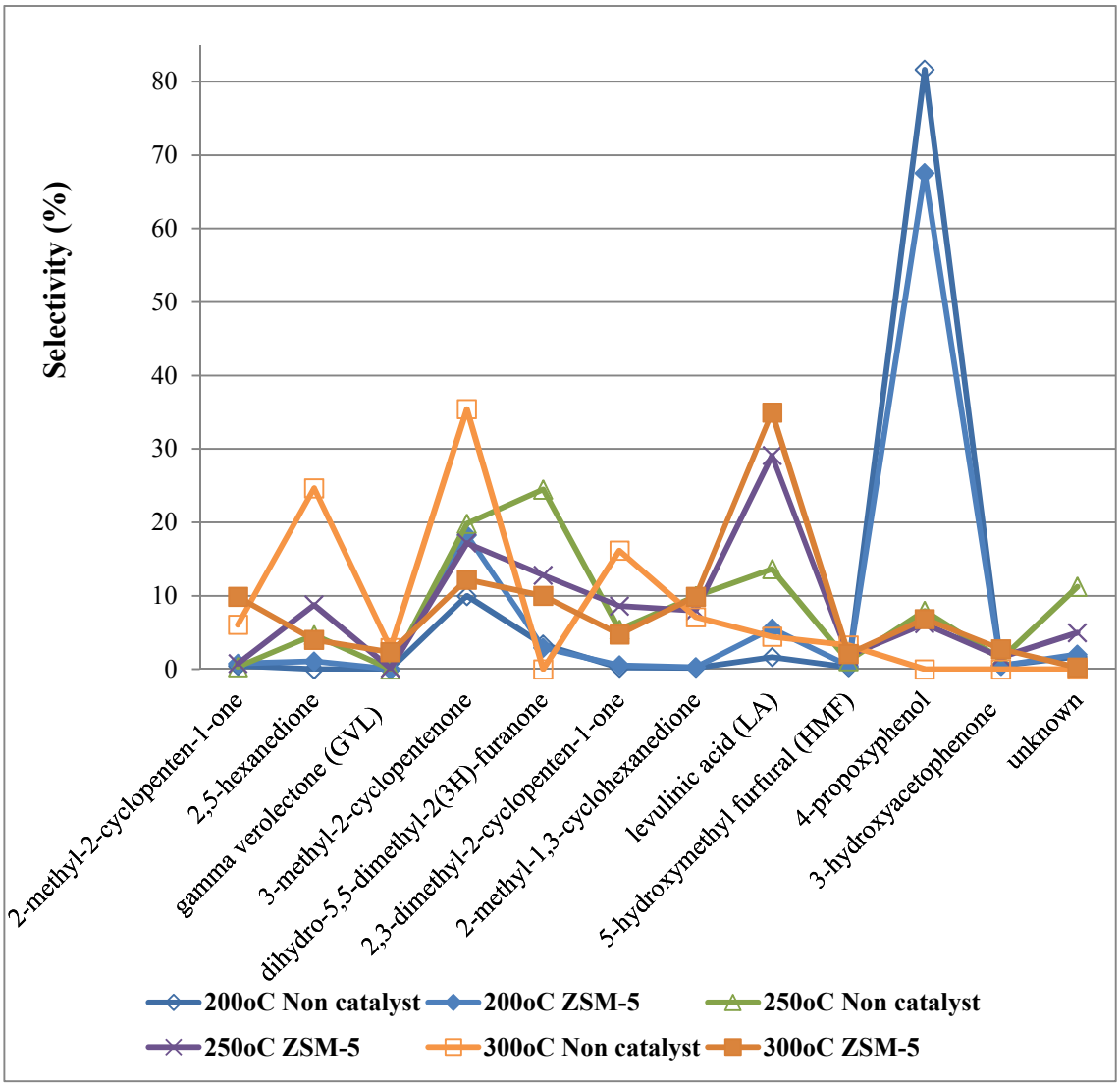

Figure 4.24 Liquid product selectivity of starch hydrothermolysis at various reaction temperatures (Condition: 10 wt.% ZSM-5 of starting material, reaction time 1 h, 10 bar N_2).

4.3.2 Effect of catalytic amount

The effect of catalytic amount on product yield and liquid product selectivity was studied using commercial ZSM-5 at various catalytic amounts of 5, 10, and 15 wt.% of starting material.

4.3.2.1 Glucose reaction

Value of product yields from glucose hydrothermolysis at 200°C with various catalytic amounts were shown in Table 4.12. The highest liquid yield (89.0%) was obtained in case of using 5 wt.% of catalyst, a bit higher than the reaction of 10 wt.% using (87.4%) and 15 wt.% using (87.4%). The gas product yield was increased when higher catalytic amount was used in the range 5-15 wt.% of starting material. The selectivity of liquid products was affected by the catalytic amount as shown in Figure 4.24. The selectivity of LA was risen when higher catalytic amount was used. The amount of 15 wt.% catalyst provided the highest LA yield as 40.1%. As a result, the choice was using 15 wt.% catalytic amount in the next experiments.

Table 4.12 Product yields from glucose hydrothermolysis over ZSM-5 at various catalytic amounts (Condition: 200°C, reaction time 1 h, 10 bar N_2)

Yield (%)	Non catalyst	ZSM-5		
		5 wt.%	10 wt.%	15 wt.%
[a]Gas	6.1	5.2	7.6	8.6
[b]Liquid	87.9	89.0	87.4	87.4
[c]Residue	6.0	5.8	5.0	4.0

[a]Deviation within 1.11%
[b]Deviation within 1.01%
[c]Deviation within 0.63%

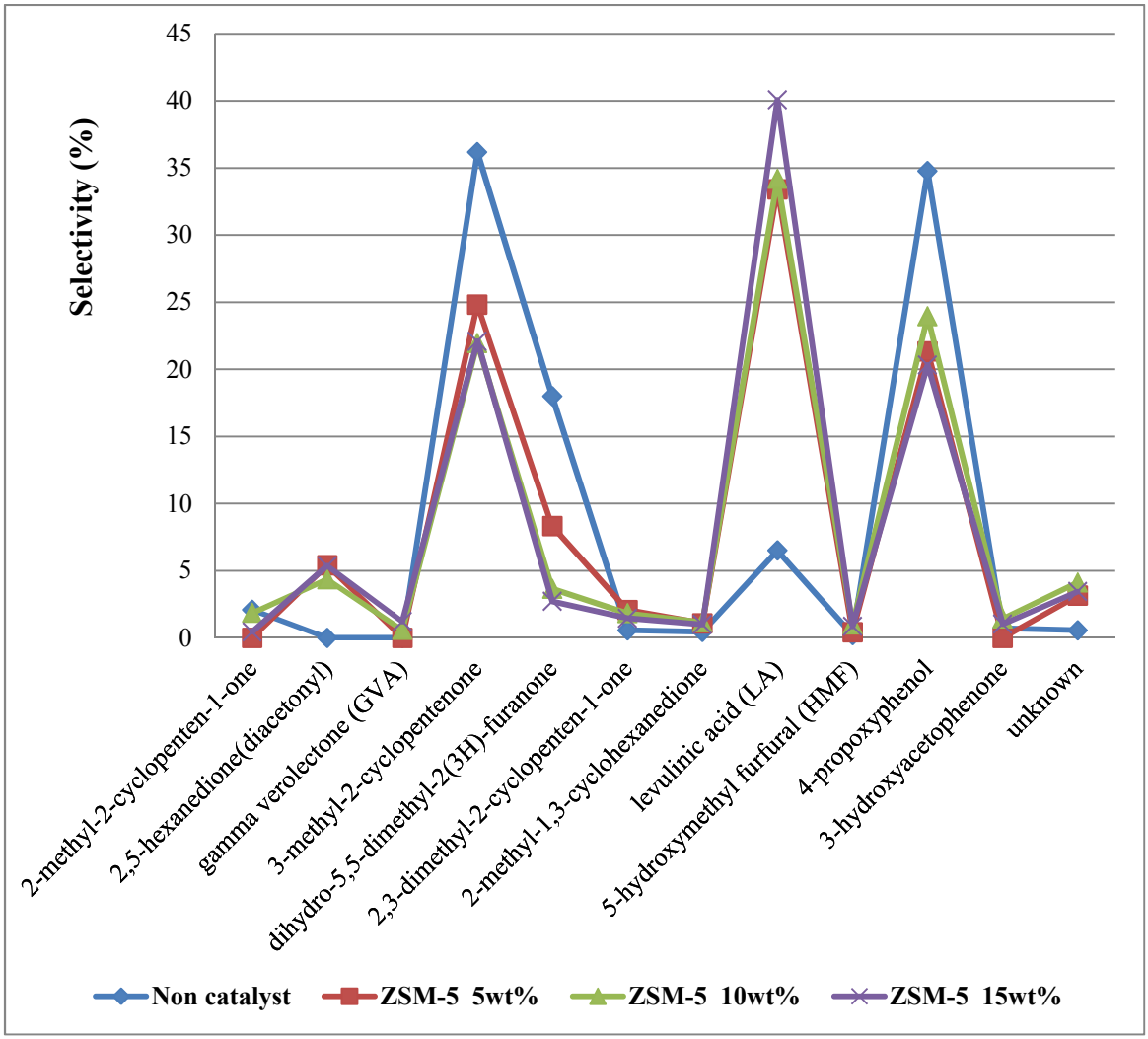

Figure 4.25 Liquid product selectivity of glucose hydrothermolysis at various catalytic amounts (Condition: 200°C, reaction time 1 h, 10 bar N_2).

4.3.2.2 Sucrose reaction

Table 4.13 presented the product yield from sucrose hydrothermolysis with various catalytic amounts at 200°C. The liquid yield of sucrose reaction using the 5 wt.% catalytic amount (88.0%) was not much different from that using 10 (87.4%) and 15 wt.% (87.9%). The selectivity of liquid products was shown in Figure 4.25. The LA selectivity of liquid product for 5 and 10 wt.% catalytic amount were not much different as 23.9 and 26.9%, respectively but showed the significantly difference from that of the 15 wt.%. When 15 wt.% catalytic amount was used, more favor to LA selectivity (37.7%) obtained. Based upon these results, the using catalytic amount in the next sucrose experiments was 15wt.% of the starting material.

Table 4.13 Product yields from sucrose hydrothermolysis over ZSM-5 at various catalytic amounts (Condition: 200°C, reaction time 1 h, 10 bar N_2)

Yield (%)	Non catalyst	ZSM-5		
		5 wt.%	10 wt.%	15 wt.%
[a]Gas	4.8	5.8	6.6	6.7
[b]Liquid	89.1	88.0	87.4	87.9
[c]Residue	6.1	6.2	6.0	5.4

[a]Deviation within 0.83%
[b]Deviation within 0.78%
[c]Deviation within 0.98%

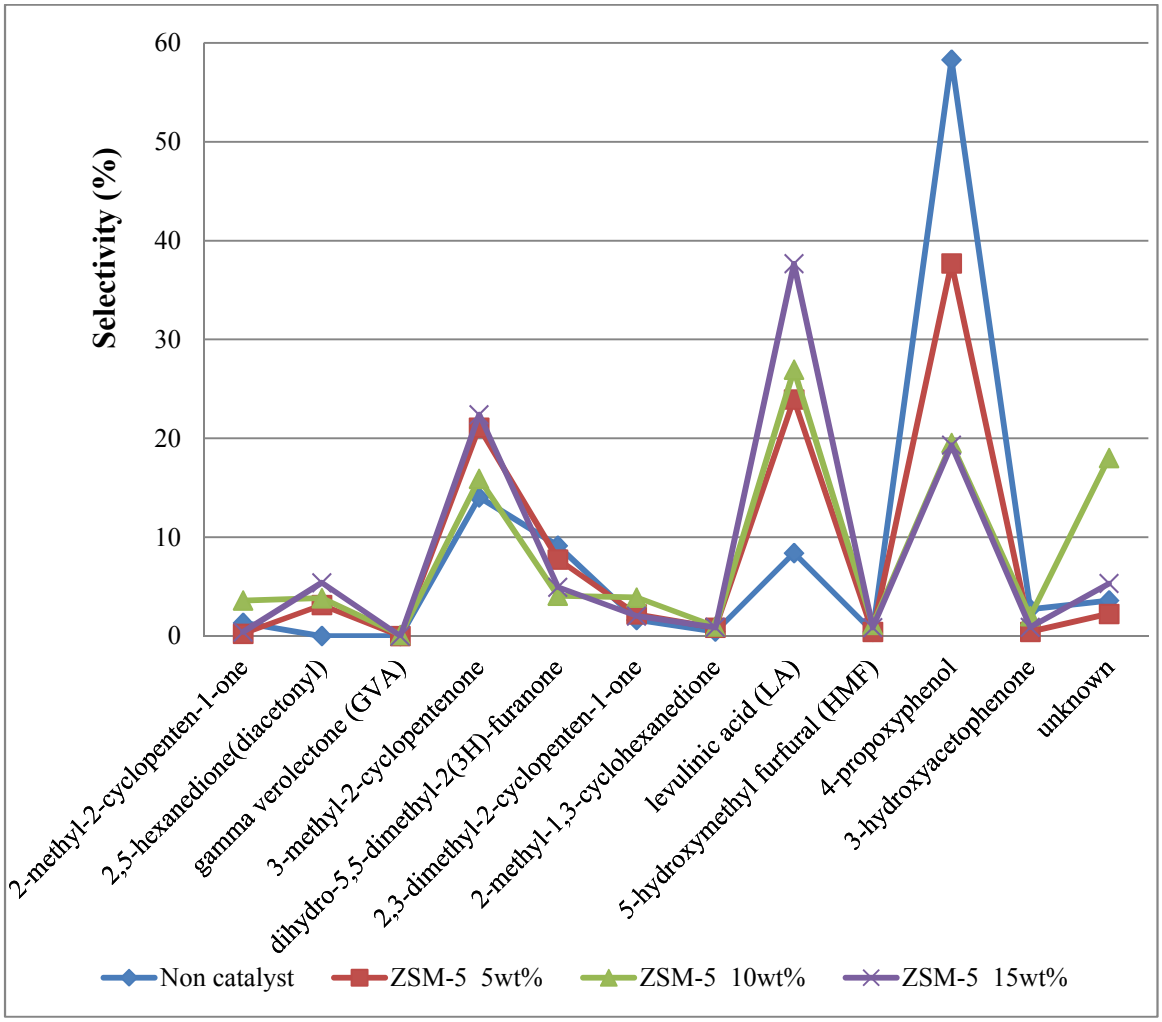

Figure 4.26 Liquid product selectivity of sucrose hydrothermolysis at various catalytic amount (Condition: 200°C, reaction time 1 h, 10 bar N_2).

4.3.2.3 Starch reaction

The effect of the catalytic amount over product yield of starch hydrothermolysis was exhibited in Table 4.14. It was obvious that all of the catalytic amounts have greater volume of liquid product than that of non catalyst reaction. And the using 10 wt.% catalyst gave highest liquid product yield (86.8%). In Figure 4.26 showed the selectivity of liquid product. The LA selectivity increased from 27.8 to 35.0% when more catalytic amount was used from 5 to 10 wt.%. When 15 wt.% of catalyst was utilized, the LA selectivity was decreased a little bit from 35.0% to 33.5% which might be caused by the excess amount of catalyst made the dissolution of starting material became worse. Thereby the used of 10 wt.% catalytic amount gave the highest LA selectivity in case of starch then it was selected to use in next starch hydrothermolysis reactions.

Table 4.14 Product yields from starch hydrothermolysis over ZSM-5 at various catalytic amounts (Condition: 300^{o}C, reaction time 1 h, 10 bar N_2)

Yield (%)	Non catalyst	ZSM-5		
		5 wt.%	10 wt.%	15 wt.%
[a]Gas	8.90	9.1	9.1	9.4
[b]Liquid	85.6	86.0	86.8	86.1
[c]Residue	5.4	4.9	4.1	4.5

[a]Deviation within 0.81%
[b]Deviation within 0.81%
[c]Deviation within 1.11%

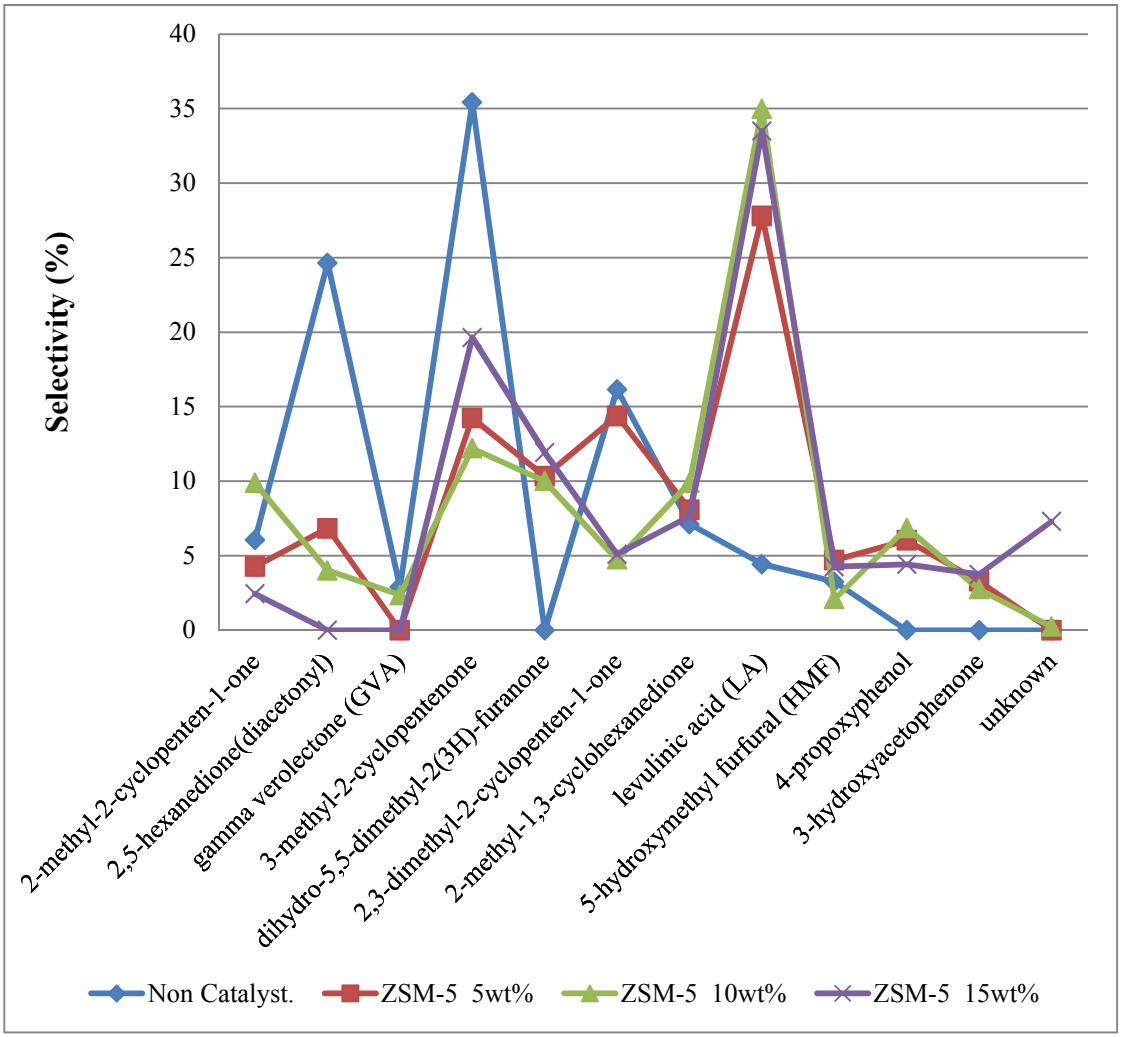

Figure 4.27 Liquid product selectivity of starch hydrothermolysis at various catalytic amounts (Condition: 300°C, reaction time 1 h, 10 bar N_2).

4.3.3 Effect of catalytic type

The hydrothermolysis of carbohydrates over various catalysts, *i.e.* ZSM-5, 20%Ru-ZSM-5, Al-SBA-15, 10%Ni-Al-SBA-15, 10%Ru-Al-SBA-15, 20%Ru-Al-SBA-15, 10%Ni-SBA-15, and 10%Ru-SBA-15 were performed at optimum conditions of each starting material compared to reaction without catalyst. In case of glucose and sucrose, catalyzed by 15 wt.% of catalyst at 200°C for 1 h and in case of starch, catalyzed by 10 wt.% of catalyst at 300°C for 1 h.

4.3.3.1 Glucose reaction

Value of product yields obtained by glucose hydrothermolysis over various catalysts at 200°C were shown in Table 4.15. All of catalytic type, the liquid yields were in range of 86-89% and yields of residue were lower than non catalytic reaction. In case of 10%Ni-SBA-15 and 10%Ru-SBA-15 were obtained higher residue than metal-Al-SBA-15 due to the lower acidity. Figure 4.28 exhibited selectivity of glucose hydrothermolysis liquid product. The highest LA selectivity was obtained in case of 20%Ru-ZSM-5 using as 44.0% and lower in the order of ZSM-5 (40.1%) > 20%Ru-Al-SBA-15 (33.6%) > 10%Ru-Al-SBA-15 (32.9%) > 10 %Ni-Al-SBA-15 (32.0%) > Al-SBA-15 (26.0%) > 10%Ru-SBA-15 (14.8%) > 10%Ni-SBA-15 (12.6%) > Non catalyst (6.5%). It was able to suggest that the high acidity and small pose size of 20%Ru-ZSM-5 suitable for glucose starting material in hydrothermolysis to produce LA product. Cheriti *et al.* [9] showed lower 10.3% of LA as main product in glucose hydrothermolysis without catalyst at 350°C.

Table 4.15 Product yields from glucose hydrothermolysis over various catalysts (Condition: 200°C, reaction time 1 h, 10 bar N_2, 15 wt.% catalyst).

[a]Yield (%)	Non catalyst	ZSM-5	20%Ru-ZSM-5	Al-SBA-15	10%Ni-Al-SBA-15	10%Ru-Al-SBA-15	20%Ru-Al-SBA-15	10%Ni-SBA-15	10%Ru-SBA-15
[a]Gas	6.1	8.6	9.7	6.5	6.6	8.4	8.9	4.7	4.9
[b]Liquid	87.9	87.4	86.5	87.8	89.0	86.4	85.3	89.3	89.0
[c]Residue	6.0	4.0	3.8	5.7	4.4	5.2	5.8	6.0	6.10

[a]Deviation within 1.18%
[b]Deviation within 0.99%
[c]Deviation within 0.72%

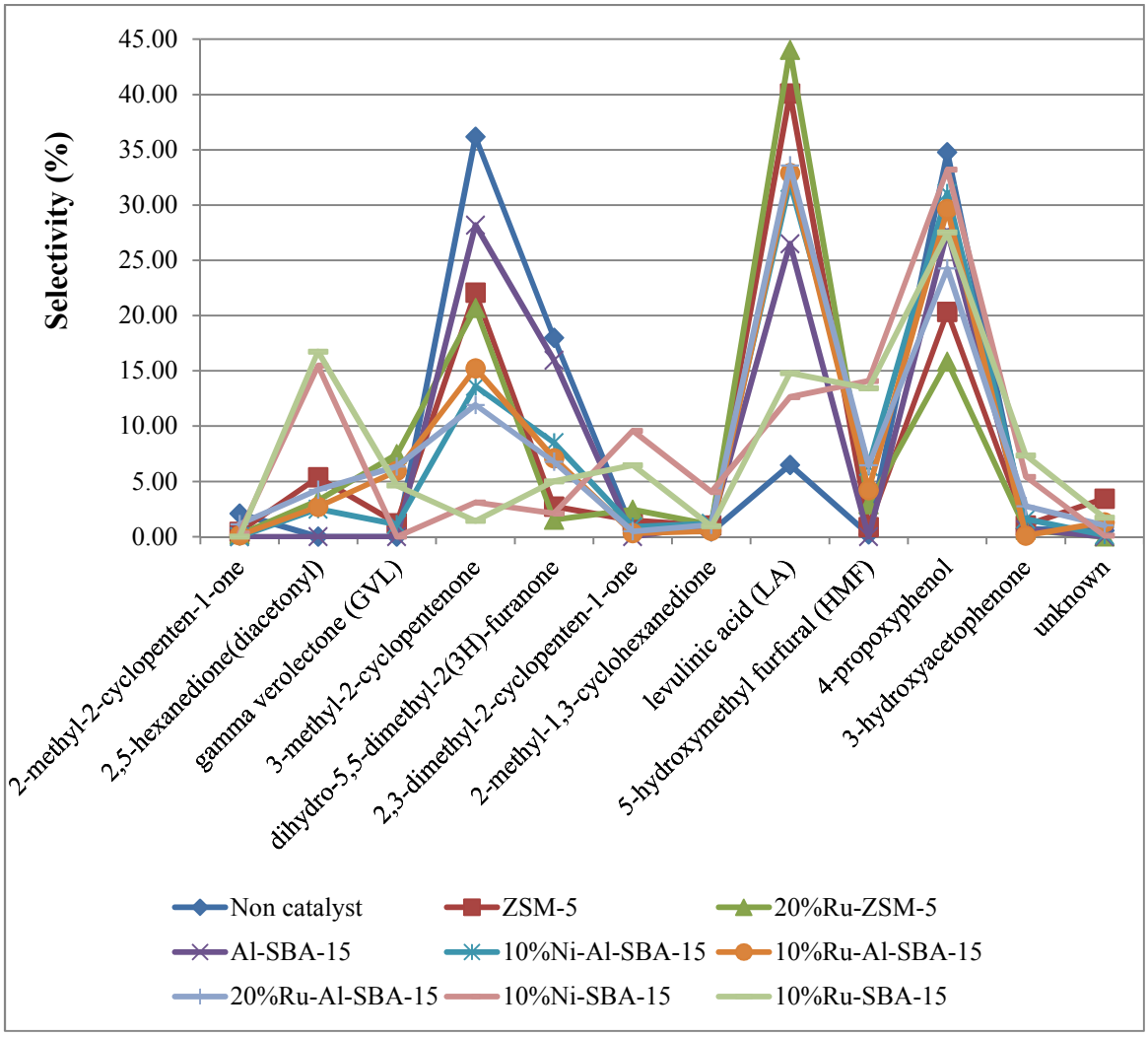

Figure 4.28 Liquid product selectivity of glucose hydrothermolysis at various catalysts (Condition: 200°C, reaction time 1 h, 10 bar N_2, 15 wt.% catalyst).

4.3.3.2 Sucrose reaction

The product yield of sucrose reaction over various catalysts and reaction without catalyst at 200°C were compared in Table 4.16. Considering the data, all of the catalytic reactions gave the gas fraction higher than non catalytic reaction and gave high yield of liquid fraction in the range of 85-89% with low residue (4-7%). The liquid product selectivity of sucrose hydrothermolysis were shown in Figure 4.28. It could be observed that all of the metal-catalysts gave the high LA selectivity in liquid product of sucrose reaction. The using of 20%Ru-Al-SBA-15 gave the highest LA yield as 40.8% slightly higher than 20%Ru-ZSM-5 (39.1%), while ZSM-5 (37.7%) gave nearly close to 10%Ru-Al-SBA-15 (37.0%) and lower in order of 10%Ni-Al-SBA-15 (35.1%) > Al-SBA-15 (26.7%) > 10%Ni-SBA-15 (17.0%) > 10%Ru-SBA-15 (16.2%) > non catalyst (8.4%).

Table 4.16 Product yields from sucrose hydrothermolysis over various catalysts (Condition: 200°C, reaction time 1 h, 10 bar N_2, 15 wt.% catalyst).

[a]Yield (%)	Non catalyst	ZSM-5	20%Ru -ZSM-5	Al-SBA-15	10%Ni-Al-SBA-15	10%Ru-Al-SBA-15	20%Ru-Al-SBA-15	10%Ni-SBA-15	10%Ru-SBA-15
[a]Gas	4.3	6.7	7.7	6.2	6.5	7.3	8.6	5.8	6.2
[b]Liquid	88.6	87.9	86.4	87.0	87.8	86.2	85.1	87.0	87.0
[c]Residue	7.1	5.4	5.9	6.8	5.7	6.5	6.3	7.2	6.8

[a]Deviation within 1.08%
[b]Deviation within 0.74%
[c]Deviation within 1.14%

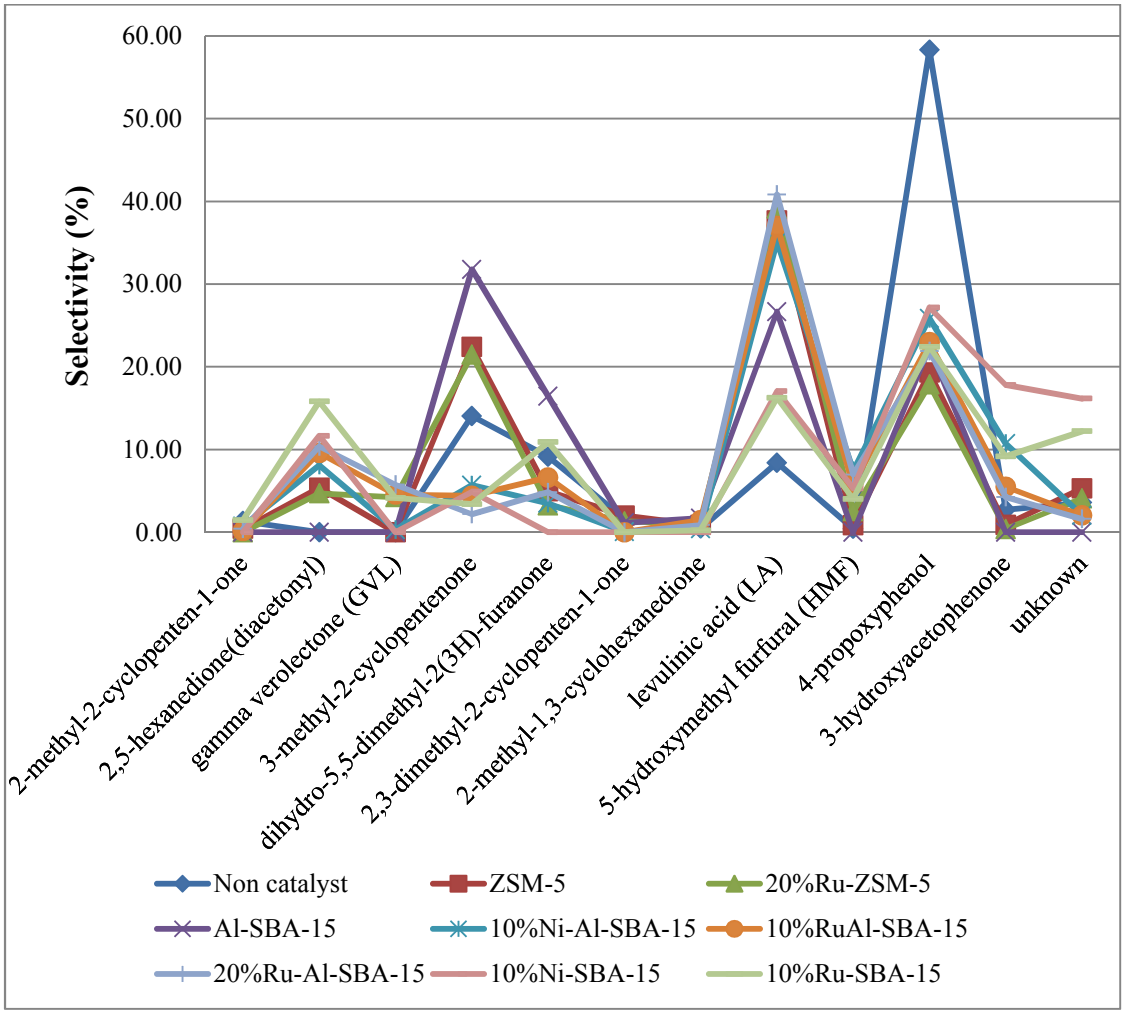

Figure 4.29 Liquid product selectivity of sucrose hydrothermolysis at various catalysts (Condition: 200°C, reaction time 1 h, 10 bar N_2, 15 wt.% catalyst).

4.3.3.3 Starch reaction

The product yields of starch hydrothermolysis over various catalysts compared to without catalytic reaction were shown in Table 4.17. Almost catalytic reactions exhibited a high performance with the liquid yield over 83% with a small amount of residue (4-7%) except the using of 20%Ru-ZSM-5 produced low liquid product (81.4%) with high residue yield (7.2%). This could be explained by the small pore size of ZSM-5 was blocked by Ru particles, therefore large molecule as starch could not access in pore of catalyst. Figure 4.30 showed the selectivity of liquid product of starch hydrothermolysis. The highest LA selectivity was obtained by using 20%Ru-Al-SBA-15 (38.6%), pretty higher than 10%Ru-Al-SBA-15 (37.9%) and lower in order of 10%Ni-Al-SBA-15 (35.2%) > ZSM-5 (35.0%) > Al-SBA-15 (31.7%) > 20%Ru-ZSM-5 (30.5) > 10%Ru-SBA-15 (15.3%) > 10%Ni-SBA-15 (13.6%) > non catalyst (4.4%). The pore size of catalyst had influence to LA selectivity of starch hydrothermolysis thus the metal-Al-SBA-15 gave the higher LA yield than that of ZSM-5. Cha *et al.* [6] reported the higher maximum LA yield (47.5%) from corn starch hydrolysis with dilute sulfuric acid by extrusion processing at 200^{o}C.

Table 4.17 Product yields from starch hydrothermolysis over various catalysts (Condition: 300^{o}C, reaction time 1 h, 10 bar N_2, 10 wt.% catalyst).

Yield (%)	Non catalyst	ZSM-5	20%Ru-ZSM-5	Al-SBA-15	10%Ni-Al-SBA-15	10%Ru-Al-SBA-15	20%Ru-Al-SBA-15	10%Ni-SBA-15	10%Ru-SBA-15
[a]Gas	8.9	9.1	11.4	9.70	9.8	11.0	12.0	8.7	9.3
[b]Liquid	85.6	86.8	81.4	84.9	85.8	83.9	83.4	85.3	84.1
[c]Residue	5.5	4.1	7.2	5.4	4.4	5.1	4.5	6.0	6.6

[a]Deviation within 0.96%
[b]Deviation within 0.98%
[c]Deviation within 1.13%

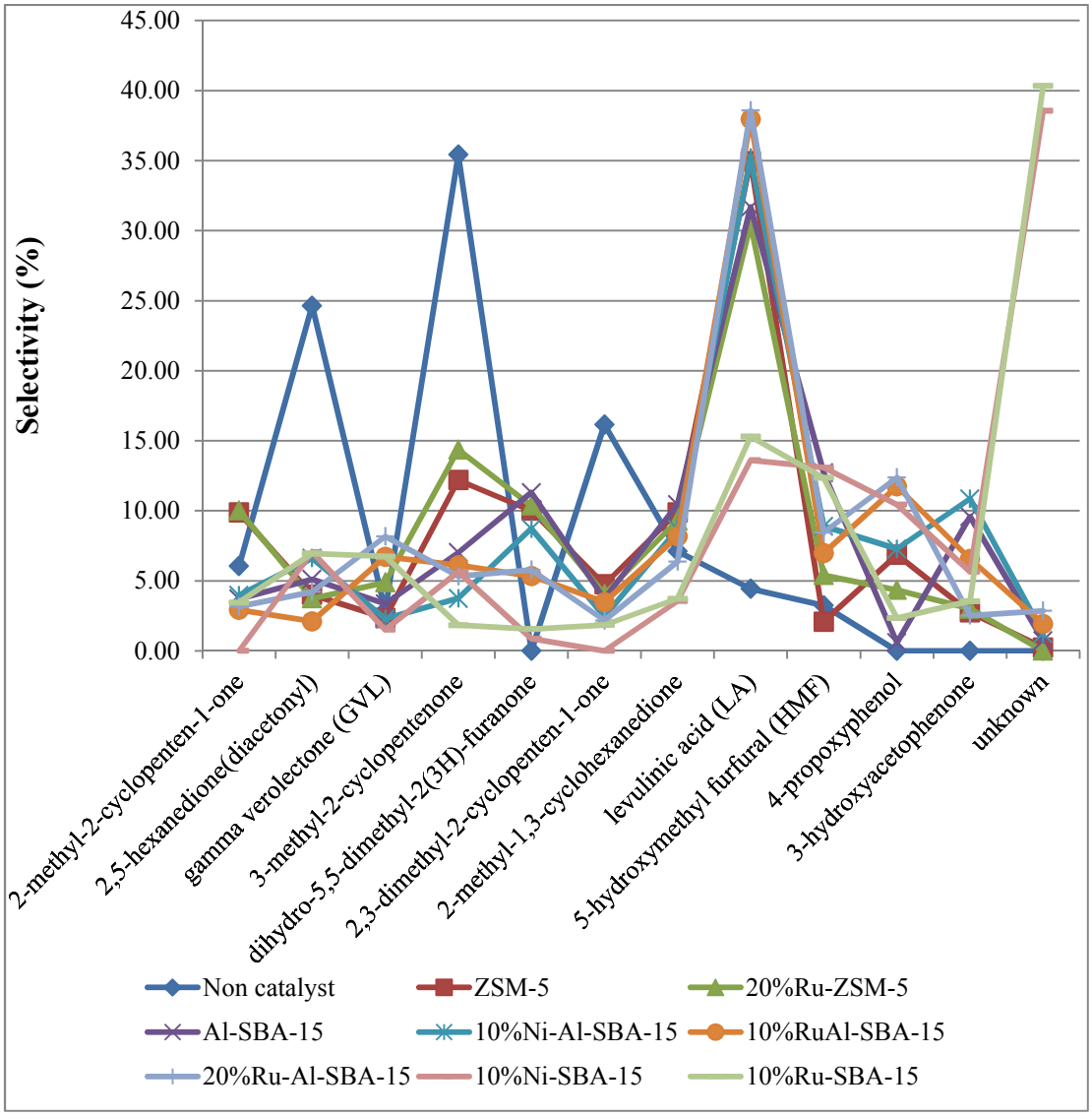

Figure 4.30 Liquid product selectivity of starch hydrothermolysis at various catalysts (Condition: 300^{o}C, reaction time 1 h, 10 bar N_2, 10 wt.% catalyst).

CHAPTER V
CONCLUSIONS

SBA-15 was successfully synthesized via hydrothermal method, exhibited only one phase of hexagonal pore mesoporous structure and Al-SBA-15 was prosperously synthesized by post-synthesis alumination method, and calcined at 550^{o}C for 5h. Also, Ni and Ru metal supported on SBA-15 and Al-SBA-15 materials were prepared by aqueous wet impregnation. All synthesized mesoporous products were characterized. XRD patterns of all samples indicated the hexagonal structure of SBA-15. N_2 adsorption-desorption isotherms displayed type IV pattern which showed typical sorption isotherm of mesoporous structure. Morphology of samples were aggregated particles with rope-like structure from SEM images. The TEM images of Al-SBA-15 showed the well-ordered hexagonal array of one-dimensional mesoporous channels of SBA-15 in which Al atoms were incorporated mainly at tetrahedral site. The aluminium framework was investigated by NMR technique. In case of metal supported samples, they were present in the form of metallic particles as measured by EDX technique indicated that metal particles enter exclusively into SBA-15 pores, observed that from the value from EDX technique was less than amount of metal in loading solution. Acid strength, measured quantitatively by acid-base titration. The alumination increased the acidity of SBA-15 due to the aluminium tetrahedral was located in framework. The metal incorporation also increased acidity of catalysts by generating more Lewis acid site.

All of catalysts were applied in the hydrothermolysis of carbohydrates (glucose, sucrose, and starch) to investigate the optimum conditions that gave highest yield of LA in liquid product. The reactions were carried out in a batch reactor for short reaction time (one hour). It was found that the hydrothermolysis of carbohydrates over high acidity showed low residue and high liquid product. The liquid product selectivity was depended on molecular size of starting material, acidity and pore size of catalyst. The small pore size of ZSM-5 was suitable for glucose molecule in hydrothermolysis to produced LA product (40.1%) when increased the acidity by Ru incorporation, the LA selectivity was increased (44.0%). The sucrose molecule was converted to LA product in high selectivity over high acidity catalyst such as metal-Al-SBA-15 and metal-ZSM-5. The large molecule of starch was specific to large pore size of SBA-15 and high acidity of catalyst that increased by metal incorporation. Thus, the 20%Ru-Al-SBA-15 gave the highest LA selectivity in starch hydrothermolysis.

The suggestion for future work

Study the catalytic activity of metal-ZSM-5 in hydrothermolysis of fructose which had pyranose ring structure that easy to convert to LA product and used cellulose and lignin, abundant and cheap starting material in hydrothermolysis over metal-Al-SBA-15 to produce high yield of LA.

REFERENCES

[1] Carlo, P., and Aldo, B. Biomass to fuels: The role of zeolite and mesoporous materials. *Mic. Mes. Mat.* 144(2011): 28-39.

[2] Huber, G.W., Iborra, S., and Corma, A. Synthesis of transportation fuels from biomass: chemistry, catalysts, and engineering. *Chem. Rev.* 106(2006): 4044-4098.

[3] Mamman, A.S., et al. Furfural-A promising platform for lignocellulosic biofuels. *Biofuel. Bioprod. Bioref.* 2(2008): 438-454.

[4] Pravin, P. U., et al. Selectivity hydrogenation of levulinic acid to ɤ-valerolactone over carbon-supported noble metal catalysts. *Ind. Eng. Chem.* 17(2011): 287-292.

[5] Lourvanij, K., and Rorrer, G.L. Reaction rates for the partial dehydration of glucose to organic acids in solid-acid, molecular-sieving catalyst powders. *J. Chem. Tech. Biotechnol.* 69(1997): 35-44.

[6] Cha, J.Y., and Hanna, M.A. Levulinic acid production based on extrusion and pressurized batch reaction. *Ind. Crop. Prod.* 16(2002): 109-118.

[7] Jinder, J., Gregory L. R., and Martin C. H. Dehydration of D-fructose to levulinic acid over LZY zeolite catalyst. *Biom. J.* 14(1987): 185-194.

[8] Khavinet, L., and Gregory, L.R. Reaction rates for the partial dehydration of glucose to organic acids in solid-acid, molecular-sieve catalyst powders. *J. Chem. Tech. Biotechnol.* 69(1997): 35-44.

[9] Cheriti, A., Draoui, B., Slimani, A., and Babadjamian A. PH effect on hydrothermolysis of the carbohydrate fraction of the biomass. *Rev. Energ. Ren*. Valorisation (1999): 117-120.

[10] Zhao, D., et al. Triblock copolymer syntheses of mesoporous silica with periodic 50 to 300 angstorm pores. *Sci.* 279(1998): 548.

[11] Yue, Y., Bonaedet, A., Melosh, J. L., and Espinose, J. B. Direct synthesis of AlSBA mesoporous molecular sieves: characterization and catalytic activities. *Chem. Commun.* (1999): 1967-1968.

[12] Kao, H.M., Ting, C.C., and Chao, S.W. Post synthesis alumination of mesoporous silica SBA-15 with high framework aluminum content using ammonium hexafluoroaluminate. *J. Mol. Catal*. 235(2005): 200.

[13] Ooi, Y.S., and Bhatia, S. Aluminum-containing SBA-15 as cracking catalyst for the production of biofuel from waste used palm oil. *Micropore. Mesopor. Mater.* 102(2007): 310.

[14] Xiu-Kai, L., Wei-Jie, J., Jing, Z., Shui-Ju, W., and Chak-Tong, A. Ammonia decomposition over Ru and Ni catalysts supported on fumed SiO_2, MCM-41, and SBA-15. *J. Catal.* 236(2005): 181-189.

[15] Yasuharu, K., et al. Preparation of highly active AlSBA-15-supported platinum catalyst for triophene hydrodesulfurization. *App. Cat.* 77(2007): 117.

[16] Vizcaino, A.J., Carrero, A., and Calles, J.A. Hydrogen production by ethanol steam reforming over Cu-Ni supported catalysts. *Int. J. Hydrogen Energy* 32(2007): 1450-1461.

[17] Yang, C., Gang, L., Fang, Y., and Song-Mei, Z. Mn/ZSM-5 participation in the degradation of cellulose under phosphoric acid media. *Polym. Degrad. Stab.* 96(2011): 863-869.

[18] Activation energy [online]. Available from : http://en.wikipedia.org/wiki/Activation_ energy [2011, February 14].

[19] Hagen, J. *Industrial Catalysis*. New York: Weinheim Wiley, 1999.

[20] Breck, D.W. *Zeolite Molecular Sieves: Structure, Chemistry, and use*, New York: John Wiley & Sons, (1997): 3-20.

[21] Barrer, R. M. *Zeolite and Clay Minerals as sorbets and Molecular Sieves*. London: Academic Press, (1978).

[22] Szostak, R. *Zeolite Molecular Sieves. Principles of Synthesis and Identification*. New York Van: Nostrand Reinhold, (1989).

[23] Zeolite [Online].Available from: http://mch3w.ch.man.ac.uk/theory/staff/student /mbdtscw/transfer_html/node1.html [2010, February 14].

[24] Argauer, R.J., and Landolt, G.R., Crystalline zeolite ZSM-5 and method of preparing the same. *U.S. Patent* 3(1972): 702-886.

[25] Smart, L., and Moore, E. *Solid State Chemistry.* London, Chapman & Hall University, 1992.

[26] Derouane, E.G. New aspects of molecular shape-selectivity: Catalytic by zeolite ZSM-5. *Stud. Surf. Sci. Catal.* 5(1980): 4.

[27] Lewis, D.W., Catlow, C.R.A., and Sankar, G. Structure of Iron-substituted ZSM-5. *J. Phys. Chem*. 99(1995): 2377.

[28] Stachowiak, G.W., and Batchelor, A.W. *Engineering tribology*. *3rd edition*. Oxford : Elsevier, 2005.

[29] Rudnick, L.R., and Shubkin, R.L. *Synthetic lubricants and high-performance functionl fluids*. *2nd edition*. New York : Marcel Dekker, 1999.

[30] Mortier, R.M., Fox, M.F., and Orszulik, S.T. *Chemistry and Technology of Lubricants*. New York : Springer Science, 2010.

[31] Beck, J. S., Leonowicz, M. E., Roth, W. J., Vartuli, J. C., and Kresge, C. T. A new family of mesoporous molecular sieves prepared with liquid crystal templates. *J. Am. Chem. Soc*. 114(1992): 10834-10843.

[32] Tanev, P. T., and Pinnavania, T. J. Mesoporous silica molecular sieves prepared by ionic and neutral surfactant templating: a comparison of physical properties. *Chem. Mater*. 8(1996): 2068-2079.

[33] Soler-Illia, G. J. A. A., Crepaldi, E. L., Grosso, D., and Sanchez, C. Block copolymer-templated mesoporous oxides. *Curr. Opin. Coll. Interf. Sci*. 8(2003): 109-126.

[34] Melosh, N.A., Lipic, P., Bates, F.A., and Stucky, G.D. Molecular and mesoscopic structure of transparent block copolymer silica monoliths. *Macromolecules*. 32(1999): 4332-4342.

[35] Stucky, G.D., et al. Triblock copolymer syntheses of mesoporous silica with periodic 50 to 300 angstorm pores. *Sci*. 279(1998): 548-552.

[36] Figueiredo, J.L., Pereira, M.M., and Faria J. *Journal of Catalysis from theory to application: an integrated course*. Portugal : Imprensa Da Universidade De Coimbra, 2008.

[37] Gabriel, B.L. *SEM: A User's Manual for Material Science*, Ohio: American Society for Metal, 1985.

[38] Luan, Z., Hartmann, M., Zhao, D., Zhou, W., and Kevan, L. Alumination and ion exchange of mesoporous SBA-15 molecular sieve. *Chem. Meter.* 11(1999): 1621.

[39] Ooi, Y., Zakaria, R., Mohamed, A.R., and Bhatia, S. Hydrothermal stability and catalytic activity of mesoporous aluminum-containing SBA-15. *Catal. Commun.* 5(2004): 441.

[40] Al-SBA-15 [online] Available from: http://mch3w.ch.man.ac.uk/theory/staff/student/mbdtscw/tranfer_htm/nodel.html [2009, September 7]

[41] Pangma, W. *Preparation of tungstic oxide supported on SBA-15 for metathesis of 1-hexane.* Master's Thesis, Program of Petrochemistry and Polymer Science, Faculty of Science, Chulalongkorn University. 2003

[42] Wouters, B.H., Chen, T.-H., and Grobet, P.J. Reversible tetrahedral-octahedral framework aluminum in zeolite Y. *J. Am. Chem. Soc.* 120(1998): 11419.

[43] Leach, B.E. *Applied Industrial Catalysis*, Vol. 2, Oklahoma, 1984

[44] Abd El-Wahab, M. M. M., and Said, A. Phosphomolybdic acid supported on silica gel and promoted with alkali metal ions as catalyst for the esterification of acetic acid by ethanol. *J. Mol. Cat. A* 240(2005): 109.

[45] Soler-Illia, G. J. A. A., Sanchez, C., Lebeau, B., and Patarin, J. Chemical strategies to design textured materials: from microporous and mesoporous oxides to nanonetworks and hierarchical structures. *Chemical. Reviews*. 102(2002): 4093-4138.

[46] Skoog, D. A. *Principles of Instrumental Analysis*. New York, Harcourt Brace College Publishers, 1997.

[47] BET [online]. Available from: Basic operating principles of the sorptomatic, http://saf.chem.ox.ac.uk./Instruments/BET/sorpoptprin [2011, February 9].

[48] Analysis software user's manual [online]. Available from: http://www.nippon-bel.co.jp/product/product_05_e.html [2011, February 9].

[49] Gabriel, B. L. *SEM: A User's Manual for Material Science*, Ohio: American Society for Metal, 1985.

[50] Transmission electron microscope [online]. Available from: Microscope, http:// www1.stkc.go.th/stportalDocument/stportal _1170654028.doc [2009, September 2].

[51] TEM [online].Available from: Transmission electron microscope (TEM) .http:// m.eb.com/assembly/110686 [2009, September 2].

[52] EDX [online]. Available from: Energy-dispersive X-rayspectroscopy, http://en. wikipedia.org/wiki/EDX [2012, March 11].

[53] EDX [online]. Available from: EDX-Energy Dispersive X-ray Analysis, http:// www.globalsino.com/micro/1/micro9999.html [2012, March 11].

[54] Szostak, R. *Molecular Sieve*. Principles of Synthesis and Identification, New York, Van Nostrand Reinhold, 1989.

[55] Clague, A.D., Alma, N.C.M., Sternhell, S., and Field, L.D., *Analytical NMR*, New York, John Wiley and son, 1989.

[56] Sudong, Y., and Zhongchao, T. Hydrothermal liquefaction of cellulose to bio-oil under acidic, neutral and alkaline conditions. *Appl. Energy.* 92(2012): 234-239.

[57] Taku, M. A., et al. Dehydration of D-glucose in high temperature water at pressures up to 80 MPa. *J. Supercrit. Fluids.* 40(2007): 381-388.

[58] Girisuta, B., Janssen, L.P.B.M., and Heeres, H.J. Green chemicals a kinetic study on the coversion of glucose to levulinic acid. *Chem. Eng. Res. Des.* 84(A5): 339-349.

[59] Joseph, J. B., et al. Production of levulinic acid and use as a platform chemical for derived products. *Res. Con. Rec.* 28(2000): 227-239.

[60] Zhaohua, L., Hartmann, M., Zhao, D.; Zhou, D., and Kevan, L. Alumination and ion exchange of mesoporous SBA-15 molecular sieve. *J. Mater. Chem.* 11(1999): 1621-1627.

[61] Mbaraka, I. K., Radu, D. R., Lin, V. S. Y., and Shanks, B. H. Organosulfonic acid-functionalized mesoporous silicas for the esterification of fatty acid. *J. Catal.* 219(2003): 329-336.

[62] Eswaramoorthi, I., and Dalai, A.K. Synthesis, characterization and catalytic performance of boron substituted SBA-15 molecular sieves, *Micro.Meso. Mater.* 93(2006): 1.

[63] Sun, Y., Zheng, Y., Su, X., Zhang, X., and Wei, W. Functionalized masoporous SBA -15 silica with propylsulfonic group as catalysts for esterification of salicylic acid with dimethyl carbonate. *Stud. Surf. Sci. Catal*. 156(2006): 205-212.

[64] Tatiana, K., Javier, R., Oliver, G., and Lilia, L. Novel bifunctional NiMo/Al-SBA-15 catalysts for deep hydrodesulfurization: Effect of support Si/Al ratio. *Appl. Catal. A.* 335(2008): 159-171.

[65] Xiu-Kai, L., Wei-Jei, J., Jing, Z., Shui-Ju, W., and Chak-Tong, A. Ammonia decomposition over Ru And Ni catalysts supported on fumed SiO_2, MCM-41, and SBA-15. *J. Catal.* 236(2005): 181-189.

[66] Amaroli, T., et al. Effect of crystal size ans Si/Al ratio on the surface properties of HZSM-5 zeolites. *Appl. Catal. A: Gen.* 306(2006): 78-84.

[67] Yang, C., Gang, L., Fang, Y., and Song-Mei, Z. Mn/ZSM-5 participation in the degradation of cellulose under phosphoric acid media. *Polym Degrad Stab.* 96(2011): 863-869.

[68] Serrano, D.P., Aguado, J., Escola J.M., and Rodriques, J.M. Influence of na nocrystalline HZSM-5 external surface on the catalytic cracking of polyolefin. *J. Anal. Appl. Pyrolysis* 74(2005): 353-360.

APPENDIX

1. % Yield

$$\% \text{ Yield} = \frac{\text{mass of product fraction}}{\text{mass of starting mixture}} \times 100$$

2. % Selectivity of liquid products (Area Normalization)

$$\% \text{ Selectivity of X} = \frac{\text{Peak area of X}}{\text{Peak area of all products}} \times 100$$

Table A-1 Retention time of the peaks and names of the corresponding chemical species identified (GC chromatogram refer to Figure A-1).

Peak No.	Retention time (min)	Compound name
1	2.08	2-methyl-2-cyclopenten-1-one
2	2.33	2,5-hexanedione
3	2.50	dihydro-5-methyl-2(3H)-furanone
4	3.50	3-methyl-2-cyclopentenone
5	5.00	dihydro-5,5-dimethyl-2(3H)-furanone
6	7.14	2,3-dimethyl-2-cyclopenten-1-one
7	24.52	2-methyl-1,3-cyclohexanedione
8	26.70	levulinic acid (LA)
9	28.12	5-hydroxymethyl furfural
10	33.12	4-propoxyphenol
11	39.04	3-hydroxyacetophenone
12	57.30	unknown
13	58.98	unknown

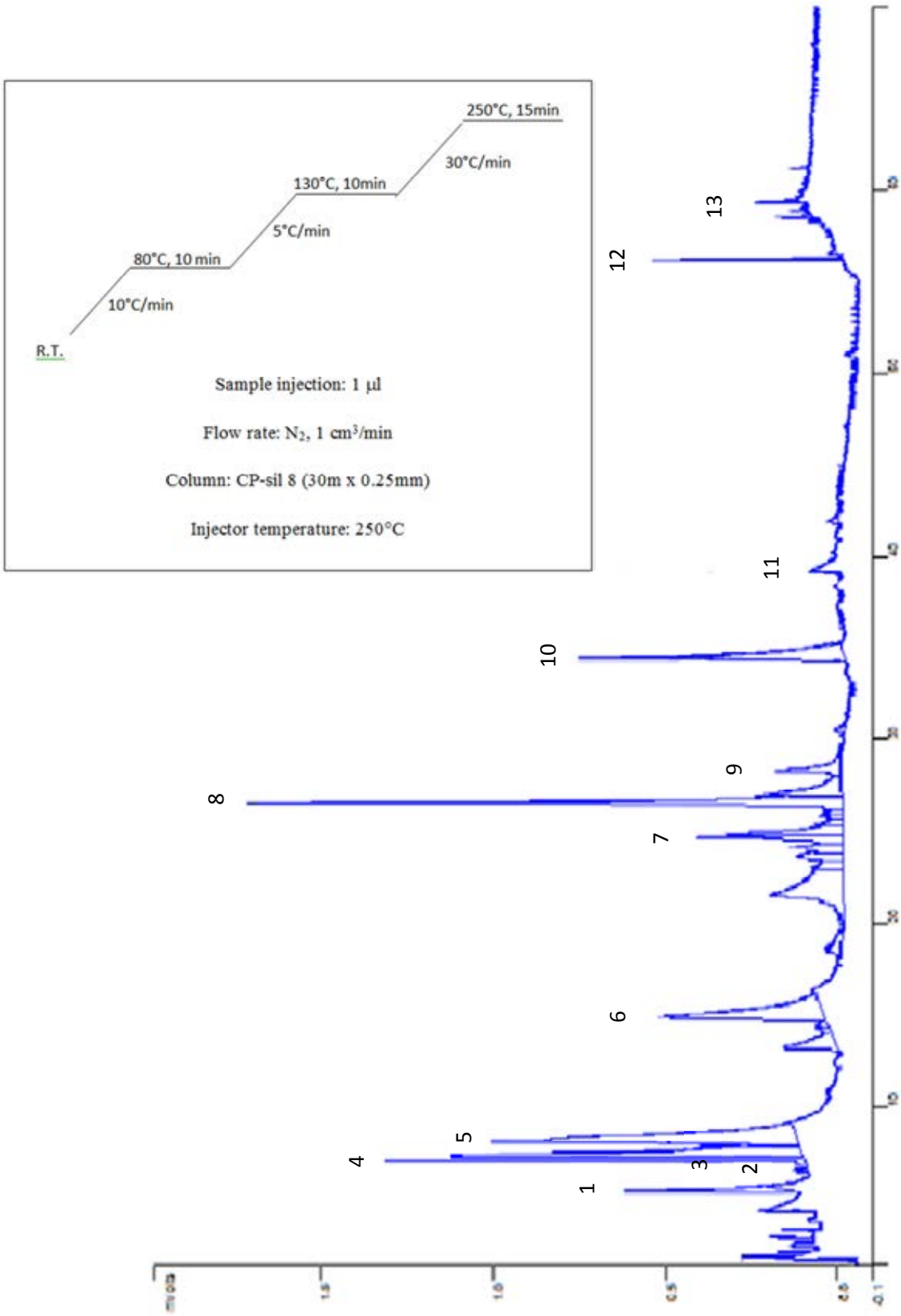

Figure A-1 GC Chromatogram of liquid product from glucose hydrothermolysis over ZSM-5 at 200°C.

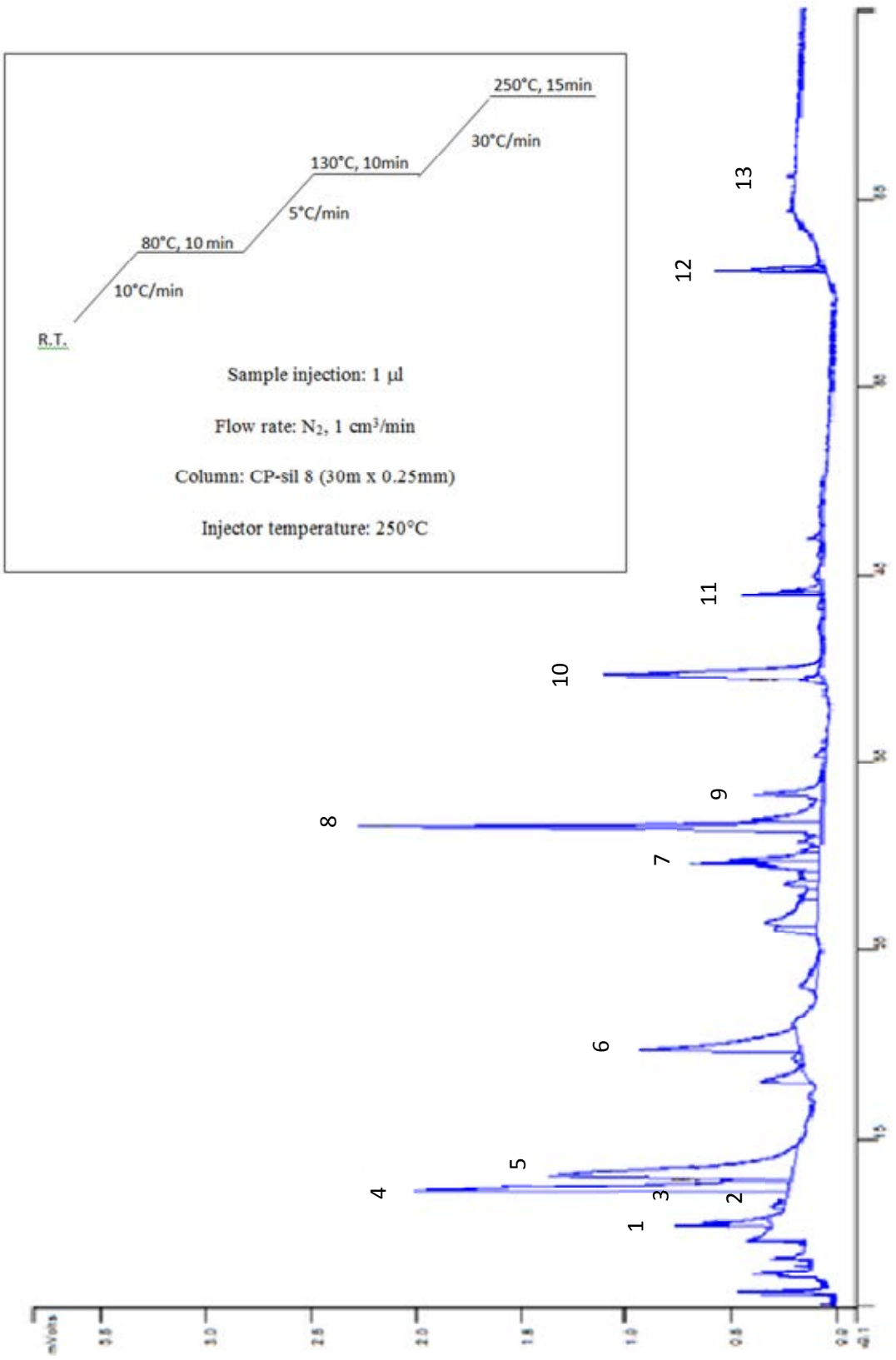

Figure A-2 GC Chromatogram of liquid product from sucrose hydrothermolysis over ZSM-5 at 200°C.

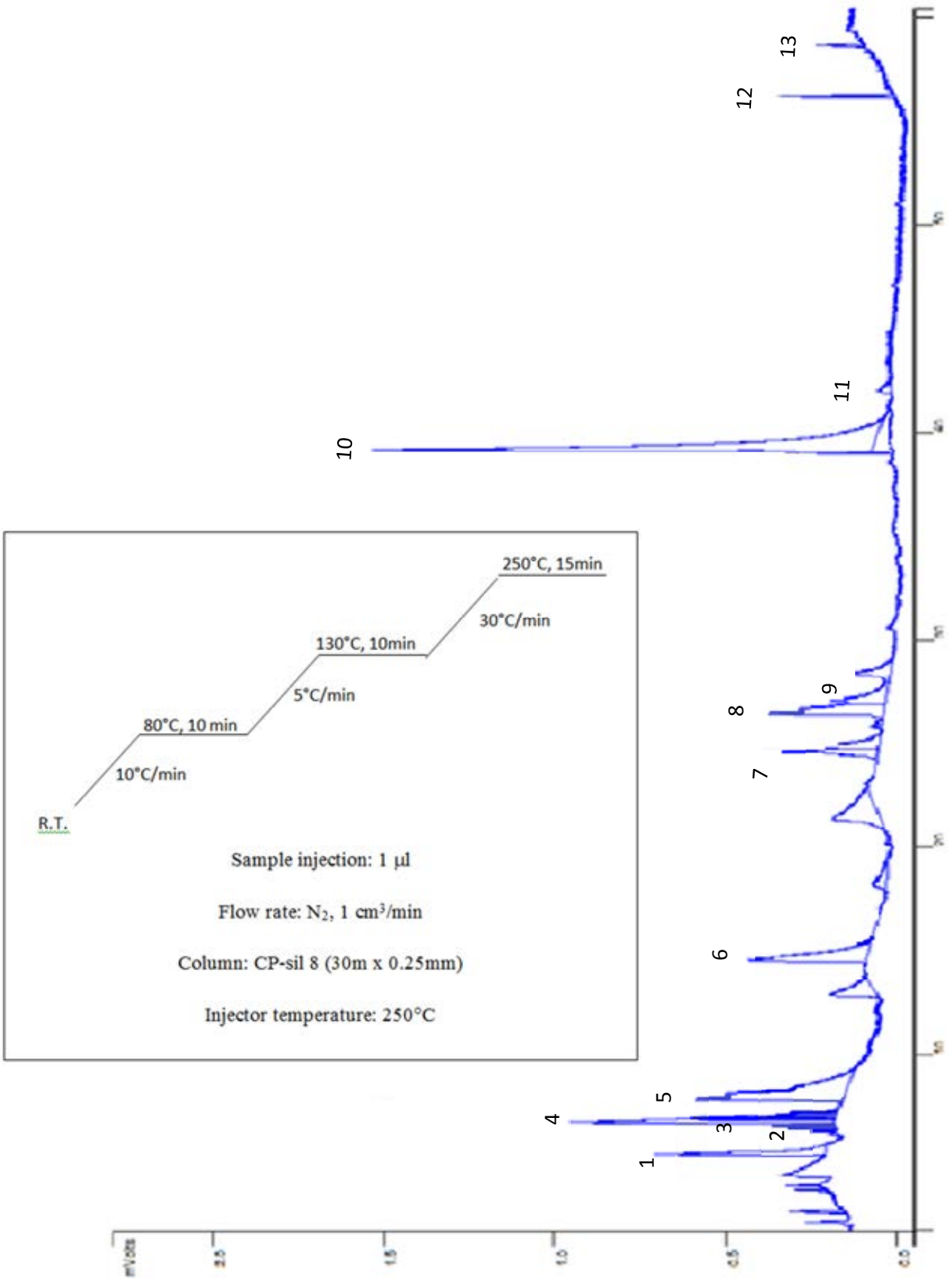

Figure A-3 GC Chromatogram of liquid product from starch hydrothermolysis over ZSM-5 at 200°C.

VITAE

Miss Sirinart Suacharoen was born on May 11, 1986 in Bangkok, Thailand. She obtained a Bachelor Degree of Science, major in Marine science, Faculty of Science from Chulalongkorn University, Bangkok, Thailand in 2008. Since 2009, she has been a graduate student in the program of Petrochemistry and Polymer Science, Faculty of Science, Chulalongkorn University and completed her Master of Science Degree in 2012.

In 11-13 January 2012, she participated in Pure and Applied Chemistry International Conference (PACCON 2012) at The M Place Hotel, Chiang mai, Thailand which had already been approved by proceeding and poster presentation in the title of "Hydrothermolysis of carbohydrates using aluminosilicate catalyst".

Her present address is 99/35 U Sabai Village, Soi Krungthepkreetha 39, Krungthepkreetha Road, Sapansung district, Bangkok, Thailand 10240.